Al-Farabi Kazakh National University

UDC 539.1

VALIOLDA DINARA SALAVATKYZY

Coulomb breakup of exotic nuclei by quantum-mechanical approach

6D060500 – Nuclear physics

Thesis is submitted in fulfillment of the requirements for the degree of
Doctor of Philosophy (PhD)

Scientific Supervisors:
Cand.of Phys.-Math. Sciences,
assoc.prof. Zhaugasheva S.A.
Doctor of Phys.-Math. Sciences,
professor Melezhik V.S.

Republic of Kazakhstan
Almaty, 2023

CONTENT

NORMATIVE REFERENCES 3
NOTATION AND ABBREVIATIONS 4
INTRODUCTION 5
1 THE HALO STRUCTURE 13
1.1 The ^{11}Be halo nucleus 15
1.2 The role of nuclear reactions 17
2 NONPERTURBATIVE TIME-DEPENDENT APPROACH IN BREAKUP REACTIONS 19
2.1 Model for describing neutron dynamics during collision 19
2.2 The computational scheme of solving TDSE 20
2.2.1 Angular-subspace discretization 21
2.2.2 Splitting up method 23
2.3 The numerical method for solving stationary Schrodinger equation for bound states of ^{11}Be 24
2.3.1 Reverse iteration method in subspace 26
2.3.2 Sweep method 29
2.4. Quasi uniform radial grid 30
2.4.1 Radial discretization of the wave function 31
2.4.2 The results of solving stationary SE: the energy spectrum of bound states 32
2.5 The parameterization of the interaction between the neutron and core 34
3 THE CALCULATION OF BREAKUP CROSS-SECTION 41
3.1 Convergence of the computational scheme and accuracy of the approach 42
3.2 Results and discussion 48
3.2.1 Influence of resonance states to the breakup cross section of ^{11}Be at 69 and 72 MeV/nucleon 48
3.2.2 Breakup cross section of ^{11} Be at low beam energies 50
3.3 The breakup cross section including neutron interaction with the core in the final state 53
3.4 Contribution to breakup of nuclear interaction between projectile and target 57
3.5 How good is the linear trajectory approach for projectile motion at low energies 61
3.6 Excitation of ^{11}Be in collision with ^{208}Pb 65
CONCLUSION 70
REFERENCES 73
APPENDIX A The system of units and some details of the solution of SE 77
APPENDIX B Details of the inclusion of nuclear interaction into the computational scheme 80
APPENDIX C The application of breakup wave function in analyzing the breakup dynamics 84

NORMATIVE REFERENCES

In this dissertation, references to the following standards are used:

GOST 7.1-84 System of standards for information, librarianship and publishing. Bibliographic description of documents. General requirements and drafting rules

GOST 7.12-93 System of standards for information, librarianship and publishing. Bibliographic record. Abbreviations of words in English. General requirements and rules

GOST 2.105-95 Unified system for design documentation. General requirements for text documents

GOST 7.32-2001 System of standards for information, librarianship and publishing. Research report. Structure and design rules

DESIGNATIONS AND ABBREVIATIONS

CDCC	–	coupled-channels with a discretized continuum
DEA	–	dynamical eikonal approximation
TDSE	–	time-dependent Schrodinger equation
DWBA	–	distorted-wave Born approximation
MeV	–	Mega electron volt, is the measure of an amount of kinetic energy gained by a single electron accelerating from rest through an electric potential difference of one volt in vacuum
ISOLDE	–	The Isotope mass Separator On-Line facility., the radioactive ion beam facility at CERN and a unique source of low-energy beams of radioactive nuclides
HIE-ISOLDE	–	High-Intensity and Energy upgrade of ISOLDE
CERN	–	European Organization for Nuclear Research
ReA12	–	The reaccelerator facility (ReA) at the National Superconducting Cyclotron Laboratory (NSCL) at Michigan State University
MSU	–	Michigan State University
DVR	–	discrete-variable representation
2D	–	two dimensional
the USA	–	United States of America
RIBs	–	Radioactive ion beams
JINR	–	Joint Institute for Nuclear Research (in Dubna, Russia)
1 n halo	–	one neutron halo nucleus
Eq.	–	equation
LU decomposition	–	lower–upper decomposition
Fig.	–	figure
SE	–	Schrodinger equation

INTRODUCTION

General description of the research. The dissertation work is devoted to the investigation of the Coulomb breakup of ^{11}Be halo nuclei within the time-dependent quantum-mechanical approach.

Exotic structures and phenomena in the proximity of the proton and neutron driplines were discovered in the 1980s due to the development of radioactive beams [1, 2]. A striking example is the halo nuclei. Halo nuclei are usually described within the few-body model: a core, which contains most of the nucleons plus one or two valence nucleons. Due to their very short lifetime, halo nuclei are studied through indirect techniques such as breakup reactions in which the halo nucleon dissociates from the core through the interaction with the target [3]. A number of breakup measurements were made even when the radioactive beam intensity was rather low. The breakup induced by the Coulomb interaction between projectile and target is one of the main mechanisms to describe exotic processes [2, 4].

The neutron halo effect is caused by the presence of weakly bound states of neutrons located near the continuum. The small value of the binding energy of a neutron (or a group of neutrons) and the short-range nature of nuclear forces lead to the tunneling of neutrons into the outer peripheral region over large distances from the core of the nucleus [5]. The most famous nuclei having the structure of a neutron halo are ^{11}Be, ^{11}Li, ^{15}C, ^{19}C and etc. They have small binding energies, anomalously large sizes, narrow momentum distributions of fragments after the breakup, large interaction cross sections and electromagnetic dissociation [5].

Among the neutron halo nuclei, the ^{11}Be nucleus is of particular interest. In the simplest approximation, it can be considered as a two-particle system consisting of a ^{10}Be core and a weakly bound neutron. A number of computational approaches were developed to describe the breakup of two-body projectiles, i.e., one-nucleon halo nuclei of ^{11}Be: perturbation expansion [6, 7], adiabatic approximation [8], eikonal model [9], coupled-channels with a discretized continuum (CDCC) [10, 11], dynamical eikonal approximation (DEA) [11] and numerical integration of a three-dimensional time-dependent Schrodinger equation (TDSE) [12, 13, 14, 15].

The methods mentioned above are mainly applied to high and intermediate beam energies in the breakup reaction of ^{11}Be on a heavy target. For intermediate beam energies (near 70 MeV/nucleon) there are rather accurate experimental data [16, 17] and theoretical analyses with different approaches [11, 18, 19]. However, for lower energies only a few theoretical works have been performed so far [11, 18-22]. For instance at [19] the breakup reaction ^{11}Be+^{208}Pb->^{10}Be+n+^{208}Pb for energies of 5, 10 and 30 MeV/nucleon was investigated within the distorted wave Born approximation (DWBA). Nevertheless, the applicability of this approach to low energies is questionable and must be justified [19].

An attempt was also made to calculate the breakup of ^{11}Be on the Pb target at a beam energy of 20 MeV/nucleon with the dynamical eikonal approximation [11, 18]. However, this approach is a high-energy reaction model [11] and its adequate extension to low-energy (below 40 MeV/nucleon) has not yet been realised [5]. Thus,

although the region around 10 MeV/nucleon is of great interest, since this is the energy range of HIE-ISOLD at CERN and the future ReA12 at MSU, it has hardly been investigated theoretically so far [3].

In the present work, we fill this gap by generalizing to this area the theoretical model developed in [12, 13, 23] and successfully applied to the breakup of halo nuclei ^{11}Be [12, 13], ^{15}C [13], and ^{17}F [23] at higher beam energies. In this model, the time-dependent Schrödinger equation for a halo-nucleon is integrated with a non-perturbative algorithm on a three dimensional spatial mesh. The use of the discrete-variable representation (DVR) in 2D angular space and high-order finite differences for the radial part of the wave function allows avoiding the multipole expansion of the time-dependent Coulomb interaction between the projectile and the target [12, 24]. Another attractive feature of the method is its flexibility to the choice of the interactions between the halo-nucleon, the core and the target [13] and in the definition of the projectile trajectory which can be quasiclassically treated simultaneously with the Schrödinger equation for the weakly-bound halo nucleon of the projectile [3, 25].

We extend the theoretical model to the low-energy region and investigate its convergence and stability here [3]. With this approach we perform calculations of the breakup cross section of ^{11}Be on a heavy target (^{208}Pb) at 5–30 MeV/nucleon taking into account Coulomb and nuclear interactions between the projectile and the target [3]. We apply the classical consideration (classical trajectories) for a heavy and fast ^{11}Be projectile and a quantum approach for a light and slow neutron, where the relation p_{Be} = (3800 − 1100) MeV/c >> p_n ~ 40 MeV/*c* for their momentums is satisfied. We consider the region E_{Be} = (770 − 55) MeV>>E_n ~ 1 MeV for the projectile and the halo neutron energies during the breakup collisions, which further justifies the semiclassical approach. To quantify how good the semiclassical approach with decreasing the projectile energy is, we also performed calculations with quantum-quasiclassical approach [25, 26], which includes the effect of deformation of the projectile trajectory and the transfer of energy from target to projectile and vice versa during a collision [3]. We also analyse in the frame of this model the influence of the ^{11}Be resonant states $5/2^+$, $3/2^-$ and $3/2^+$ [17, 27, 28] on the breakup processes. This analysis demonstrates the possibility of studying low-lying resonances in halo nuclei using their breakup reactions. The method can potentially be useful for interpretation of low-energy breakup experiments on different targets in studying the halo structure of nuclei [3].

Relevance of the research topic. Nowadays the greatest interest in nuclear physics is associated with the investigations of the behavior of atomic nuclei under extreme conditions that can be created in modern laboratories. The parameters, which characterize nuclear states and take extreme values, can be different: energy, deformation, angular momentum, etc. [29]. The study of radioactive nuclei is of the particular interest. These are neutron or proton-excess nuclei, which are unstable and decay via β-decay. The investigations with beams of radioactive nuclei have opened new prospects in studying the structure of the atomic nucleus and have found wide applications in other areas of physics, including nuclear astrophysics. The

fundamental problems of nuclear physics, for example, the determination of the nucleon drip-line, the synthesis of superheavy elements, the evolution of the shell structure on the way to the limits of the existence of atomic nuclei (the disappearance and appearance of magic numbers) are studied in the reactions with beams of unstable nuclei [29]. New facilities for studying exotic nuclei with parameters that far exceed existing ones are planned and built in Japan, Germany, Canada and the USA. In the future, it is expected to get important results concerning the fundamental questions of the structure of atomic nuclei and the mechanisms of nuclear reactions. The studies with radioactive nuclei have already led to a fundamental result: in some weakly coupled light nuclei located on the boundary of nucleon stability, an interesting phenomena of nuclear structure - the halo has been discovered. The structure of nuclei with halo, located on the drip-line, is one of the most interesting problems in the physics of radioactive ion beams (RIBs)[29].

A characteristic feature of the physics of exotic nuclei is the close relationship between the mechanism of nuclear reaction and the structure of the nucleus. The most widely used reaction for studying halo nuclei is the Coulomb breakup reaction, which can be considered as the transition of a nucleon from a halo nucleus to a continuum due to varying Coulomb field between the nucleon and the target in collisions. Thus, the Coulomb breakup is one of the main tools in the study of halo nuclei. The breakup cross section provides useful information on the halo structure [30].

Within the framework of the dissertation work, for a more detailed study of the mechanism of the halo structure, it was planned to include low-lying resonances in various partial and spin states of the ^{11}Be nucleus in the calculation of the breakup cross section [3, 31]. The Coulomb breakup of the halo nuclei is studied numerically, by solving the time-dependent Schrödinger equation on an angular Lagrange and quasi-uniform radial grid. The developed computational scheme opens up new possibilities in the study of the Coulomb, as well as nuclear, breakup of halo nuclei on both heavy and light targets [3].

One of the relevant problems of the work is to study the contribution of low-lying resonances to the breakup cross section. Since in the previous calculations only two bound states of the ^{11}Be nucleus were taken into account (the ground state $½^+$ and the first excited state $½^-$) [11-13, 24, 32], it is assumed that taking into account low-lying resonances will improve the theoretical description of the experimental data on the cross section for the breakup reaction $^{11}\text{Be} + {}^{208}\text{Pb} \rightarrow {}^{10}\text{Be} + \text{n} + {}^{208}\text{Pb}$ at intermediate energies [16, 17] and explain the appearance of visible peaks in the energy range 1.23, 2.78, and 3.3 MeV, which corresponds to the position of the peaks of resonances $5/2^+$, $3/2^-$ and $3/2^+$ [27, 28]. It should be noted that these resonances were identified by the states obtained experimentally by the group of Fukuda et al. [17] in the $^{11}\text{Be} + {}^{12}\text{C}$ breakup reaction at 70 MeV/nucleon. Also, special attention should be paid to study of the influence of nuclear effects on the breakup cross section, which makes it possible to extract more detailed information on the structure of exotic nuclei.

Thus, the presented tasks of this dissertation work have priority directions not only in Kazakhstan, but also in the worldwide. Research on this topic is one of the

rapidly developing fields of modern nuclear physics of all major scientific centers of the world. The obtained results are quite competitive on the international level. These studies are not only of academic interest, but also of great practical importance. The expected results are very important and relevant for the interpretation and planning of future experiments with exotic nuclei, since at the present time there is a substantial lag in the theoretical models from the needs of the experiment in this field. The key problem to be solved by the tasks of the dissertation work is the expansion of our approach to the low-energy area, since this area has hardly been studied both theoretically and experimentally. Thus, the obtained results will be important for testing existing theoretical models and for the practical application of theoretical calculations in experiments to investigate the breakup of halo nucleus at low-energy radioactive beams.

The goals of the research is an investigation of low-lying resonances in the Coulomb breakup of ^{11}Be halo nuclei on heavy target (^{208}Pb) from intermediate (70 MeV/nucleon) to low energies (5 MeV/nucleon) within non-perturbative time-dependent quantum-mechanical approach.

To achieve these goals, it is necessary to solve the following **objectives:**

– to select and analyse parameters of the potentials between the neutron and ^{10}Be core for description of different partial and spin states of the ^{11}Be nucleus;

– to investigate the influence of low-lying resonance states ($5/2^+$, $3/2^-$ and $3/2^+$) to the Coulomb breakup of ^{11}Be nucleus on a heavy (^{208}Pb) target within the semiclassical and quantum-quasiclassical time-dependent approaches;

– to study the contribution to breakup of nuclear interaction between projectile and target;

– to probe how good is the linear trajectory approach for projectile motion at low beam energies;

– to explore the excitation of ^{11}Be in collision with ^{208}Pb target.

The objects of the research are a halo nucleus, ^{11}Be, low-lying resonances and breakup cross-section.

The subject of the research is quantum mechanics, the work is devoted to the numerical solution of the time-dependent Schrödinger equation, exact calculations of the breakup cross sections by quantum-mechanical approach.

Research methods: numerical methods for solving the stationary and time-dependent Schrödinger equations: reverse iteration method, sweep method, the splitting up method, the discrete variable representation, finite-difference technique in quasi uniform radial grid.

The main statements for defense:

1) An account of the low-lying resonance states of ^{11}Be describes the experimental data on the breakup reaction ^{11}Be+^{208}Pb->^{10}Be+n+^{208}Pb cross sections at 69 MeV/nucleon with the accuracy of 1-2% and explains the appearance of visible peaks at energies of 1.23, 2.78, 3.3 MeV, which correspond to the positions of the $5/2^+$, $3/2^-$ and $3/2^+$ resonances, respectively.

2) The breakup cross sections of the halo nucleus ^{11}Be on a heavy (^{208}Pb) target at low collision energies (30-5 MeV/nucleon), demonstrate a visible peak due to the $5/2^+$ resonant state (E_r=1.23 MeV).

3) The differences between the linear and curvilinear (realistic) trajectories of the projectile in the analysis of the breakup reaction ^{11}Be+^{208}Pb->^{10}Be+n+^{208}Pb is about several percent in the energy range 30-20 MeV/nucleon, for 10 MeV/nucleon the discrepancy is 10% and reaches a value of more than 20% at 5 MeV/nucleon, which exceeds the effect of nuclear interaction.

Scientific novelty of the work. The novelty and originality of research lies in the fact that for the first time**:**

1) The low-lying resonant states ($5/2^+$, $3/2^-$ and $3/2^+$) of the ^{11}Be were included in the analysis of the breakup reaction ^{11}Be+^{208}Pb->^{10}Be+n+^{208}Pb by the numerical integration of the time-dependent Schrödinger equation.

2) The breakup cross sections of one-neutron halo nucleus of ^{11}Be on a heavy (^{208}Pb) target are calculated by solving the time-dependent Schrödinger equation with a non-perturbative algorithm in a wide range of beam energies (70-5 MeV/nucleon).

3) The inelastic cross sections for the excitation of the ½- state of ^{11}Be in a collision with ^{208}Pb target at low beam energies are evaluated with inclusion of Coulomb and nuclear interactions between the target and projectile. The influence of the curvilinear trajectory for projectile motion is analyzed with decreasing the collision energies.

The theoretical and practical significance of the research outcomes.

Theoretical significance of the study: exotic nuclei are one of the most intensively studied objects in modern few-nucleon nuclear physics. The theoretical study of halo nuclei within the framework of the non-stationary quantum-mechanical approach is relevant in connection with planning experiments on the study of light nuclei in radioactive beams.

The developed computational scheme in this dissertation work opens new possibilities in investigation of Coulomb, as well as nuclear, breakup of exotic nuclei on heavy, as well as, light targets. This theoretical model can potentially be useful for interpretation and planning of low-energy experiments in studying the halo structure of the nuclei. The obtained results at lower energies are important in connection with the research program in this area at HIE-ISOLD (CERN) and ReA12 (MSU).

The validity and reliability of the research results.

The results of dissertation work were successfully presented at high-level international scientific conferences and formed the basis of publications in high-ranking journals such as European Physical Journal A, Physics of Particles and Nuclei letters, Acta Physica Polonica B Proceedings Supplement, Eurasian Journal of Physics and Functional Materials. The achieved scientific results are in good agreement with the existing works of other foreign authors in this field.

Personal contribution of the author.

In the framework of the dissertation research, the author was directly involved in setting goals, in writing and debugging a computational program, processing and analyzing of obtained data, interpreting the results, preparing articles for publication

as a full member of the scientific group. The contribution of the applicant to the results of the dissertation is essential.

Approbation of dissertation work. The materials of the dissertation work were reported at the following international conferences:

1 "IV International Scientific Forum-Nuclear Science and Technology". RSE ME INP (Almaty, Kazakhstan, 2022).

2 The LXXI International conference "NUCLEUS – 2022. Nuclear physics and elementary particle physics. Nuclear physics technologies", Moscow State University, (Moscow, Russia, 2022).

3 The International Workshop on Elementary Particles and Nuclear Physic, RSE ME INP (Almaty, Kazakhstan, 2022).

4 I International School-Conference “Atom. The science. Technology" RSE ME INP (Almaty, Kazakhstan, 2021).

5 The XXV International Scientific Conference of Young Scientists and Specialists (AYSS-2021), Joint Institute for Nuclear Research (JINR), (Almaty, Kazakhstan, 2021).

6 XXIII International School on Nuclear Physics, Neutron Physics and Applications, Institute for Nuclear Research and Nuclear Energy, (Varna, Bulgaria, 2019).

7 Euroschool on Exotic Beams, KU Leuven, (Aarhus, Denmark, 2019).

8 European Nuclear Physics Conference EuNPC, INFN, (Bologna, Italy, 2018) and others.

The results of the research were reported at the seminar of the N.N. Bogolyubov Laboratory of Theoretical Physics, Joint Institute for Nuclear Research on July 2020.

Publications.

Based on the results of the dissertation work, 6 printed works were published, 4 of that were published in journals included in the database indexed by SCOPUS scientometric databases, 2 - in the journals included in the list recommended by the Committee for Quality Assurance in the Sphere of Education of the Ministry of Education of the Republic of Kazakhstan.

Articles in journals indexed by scientometric databases SCOPUS and Web of Science:

1 Valiolda D., Melezhik V.S., Janseitov D. Investigation of low-lying resonances in breakup of halo nuclei within the time-dependent approach // The European Physical Journal A. – 2022. – Vol. 58. –P 34 1-34 13.

2 Valiolda D., Melezhik V.S., Janseitov D. Study of bound and resonance states of ^{11}Be in breakup reaction // Eurasian Journal of physics and functional materials. –2022. –Vol. 6, № 3. –P. 165-173.

3 Valiolda D., Melezhik V.S., Janseitov D. Study of nuclear contribution to breakup cross section of ^{11}Be halo nuclei within time-dependent approach // Physics of Particles and Nuclei Letters. –2022. –Vol. 19, №5. –P. 477-480.

4 Valiolda D., Melezhik V.S., Janseitov D. Contribution of Low-lying Resonances in the Coulomb Breakup of ^{11}Be Halo Nuclei// Acta Physica Polonica B Proceedings Supplement. –2021. –Vol. 14, № 4. –P. 687-692.

Articles in scientific journals of the Republic of Kazakhstan:

1 Valiolda D.S., Zhaugasheva S.A., Janseitov D.M., Zhussupova N.K. The study of the neutron halo of the ^{11}Be nucleus taking into account the influence of an external field// NEWS of the National Academy of Sciences of the Republic of Kazakhstan. –2018. –Vol. 318, №2. –P. 12-20.

2 Valiolda D.S., Janseitov D.M., Zhaugasheva S.A., Zhussupova N.K. Investigation of the neutron halo of the ^{11}Be nucleus// Recent Contributions to Physics. –2018. –Vol. 64, №1. –P. 81-88.

The structure and volume of the thesis. The dissertation consists of an introduction, three sections, a conclusion, a list of references and 3 appendices. The volume of the dissertation is 90 pages, containing 34 figures and 11 tables, the number of used literature sources is 62.

The first section is devoted to the determination of the exotic nuclei and the description of the ^{11}Be nucleus as a halo structure. The main features of the halo structure, such as nuclear density, large radii, and low binding energies and others are considered. A literature review carried out on theoretical studies of the ^{11}Be halo nucleus, as well as the experiments performed for the breakup reaction of ^{11}Be are discussed in this section.

The second section formulates the nonperturbative time-dependent approach in breakup reactions. The modeling of the physical problem is described here. In this model, the time-dependent Schrödinger equation for a halo-nucleon is integrated with a non-perturbative algorithm on a three dimensional spatial mesh. The use of the discrete-variable representation in 2D angular space and high-order finite differences for the radial part of the wave function allows avoiding the multipole expansion of the time-dependent Coulomb interaction between the projectile and the target. The computational methods used for solving stationary and non-stationary Schrodinger equations are described in section II. Also the results of solving eigenvalue problem: the radial wave functions and energy spectrum, the parameterization of the interaction between the neutron and core are presented.

The third section is devoted to the discussion of obtained results: the calculation of breakup reactions. A considerable contribution of low-lying resonances ($5/2^+$, $3/2^-$ and $3/2^+$) and the nuclear interaction between the target and projectile into breakup of ^{11}Be on the ^{208}Pb target were found at low beam energies (5 - 30 MeV/nucleon). The satisfactory accuracy of the semiclassical approach with linear trajectories of the projectile was also demonstrated for the ^{11}Be breakup cross sections up to 20 - 30 MeV/nucleon. It is shown that this approach is also useful at lower energies, where, however, a more adequate description is provided by the quantum-quasiclassical approach. The convergence of the computational scheme and accuracy of research are demonstrated in the considered energy range (5 - 69 MeV/nucleon), including low-lying resonances in various partial and spin states of ^{11}Be.

The Conclusion formulates the main results obtained in the dissertation and is devoted to concluding remarks.

1 THE HALO STRUCTURE

Due to the rapid development of accelerators and becoming of them more sophisticated and powerful, in the following 40 years, besides the 300 stable nuclear species, 1300 radioisotopes were produced, identified and studied (see nuclear map in figure 1). Most of the knowledge acquired until now in the field of nuclear physics, has been obtained through nuclear reactions [30].

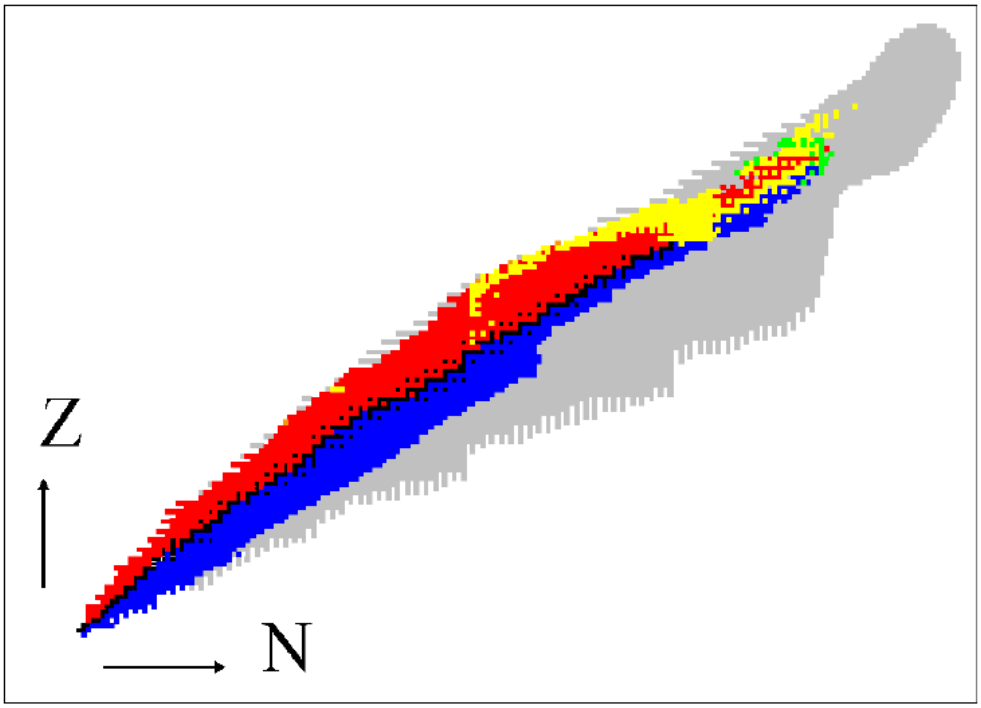

Figure 1 – Nuclide chart. In black the stable isotopes, forming the valley of stability are presented. In red the nuclei decaying by β^- and in blue the nuclei decaying by β^+ processes are illustrated. The line that separates the (coloured) unstable nuclei from the unbound ones (not represented or in grey) is called the dripline [33].

In the late XX century, a crucial step forward was taken. In 1985, at the Lawrence Berkley Laboratory, I. Tanihata and his collaborators performed the first experiment using a beam of a radioactive ion [1]. This experiment consisted on beams of Li and Be isotopes impinging on Be, C and Al targets at energies of 790 MeV/nucleon. In this high energy regime, the interaction cross section (σ_I) is approximately equal to the area calculated from the sum of the nuclear radius of target (R_t) and projectile (R_p),

$$\sigma_{I=}\pi(R_t + R_p)^2. \tag{1.1}$$

"The nucleus ^{11}Li showed a remarkably large radius, suggesting a large deformation or a long tail in the matter distribution" [1]. These were the first words pointing to a new structure, which later was labeled as halo.

The term halo was first coined by P.G Hansen and B. Jonson in 1987 [34]. They ruled out the possibility of a nuclear deformation of ^{11}Li and calculated, considering a two body structure with ^{9}Li and 2n, the decay length of the 2n wave function was $\rho = 8.2$ fm,

$$\rho = \frac{\hbar}{(2\mu B)^{1/2}}, \tag{1.2}$$

with μ is the reduced mass and B is the binding energy. The "long tail in the matter distribution" suspected by Tanihata and collaborators [1] was called a neutron halo and other nuclei with similar properties were found later. Examples of halo nuclei are ^{6}He, ^{11}Li (which are two-neutron halo nuclei), ^{11}Be, ^{17,19}C, ^{22}N (which are one neutron halo nuclei), or ^{8}B (which is a candidate for a proton halo nucleus) and others.

In general, a halo nucleus is a system composed of a compact core, formed by most of its nucleons, and a diffuse halo formed by one or two weakly bound nucleons. In principle both, proton and neutron, can form a halo. However, in the case of protons, the Coulomb barrier tends to confine the nucleons inside the nucleus, thereby preventing the development of a halo structure. Such structures are observed close to the driplines, where there is an excess of either protons or neutrons that still can be bound to the nucleus but with very low binding energy. Since the core attraction is weak, these nucleons can be found at large distances of the center of the nucleus. In particular, when the last nucleon is in an *s*-orbit, it has no centrifugal barrier and, hence, it may be found particularly far. Saying it with quantum mechanics correctness, the wave function of these particles has a long tail, i.e. their density is not negligible up to abnormally large radii, compared to other nuclei with the same mass [33].

An often suitable representation of the nuclear density is given by the Fermi-Dirac distribution:

$$\rho = \frac{\rho_0}{1+exp\frac{r-R}{a}}, \tag{1.3}$$

where r is the radius from the center of the nucleus, $R = r_v \times A^{1/3}$ being $r_v -$ a constant between 1.2 and 1.44 fm, A is the mass number of the nucleus and a the diffuseness, that models the sharpness of the density fall, which can also be understood as a measure of the thickness of the surface. Large radius and diffuseness parameters can be used for describing the densities of halo nuclei [33].

Up to now, there is no generally accepted definition of halo nuclei. However, following the definition of Riisager, Fedorov, and Jensen [35]: "Quantum halos are defined as systems with dominating few-body structure and radii large compared to the sizes of the classically allowed regions". This definition emphasises the three main halo characteristics:

1) Halo nuclei exhibit a strong cluster structure. That is to say, they are well described as a core plus one or two neutrons;

2) Halo nuclei have a large matter radius in comparison with the range of the nuclear interaction. This is explained in the few-body model by the fact that the halo neutrons have a high probability of being at a large distance from the core. In other words, their wave function is assumed to tunnel far outside the classically allowed region. This region corresponds to the positions the halo neutrons would occupy if their relative motions to the core were treated classically. For example, in a two-body structure (i.e. for one- neutron halos) these positions are those at which the interaction potential is lower than the binding energy of the system. This second condition implies the third one;

3) Halo nuclei are weakly bound, i.e. the separation energy of the halo neutrons is very low. This two- or three-body structure can therefore be easily broken.

This exotic feature in nuclear physics is of great interest not only because it constitutes a stringent test for the available nuclear models, but also because it opens up new research fields in nuclear science. Halo nuclei are therefore the focus of numerous theoretical and experimental studies [33].

1.1 The ^{11}Be halo nucleus

Among the halo nuclei, the ^{11}Be nucleus is of particular importance, since the relative simplicity of its structure allows accurate theoretical studies. In fact, bound states of the ^{11}Be nucleus can be described quite well as a ^{10}Be core and a weakly bound neutron, as illustrated schematically in figure 2.

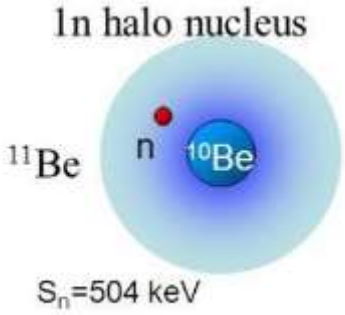

Figure 2 − A schematic representation of 1 n halo nucleus of ^{11}Be.

The berillium is the fourth element in the periodic table, what in turn means that it has 4 protons. The particular case of ^{11}Be has, as its name indicates, 11 nucleons, the 4 protons plus 7 neutrons. The only stable isotope of berillium is ^{9}Be which has an structure that may be thought of as two alpha particles bound together by a neutron. That neutron plays a role comparable to the one that the electron does in a covalent bond. Adding another neutron ^{10}Be is obtained, which has the same structure, but with two neutrons making this kind of covalent binding. The ^{10}Be nucleus ($J^{\pi} = 0^{+}$) decays through β^{-} to ^{10}B ($j^{\pi} = 3^{+}$) with a half-life of $t_{1/2} = 1.6 *$

10^6 years, so it may be said to be such an stable one. The addition of an extra neutron brings a completely different structure to the stage. The half-life of ^{11}Be ($J^\pi = 1/2^+$), decaying through β^- to ^{11}B ($j^\pi = 3/2^-$), is $t_{1/2} = 13{,}76$ s (10^{12} times lower) [36], so the experimental requirements to study this nucleus will be more challenging.

Using the standard independent-particle level ordering (see figure 3a), as the ^{10}Be (Z=4, N=6, $j^\pi = 0^+$) does not present a closed shell structure, an additional neutron should just occupy the close-in-energy $p_{1/2}$ orbit, as it happens in ^{15}O. Despite that, as it is observed in figure 3b, this is not what happens. Within this simple single-particle picture, the ground state of ^{11}Be is formed by adding a neutron to the *s* orbit *sd*-shell (J^π= 1/2$^+$) due to an inversion between the $s_{1/2}$ and the $1p_{1/2}$ levels [33].

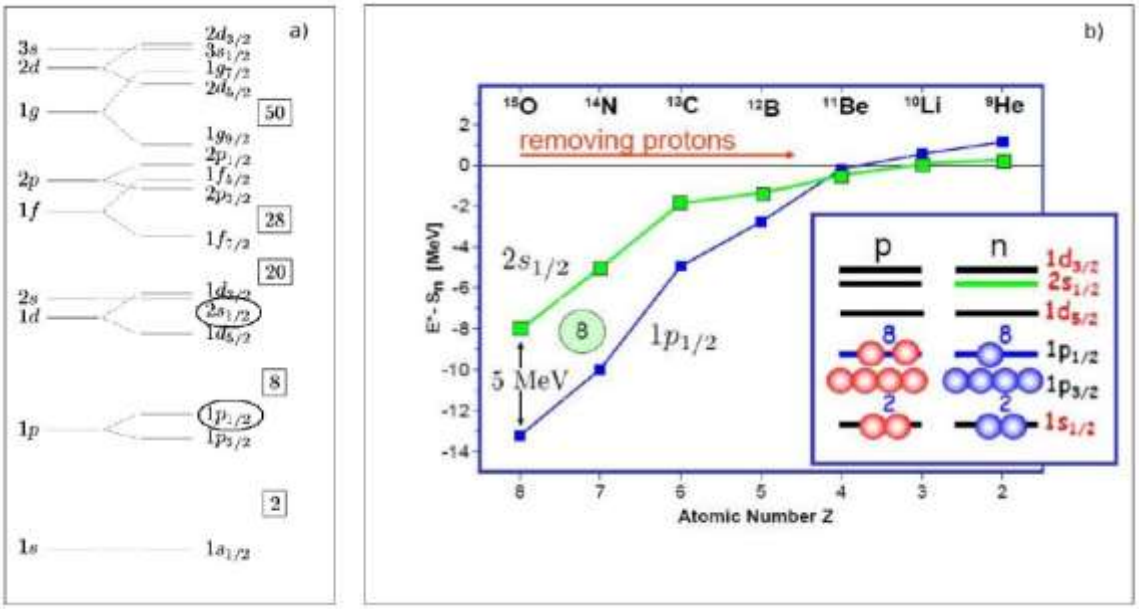

Figure 3 − a) Shell distribution and gaps between them following the Standard Nuclear Shell Model.
b) Energy difference between the $p_{1/2}$ and the $s_{1/2}$ shells for N = 7 as the number of protons is reduced. Plot from P.G. Hansen and J.A. Tostevin [37].

The comparison of the energy needed for exciting the ^{10}Be (3368 keV) compared to the energy of the first excited states of ^{11}Be (320 keV) and ^{12}Be (2101 keV) reinforces the statement that the shell is closed at N = 6. The closed shell of the ^{10}Be nucleus, the *s*-orbit of the last neutron and the low binding energy, all together sum up into becoming the ^{11}Be a weakly bound one-neutron halo nucleus with a ^{10}Be core.

Schematically, the wave function of the ground state of ^{11}Be can be written as

$$|^{11}\mathrm{Be}(g.s.)>_{\frac{1}{2}+} = |^{10}\mathrm{Be}\ (0^+) \otimes \nu(s1/2)>_{1/2^+}. \qquad (1.4)$$

The neutron separation energy is S_n=501.6 keV. Despite being low, it is high enough for the inverted *p*-orbit to be below the threshold, so there is one bound

excited state ($J^{\pi} = ½^{-}$), which lies at E_x= 320.04(10) keV above the ground state (S_n = 181.6 keV*),*

$$|^{11}\text{Be}*>_{1/2-} = |^{10}\text{Be}\ (0+)\otimes\nu(p1/2)>_{1/2-}. \quad (1.5)$$

It is possible to populate this state through an E1 transition from the ground state, and it is remarkable that with a strength of B(E1) = 0.116 ± 012 e^2fm^2 [38], it is the strongest B(E1) measured between bound states.

In [39], the extra configurations resulting from the coupling of excited states of the core with the valence particle, have been interpreted within the particle-rotor model, assuming a permanent deformation of the ^{10}Be nucleus (β= 0.67). Other works [40,41], use a particle-vibrator model, treating the excitation as a result of surface excitations of the ^{10}Be core. Independently of the model, in these extra configurations the neutron is in a d-orbit, so they are not halo configurations (halos are only observed in s and p orbits). In the ground state, the halo structure is only due to the first and main term $|^{10}Be(0^+)\otimes vs(1/2)>_{\frac{1}{2}+}$, which will determine in a large extent the dynamics of the reaction.

1.2 The role of nuclear reactions

The energies used for studying nuclear reactions range from the few keV to hundreds of GeV. The different energy regimes are used for exploring different features of the nuclei and for exploring different areas of the nuclide chart. The higher the energy, the more reaction channels will be opened and the deeper the structure can be digged in. On the other hand, reactions at low energies are useful for studying low-lying excited states, the shell structure (by means of transfer reactions, for instance) and dynamic phenomena, like the Coulomb nuclear interplay. This is the case of reactions at energies around the Coulomb barrier.

The energy of the reaction is not the only parameter to take into account in nuclear reactions. Different experiments may explore different features of the nuclei focusing on different reaction channels. In the case of loosely bound nuclei, the assortment of experiments that can provide relevant data is extensive. Some examples of experiments that studied ^{11}Be have been selected from literature data [17, 36, 38, 42, 43, 44] to illustrate the information on the structure and the reaction dynamics that can be extracted from experiments of different nature.

– ^{11}Be(p,p)^{11}Be, ^{11}Be(p,p')^{11}Be: The elastic and inelastic scattering with protons, usually referred to as (p,p) and (p,p') reactions, respectively, has been studied in inverse kinematics at E(^{11}Be) = 63 MeV/A, ^{1}H(^{11}Be,^{11}Be)^{1}H, ^{1}H(^{11}Be,^{11}Be′)^{1}H [42]. With this experiment the bound states in ^{11}Be could not be resolved, but the resonance at E_x =1.78 MeV (J^{π}= 5/2$^+$) was observed. Other resonances at higher energies were not resolved either.

– ^{9}Be(t,p)^{11}Be: The protons detected after the two-neutron transfer to a ^{9}Be target giving information on the states of the ^{11}Be populated. Measuring the gamma ray emitted after the population of the bound excited state, the energy and the lifetime

were determined to be E_x = 320.04± 0.10 keV, τ_m= 116±15fs, respectively. From this lifetime measurement the extracted strength is B(E1) = 0.116± 0.012 e^2fm^2 [38].

– ^{208}Pb(^{11}Be, ^{10}Be+n)^{208}Pb: Exclusive breakup measurements, in which the outgoing neutron and ^{10}Be are measured in coincidence, have been performed at RIKEN at energies ~70 MeV/u [16, 17] and at GSI at energies ~520 MeV/u [44]. They have provided information on the direct Coulomb breakup probability, which in loosely bound nuclei on heavy targets is dominated by an E1 transition. Although the extracted B(E1) distributions differ quantitatively among the different experiments, they all predict a large B(E1) strength near the breakup threshold, as expected for a halo nucleus.

– ^{12}C(^{11}Be, ^{10}Be+n)^{12}C: The breakup measurements on light targets (ej. ^{12}C), in which nuclear effects are dominant, allowed the identification of low-lying resonances and their spin-parity assignment. In [17] the resonance states at E_x = 1.78 MeV (J^π= 5/2$^+$) and E_x = 3.41 MeV (J^π= 3/2$^+$) are observed.

As already indicated above, experiments aimed at studying the breakup of ^{11}Be halo nucleus at a heavy target (^{208}Pb) were performed at intermediate (69 and 72 MeV/nucleon) [16, 17] and at high beam (520 MeV/nucleon) [39] energies. Also many theoretical calculations and processing of these experiments [11, 12, 13, 14, 45, 46] have been carried out. However, in that works only the bound states of ^{11}Be were included in calculations. Note that at Riken (Japan) Fukuda et.al. observed experimentally the low-lying resonances in the nuclear induced breakup of ^{11}Be on the light target (^{12}C) at 70 MeV/nucleon [17]. In particular, we assume that in the experimental data for the reaction ^{11}Be + ^{208}Pb -> ^{10}Be+n+^{208}Pb [16, 17], there are visible peaks near the energies 1.23, 2.78 and 3.3 MeV [27, 28], which correspond to position of resonances: 5/2$^+$, 3/2$^-$ and 3/2$^+$ [27, 3]. We suppose that taking into consideration of the resonant states 5/2$^+$, 3/2$^-$ and 3/2$^+$ improve the theoretical model describing the Coulomb breakup [3].

In the framework of this PhD thesis, we also extend the non-perturbative time-dependent approach [12, 13, 23], for calculations of breakup cross section at low beam energies down to 5 MeV/nucleon, where no experimental data exists and investigate the contribution of the ^{11}Be resonance states in this region [3, 31]. In addition, by comparing our calculations with few existing theoretical results [11, 18, 19], we show the benefits of our approach.

2 NONPERTURBATIVE TIME-DEPENDENT APPROACH IN BREAKUP REACTIONS

2.1 Model for describing neutron dynamics during collision

The halo neutron is treated as a structureless particle weakly bound by the potential $V(\boldsymbol{r})$ to the ^{10}Be core nucleus, where $\boldsymbol{r}$ is the relative variable describing the distance between the neutron and the core. The dynamics of the halo neutron relative to the ^{10}Be core in the breakup reaction ^{11}Be+^{208}Pb → ^{10}Be+n+^{208}Pb is described by the time-dependent Schrodinger equation

$$i\hbar\frac{\partial}{\partial t}\Psi(\boldsymbol{r},t) = H(\boldsymbol{r},t)\Psi(\boldsymbol{r},t) = [H_0(\boldsymbol{r}) + V_C(\boldsymbol{r},t)]\Psi(\boldsymbol{r},t), \quad (2.1)$$

in the projectile rest frame, where $\Psi(\boldsymbol{r},t)$ is the wave packet of the neutron relative the ^{10}Be core. In this expression

$$H_0(\boldsymbol{r}) = -\frac{\hbar^2}{2\mu}\Delta_r + V(\boldsymbol{r}), \quad (2.2)$$

$H_0(\boldsymbol{r})$ is the Hamiltonian describing relative halo nucleon-core motion with reduced mass $\mu = m_n m_c/M$, where m_n, m_c and $M = m_n + m_c$ are the neutron, ^{10}Be-core, and ^{11}Be masses, respectively. The potential $V(\boldsymbol{r})$ represents the sum of the l-dependent central potential $V_l(r)$ and a spin-orbit interaction $V_l^s(r)(\boldsymbol{ls})$**.** The interaction of the target nucleus with the projectile corresponds to the time-dependent Coulomb potential $V_C(\boldsymbol{r},t)$, which is defined as

$$V_C(\boldsymbol{r},t) = \frac{Z_c Z_T e^2}{|\frac{m_n \boldsymbol{r}}{M}+\boldsymbol{R}(t)|} - \frac{Z_c Z_T e^2}{R(t)}, \quad (2.3)$$

where Z_c and Z_T are charge numbers of the core and target, respectively, and $\boldsymbol{R}(t)$ is the relative coordinate between the projectile and the target, which represents the straight-line trajectory $\boldsymbol{R}(t) = \boldsymbol{b} + \boldsymbol{v}_0 t$, where $\boldsymbol{b}$ is the impact parameter orthogonal to the initial velocity of the projectile $\boldsymbol{v}_0$. This definition corresponds to previous models, accepted in the works [12, 14, 15].

The time-dependent Coulomb potential $V_C(\boldsymbol{r},t)$ is written in the center of mass system associated with ^{11}Be. When ^{11}Be is far from the target, the Coulomb potential is zero. It acquires a maximum value, as seen in formula (2.3), if the target and the projectile approach at a minimum distance. After the collision, this time-dependent interaction $V_C(\boldsymbol{r},t)$ vanishes. Our task is to integrate the equation from the initial moment of time, where the target and the projectile are at a large distance, and then they approach each other and again scatter over large distances. We write down the system of two bodies ^{10}Be + n, between them there is a nuclear interaction $V_n(\boldsymbol{r},t)$, which is described at section 3.4. When a system of ^{10}Be+n approach the target (T

(^{208}Pb) as displayed at figure 4), the interaction between the target and the projectile must also be taken into account. This interaction is described by the Coulomb potential (Eq.(2.3)).

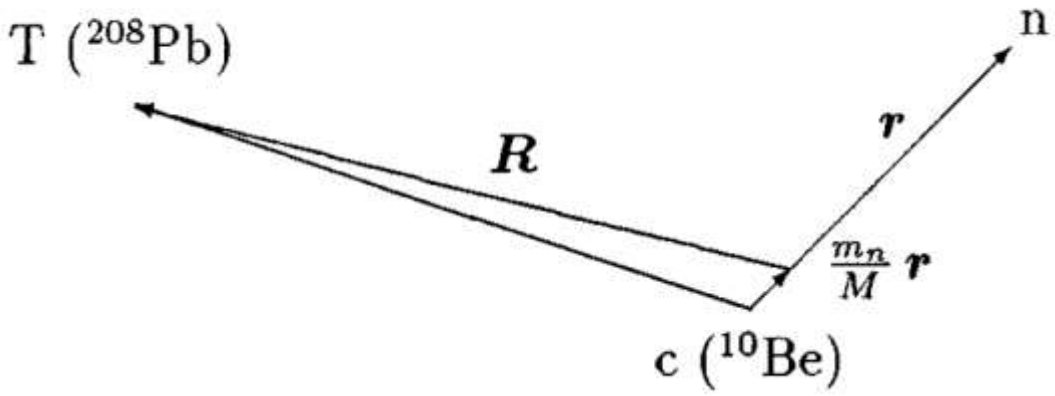

Figure 4 − Coordinates appearing in the definitions of Coulomb potential $V_C(\boldsymbol{r}, t)$ [Eq. (3)] [12, Fig 1.].

For the considered collisions, the approximation of linear trajectories is works well in this case. In [12], it was studied that taking into account the curvature of this trajectory gave a negligible correction at higher beam energies (~70 MeV/nucleon). How good is the linear trajectory approach for projectile motion at lower beam energies is studied at Section 3.5.

2.2 The computational scheme of solving TDSE

In order to correctly describe the breakup process, it is necessary to formulate the problem in a non-perturbative way. In this work, the time-dependent Schrödinger equation is integrated with a non-perturbative algorithm on a three-dimensional spatial grid, where it is assumed that the projectile moves along a classical trajectory and its interaction develops due to the difference between the Coulomb and nuclear interactions around the target. The method uses wave function values at grid points in angular space in the spirit of Discrete Variable Representation (DVR) methods (or Lagrange grid methods) [12, 24]. The radial functions are approximated using the high-order finite difference method (with a variable step) on a quasi-uniform grid [12, 24, 47]. For the initial approximation of the wave function, an auxiliary problem is solved - a stationary SE with boundary conditions. The stationary problem is solved in the standard way, the angular variables are separated because there is no interaction with the target, and the radial SE is solved by the finite difference method [47 p.180-184]. The radial equation is solved on the same grid as the TDSE. But when a time-dependent equation is integrated, the angular part of TDSE is not separated from the radial variable due to the interaction [3] (the numerical methods used in the thesis are described at subsections 2.2 - 2.4).

2.2.1 **Angular-subspace discretization**

We seek a solution $\Psi(\boldsymbol{r},t)$ of TDSE (2.1) in spherical coordinates $(r,\Omega) \equiv (\mathrm{r},\theta,\phi)$ as an expansion [12],

$$\Psi(\boldsymbol{r},t) = \frac{1}{r}\sum_s \sum_{\nu j}^{N} \varphi_\nu(\Omega)(\varphi^{-1})_{\nu j}\psi_j^s(r,t), \tag{2.4}$$

over the two-dimensional basis

$$\varphi_\nu(\Omega) = \sum_{\nu'} C_{lm}^{l'm'} P_{l'}^{m'}(\theta)e^{im'\phi}. \tag{2.5}$$

In this basis, $C_{lm}^{l'm'} = \delta_{ll'}\delta_{mm'}$, in general and thus $\varphi_\nu(\Omega)$ coincides with an usual spherical harmonic with a few possible exceptions for high ν as explained below after Eq. (2.7). The symbol ν represents the combination of the orbital momentum and its projection (*l, m*), and the sum over ν is equivalent to the double sum

$$\sum_{\nu=1}^{N} = \sum_{l=0}^{\sqrt{N}-1} \sum_{m=-l}^{l}. \tag{2.6}$$

The basis (2.5) is associated with a mesh. For the θ variable, the $N_\theta = \sqrt{N}$ mesh points θ_{j_θ} are defined as zeros of the Legendre polynomial $P_{\sqrt{N}}(\cos\theta_{j_\theta})$. For the ϕ variable, the $N_\varphi = \sqrt{N}$ mesh points are chosen as $\phi_{j_\phi} = \pi(2j_\phi - 1)/\sqrt{N}$. The total number N ($where\ N = N_\theta \times N_\varphi$) of grid points $\Omega_j = \left(\theta_{j_\theta}, \phi_{j_\phi}\right)$ is equal to the number of basis functions (2.5) in expansion (2.4) [24, 25]. This mesh is associated with the N weights λ_j that are the products of the standard Gauss-Legendre weights over θ by $2\pi/\sqrt{N}$. The $(\varphi^{-1})_{\nu j}$ are the elements of the $N\times N$ matrix φ^{-1} inverse to the matrix with the elements $\varphi_{j\nu} = \varphi_\nu(\Omega_j)$ defined at the grid points Ω_j. The polynomials $\varphi_\nu(\Omega)$ are constructed from the Legendre polynomials $P_l^m(\theta)$ and $e^{im\varphi}$ so that they are orthogonal on the grid Ω_j

$$\int \varphi_\nu^*(\Omega)\varphi_{\nu'}(\Omega)d\Omega = \sum_j \lambda_j \varphi_{\nu j}^*\varphi_{\nu' j} = \delta_{\nu\nu'}, \tag{2.7}$$

for all ν and $\nu' \le N$. For most ν and ν', property (2.7) is automatically satisfied because the basis functions $\varphi_\nu(\Omega)$ are orthogonal and the Gauss quadrature is exact. For these ν the coefficients $C_{lm}^{l'm'} = \delta_{ll}\delta_{mm}$ in Eq.(2.5). However, in a few cases with the highest *l* and *m* values, some polynomials $\varphi_{lm}(\Omega)$ have to be specially made orthogonal in the sense of the Gauss quadrature. With this choice, the matrix ${\lambda^{1/2}}_j\varphi_{\nu j}$ is orthogonal.

The radial components $\psi_j^s(r,t)$ in expansion (2.4) correspond to $r\psi(r,\Omega_j,t)|s>$ where $|s>=|\pm\frac{1}{2}>$ is a spin state of a nucleus and $r\psi(r,\Omega_j,t)$ are the values of the spatial part of the nuclear wave function at the angular grid points Ω_j. Let us introduce the 2*N*-component vector $\mathbf{\Psi}(r,t)=\{\lambda_j^{\frac{1}{2}}\psi_j^s(r,t)\}$. With respect to the unknown coefficients in expansion (2.4), the problem is reduced to a system of Schrodinger-type equations

$$i\hbar\frac{\partial}{\partial t}\mathbf{\Psi}(r,t)=\left[\widehat{H}_0(r)+\hat{h}(r,t)\right]\mathbf{\Psi}(r,t). \tag{2.8}$$

In this system, $\widehat{H}_0(r)$ and $\hat{h}(r,t)$ are 2*N*×2*N* matrix operators representing H_0 and V_c [Eq. (2.2) and (2.3)] on the angular grid. The elements of matrix $\widehat{H}_0(r)$ are defined by

$$H_{0kj}^{ss'}(r)=\left\{-\frac{\hbar^2}{2\mu}\frac{\partial^2}{\partial r^2}\delta_{kj}+(\lambda_k\lambda_j)^{-\frac{1}{2}}\sum_{\nu=\{l,m\}}^{N}(\varphi^{-1})_{k\nu}\times\right.$$
$$\left.\times\left[V_l(r)+V_l^s(r)+\frac{\hbar^2 l(l+1)}{2\mu r^2}\right](\varphi^{-1})_{\nu j}\right\}\delta_{ss'}, \tag{2.9}$$

where $V_l(r)$ is the *l*-dependent central potential between the neutron and the core and $V_l^s(r)$ is the spin dependent spin-orbit neutron-core interaction in the spin state $|s>$ [12, 13,14]. We neglect here the spin-mixing term in the interaction between the core and the nucleon during the collision with the target as in [12]. The time-dependent Coulomb operator $\hat{h}(r,t)$

$$h_{kj}^{ss'}(r,t)=[V_C(r,\Omega_k,t)\delta_{ss'}]\delta_{kj}, \tag{2.10}$$

defined in Eq. (2.3) is diagonal in this representation and does not require the multipole expansion unlike other approaches based on the numerical integration of the Schrodinger equation for the halo neutron [14, 15].

The DVR (2.9), (2.10) of the TDSE (2.1) permits different kinds of modeling *l*- and *s*-dependent interactions $V_l(r)$ and $V_l^s(r)$ between the core and the halo neutron. It allows one to include resonance interactions in various partial *l* and spin *s* states in the ^{11}Be Hamiltonian (2.9).

An attractive feature of the DVR is that the only nondiagonal part of the Hamiltonian is the angular part of the kinetic energy operator (2.9), which can be diagonalized fast by using of a split-operator method (it is described in detail at next subsection (2.2.2)). The splitting up method gives a fast convergence with respect to the numbers of grid points N (the number of basis functions in expansion (2.4)). The convergence of the method with respect to angular grid points N is discussed below at section (3.1).

2.2.2 Splitting-up method

As it is discussed above, the problem is reduced to the Schrodinger-type time-dependent radial equations coupled only through the nondiagonal angular part of the kinetic energy operator. This equation is propogated using a split-operator method, which permits fast diagonalization of the remaining nondiagonal part. The only nondiagonal part of the Hamiltonian in Eq. (8) is in the block matrices $\widehat{H_0^{ss}}(r,t)$ (Eq.(9)). For each spin state, they can be diagonalized by the simple unitary transform $S_{\nu k} = \lambda_k^{1/2}\varphi_{\nu k}$ [12]. The splitting-up method has been applied for the propagation in time $t_n \to t_{n+1} = t_n + \Delta t$ as

$$\boldsymbol{\Psi}(r, t_n + \Delta t) = \left(1 + \frac{1}{2} i\Delta t\hat{h}\right)^{-1} \left(1 - \frac{1}{2} i\Delta t\hat{h}\right) \times \left(1 + \tfrac{1}{2} i\Delta t\widehat{H_0}\right)^{-1} \left(1 - \tfrac{1}{2} i\Delta t\widehat{H_0}\right) \boldsymbol{\Psi}(r, t_n). \quad (2.11)$$

Thus, the problem is split up into two steps involving the intermediate time $t_n + \frac{1}{2} i\Delta t$ [12].

At the initial step, the vector function $\boldsymbol{\Psi}\left(r, t_n + \frac{1}{2}\Delta t\right)$ is evaluated from the known vector function $\boldsymbol{\Psi}(r, t_n)$ with the system of N differential equations

$$\left[1 + \tfrac{1}{2} i\Delta t\hat{S}\, \widehat{H_0}(r)\hat{S}^{+}\right] \bar{\boldsymbol{\Psi}}\left(r, t_n + \tfrac{1}{2}\Delta t\right) = \left[1 - \tfrac{1}{2} i\Delta t\hat{S}\, \widehat{H_0}(r)\hat{S}^{+}\right] \bar{\boldsymbol{\Psi}}(r, t_n), \quad (2.12)$$

where

$$\bar{\boldsymbol{\Psi}}(r, t_n) = \hat{S}\, \boldsymbol{\Psi}(r, t_n). \quad (2.13)$$

The system of equations (2.12) is uncoupled since

$$(\hat{S}\, \widehat{H_0}\hat{S}^{+}) = \left[-\frac{\hbar^2}{2\mu}\frac{\partial^2}{\partial r^2} + V_l(r) + V_l^S(r) + \frac{\hbar^2 l(l+1)}{2\mu r^2}\right] \delta_{ss'}\delta_{\nu\nu'}\,, \quad \nu=\{l,m\}. \quad (2.14)$$

It is solved with boundary conditions

$$\bar{\boldsymbol{\Psi}}\left(0, t_n + \tfrac{1}{2}\Delta t\right) = \bar{\boldsymbol{\Psi}}\left(r_m,\ t_n + \tfrac{1}{2}\Delta t\right) = 0, \qquad r_m \to \infty. \quad (2.15)$$

Then the wave function at time $t_n + \frac{1}{2}\Delta t$ is obtained as

$$\bar{\boldsymbol{\Psi}}\left(r, t_n + \tfrac{1}{2}\Delta t\right) = \hat{S}^{+}\, \bar{\boldsymbol{\Psi}}\left(r,\ t_n + \tfrac{1}{2}\Delta t\right). \quad (2.16)$$

The most time consuming part in performing the initial step $t_n \to t_n + \Delta t$ (Eqs. (2.13) - (2.16)), i.e. solving the boundary-value problem (2.12) and (2.15), demands

only N computational operations. Moreover, the $\hat{S}$ transformation is time independent and r independent and, as a consequence, the matrix $S_{\nu k} = \lambda_k^{1/2}\varphi_{\nu k}$ has to be evaluated only once.

At the second step, the system of N uncoupled algebraic equations

$$\left[1 + \tfrac{1}{2} i\Delta t\, \hat{h}(r, t_n)\right] \boldsymbol{\Psi}(r, t_n + \Delta t) = \left[1 - \tfrac{1}{2} i\Delta t\, \hat{h}(r, t_n)\right] \boldsymbol{\Psi}\left(r, t_n + \tfrac{1}{2}\Delta t\right). \quad (2.17)$$

with the matrix $\hat{h}(r, t_n)$ defined in Eq.(2.10) which is nondiagonal only in the spin space, is then solved. Applying the split-operator method (2.13) – (2.17) to problem (2.8) demands that the two-dimensional basis $\varphi_\nu(\Omega)$, used in Eq.(2.4), is orthogonal on the grid Ω_k [12].

2.3 The numerical method for solving the stationary Schrodinger equation for bound states of ^{11}Be

This section is devoted to discussion of the eigenstates of the two-body Hamiltonian of ^{11}Be (described in section 2.1 by formula (2.2)). In other words, we detail the wave functions $\phi(r)$ solution of

$$H_0\phi(r) = E\phi(r). \quad (2.18)$$

This eigenvalue problem leads to two kinds of solution: the negative-energy states (with E < 0) and the positive-energy states (with E > 0). The former correspond to the bound states of the system with binding energy E. They describe either the physical bound states of the system or the Pauli forbidden states. The positive-energy states describe the unbound system. They correspond to the scattering of the fragment and the core with a relative kinetic energy E. It is known that the two-body Hamiltonian $H_0(r)$ (Eq.(2.2)) is invariant under rotation. This means that its eigenstates can be expanded into partial waves. Their wave functions can be expressed as the product of radial part and a spin-angular part:

$$\phi_{ljm}(r, \Omega) = r^{-1} R_{lj}(r) \langle \Omega | ljm \rangle \quad (2.19)$$

where l, j and m are quantum numbers associated to the orbital momentum and the total angular momentum (see below), and $\Omega = (\theta, \varphi)$ is the solid angle defining the direction of r. The spin-angular part of the wave function appearing in this expression corresponds to the eigenvector $|ljm\rangle$ of operators L^2, J^2 and J_z^2 (with $J=L+I$ denoting the total angular momentum)

$$L^2|ljm\rangle = \hbar^2 l(l+1)|ljm\rangle, \quad (2.20)$$

$$J^2|ljm\rangle = \hbar^2 j(j+1)|ljm\rangle, \quad (2.21)$$

and

$$J_z|ljm\rangle| = \hbar^2 m|ljm\rangle. \tag{2.22}$$

It is also an eigenstate of the operator I^2 related to the projectile spin:

$$I^2|ljm\rangle = \hbar^2 I(I+1)|ljm\rangle. \tag{2.23}$$

Since I is assumed to be fixed, this quantum number is understood in our notations. This part of the wave function can be expressed as a linear combination of spin eigenvectors $|Im_I\rangle$ and orbital-momentum eigenfunctions $Y_l^{m_l}$ [48, Appendix A-VI]:

$$\langle\Omega|ljm\rangle = \sum_{m_l m_I} < lIm_l m_I|jm > Y_l^{m_l}|Im_I >, \tag{2.24}$$

where $<lIm_l m_I|jm>$ are the Clebsch-Gordan coefficients.

From the above, we see that the radial part R_{lj} of the wave function (2.3.2) is the solution of the following eigenvalue equation

$$-\frac{\hbar^2}{2\mu}\frac{d^2}{dr^2}R_{lj}(r) + \left\{\frac{\hbar^2}{2\mu}\frac{l(l+1)}{r^2} + V_0(r) + \frac{1}{2}[j(j+1) - l(l+1) - I(I+1)\,V_{LI}(r)]\right\} R_{lj}(r) = E_n R_{lj}(r). \tag{2.25}$$

Since the bound spectrum is discreet, the solutions of (2.25) can be distinguished by an integer. We choose this integer equal to the number n of nodes exhibited by the radial wave function. Subsequently, these states and their energies will be referred to by ϕ_{nljm} and E_{nlj} respectively. According to (2.20), their wave functions read

$$\phi_{nljm}(r) = r^{-1}R_{nlj}(r)\langle\Omega|ljm\rangle \tag{2.26}$$

These states are normalised to unity:

$$||\,\phi_{nljm}(r)\,||^2 = \int_0^\infty [R_{nlj}(r)]^2 dr = 1. \tag{2.27}$$

In the following, the physical ground state will be denoted by ϕ_{nljm}, and its energy by E_n. The solutions corresponding to the continuum are distinguished by the wave number $k = \sqrt{2\mu E/\hbar^2}$. In the following, these scattering states will be refeired to by ϕ_{kljm}. Their wave functions read

$$\phi_{kljm}(r) = r^{-1}R_{klj}(r)\langle\Omega|ljm\rangle. \tag{2.28}$$

More details of calculating and normalization of the wave functions of the continuum is discussed below at section 2.5.

With the details given in the preceding sections, the time-dependent Schrodinger equation is solved with the initial condition that at time $t_{in} \to -\infty$ the system is in its physical ground state,

$$\Psi^{m_0}(r, t_{in}) = \phi_{n_0 l_0 j_0 m_0}(r). \tag{2.29}$$

Since m_0 is not known, the eigenvalue problem (2.3.1) has to be solved for all the values it can take. In general, in the initial state, there should be summation for all m_0 according to the statistical distribution of the neutron relative to the core with static populations (averaging over m_0).

Further, using numerical methods, including the reverse iteration method and the sweep method, this problem was solved and describe the computational scheme in next subsections.

2.3.1 Reverse iteration method in subspace

The radial part of the eigenvalue problem (2.18) was solved by the reverse iteration method. The solution scheme looks like this:

$$\begin{cases} \hat{A}\,\vec{R} = E\vec{R} \\ (\widehat{A} - \hat{I}E^{(0)})\,\vec{R}^{(i)} = \vec{R}^{(i-1)} \\ E = E_0 + \frac{1}{\hat{R}^{(i)}, \hat{R}^{(i-1)}} \end{cases}, \; i = 1,2, \ldots \, i_{max}\,, \tag{2.31}$$

where E_0 – is the initial approximation of the energy level, $\hat{R}^{(0)}$ – is the initial vector, and the computed vector $\hat{R}^{(i)}$ is normalized at each iteration $\hat{R}(r) = \hat{\varphi}^{(i_{max})}$, to satisfy the normalization condition (2.27). If we describe this method in more detail for our case, then equation (2.31) for first iteration i=1 will be written as:

$$(\widehat{A} - \hat{I}E^{(0)})\,\vec{R}^{(1)} = \vec{R}^{(0)}\,. \tag{2.31'}$$

The solution of the equation:

$$\frac{1}{\sqrt{C}}\,\vec{R}^{(1)} = (\widehat{A} - \hat{I}E^{(0)})^{-1}\vec{R}^{(1)}, \tag{2.32}$$

where C- normalization coefficient of the radial wave function:

$$\int_0^{r_m} \bar{R}^{(1)^2} dr = C\,, \tag{2.32'}$$

i.e. normalized wave function $R^{(1)} = \frac{1}{\sqrt{C}}\,\vec{R}^{(1)}$ for the first iteration. For iterations i:

$$\widehat{(A} - \hat{I}\,E^{(i-1)})\bar{R}^{(i)} = \bar{R}^{(i-1)}, \tag{2.33}$$

$$\text{C}= \int_0^{r_m} \bar{R}^{(i)^2} dr,\ R^{(i)} = \frac{1}{\sqrt{C}}\,\bar{R}^{(i)}. \tag{2.34}$$

Then the next iteration:

$$\widehat{(A} - \hat{I}E^{(i-1)})\,\bar{R}^{(i+1)} = R^i. \tag{2.35}$$

Let us denote as

$$\text{D}=\int R^i\ \bar{R}^{(i+1)} dr. \tag{2.36}$$

So the energy comes from:

$$E^{(i)} = E^{(i-1)} + \frac{1}{D}\,. \tag{2.37}$$

Thus, the backward iteration method makes it easy to find an unknown eigenvector, and corresponding eigen energy. The advantage of this method is that the final answer will not depend on the choice of initial approximation, since the answer quickly converges. But this must be checked by the residual [49]. From equation (2.33) we can find that the calculation accuracy is equal to

$$\Delta_i = \left|E^{(i)} - E^{(i-1)}\right| < 10^{-6}, \tag{2.38}$$

the iteration stopped when it reached a discrepancy $\delta_i < 10^{-6}$:

$$\widehat{(A} - \hat{I}E^{(i)})\,R^{(i)} = \delta_i. \tag{2.39}$$

When the required discrepancy δ_i is reached, the computed iterations are stopped. That is, the accuracy is controlled. The computation practice shows that the scheme gives a convergent result and does not depend on the choice of the initial approximation $E^{(0)}$ [50].

This subchapter provides a scheme for calculating energy using the reverse iteration method. If we set the explicit form of the matrix $\hat{A}$ for Schrodinger equation

$$\left[-\frac{\hbar^2}{2\mu}\Delta + \frac{\hbar^2 l(l+1)}{2\mu\, r^2} + V_{cf}(r)\right] R_l(r) = E\ R_l(r), \tag{2.40}$$

we see that the matrix $\hat{A}$ will be in the form of a three-diagonal matrix. Thus, to solve the system and find the inverse matrix $\hat{A}^{-1}$ one could use the sweep method or LU decomposition [51] .

2.3.2 The sweep method

We seek the solution of SE (2.40) in the form (2.32) with the initial conditions:

$$\begin{Bmatrix} R_{Nl}(r) \to const, & r \to 0 \\ R_{Nl}(r) \to 0, & r \to \infty \end{Bmatrix}, \tag{2.41}$$

The equation contains a second-order differential, which we can simplify for the computational scheme using the finite-difference method by the formula

$$\frac{\partial^2 f}{\partial x^2} = \frac{f(x+\Delta x)-2f(x)+f(x-\Delta x)}{\Delta^2}.$$
$$\frac{d^2}{dr^2}\left(R_j^{(1)}\right) = \frac{R_{j+1}^{(1)}-2R_j^{(1)}+R_{j-1}^{(1)}}{h^2}. \tag{2.42}$$

Here we have introduced a radial grid along r_j, where h is the step along the grid r_j; for convenience, we introduced the designation $R(r_j)=R_j$. SE goes to the next form

$$\hat{c}_j\,\vec{R}_{j+1}^{(1)} + \hat{d}_j\vec{R}_j^{(1)} + \hat{e}_j\,\vec{R}_{j-1}^{(1)} = \vec{R}_j^{(0)}. \tag{2.43}$$

It can be seen that (2.43) consists of a tridiagonal matrix. We will look for a solution in the form:

$$\overline{\psi}_j = \alpha_j\overline{\psi}_{j+1} + \beta_j,$$
$$\overline{\psi}_{j-1} = \alpha_{j-1}\overline{\psi}_j + \beta_{j-1}. \tag{2.44}$$

For the radial wave function

$$\bar{R}_{j-1} = \alpha_{j-1}\overline{R}_j + \beta_{j-1}\,. \tag{2.45}$$

Substituting (2.45) into equation (3.20) we find that

$$\bar{R}_j = \alpha_j'\overline{R}_{j+1} + \beta_j',$$

where the coefficients:

$$\alpha_j' = -\left(\hat{d}_j + \alpha_{j-1}\hat{e}_j\right)^{-1}\cdot\hat{c}_j,$$
$$\beta_j' = \left(\hat{d}_j + \alpha_{j-1}\hat{e}_j\right)^{-1}\left(\vec{R}_j^{(0)} - \beta_{j-1}\cdot\hat{e}_j\right). \tag{2.46}$$

Using this scheme, at first the coefficients α_j' and β_j' is found (forward sweep), then the radial wave function $\vec{R}_j^{(1)}$ by backward sweep. Next, the normalization will be checked. Thus, as a result the radial part of the wave function and the ^{11}Be energy level of bound states are found. Negative energy states are normalized and describe either physical bound states of the projectile or states forbidden by the Pauli principle [12].

The solution of the eigenvalue problem (2.18) - the radial part $\phi_{lj}(E,r)$ of the bound states ($1/2^+$ and $1/2^-$) of ^{11}Be wave function $\phi_{ljm}(E,\boldsymbol{r}) = \phi_{lj}(E,r)Y_{lm}(\hat{r})$ (E<0) and the radial wave function $\phi_{lj}(kr)$ of the scattering states ($3/2^-$, $3/2^+$, $5/2^+$ resonances) in the continuum spectrum (E> 0) are presented in section 2.5.

2.4. Quasi uniform radial grid

As already explained, at initial time, the projectile is assumed to be in its ground state. The corresponding wave function is significant at small distance and decreases exponentially at large distance. The radial grid must then contain enough points near the origin to allow a good description of this initial state.

Through the interaction with the target, the projectile wave function develops a long-range tail which evolves rather quickly towards large distance. It corresponds mainly to the breakup component. Because this tail is a slowly varying function of r, its description requires less points than that of the bound states.

In order to take both aspects into account, V.S. Melezhik [12, 52] proposed to make use of a quasiuniform radial mesh with small steps near the origin and larger ones at large distances. In order to obtain such a mesh, we introduce a variable $x\epsilon$ [0,1] such that

$$r(x) = r_m\, g(x)/g(1), \tag{2.47}$$

where $r_m$is the upper bound of the radial interval we consider, and g is a $C^2([0,1])$ monotonous function such that *g(0)=0*.

The quasiuniform grid is obtained by mapping a uniform mesh over x with constant step $h = 1/N_r$ (where $N_r -$ is a number of points in radial grid) onto the radial interval $[0, r_m]$, . Its points r_j are calculated from the equally-spaced points of the uniform mesh $x_j = jh$ ($j = 0, \dots,$ N_r is a number of points at radial grid) through Eq. (2.47):

$$r_j = r(x_j)\ . \tag{2.48}$$

The functions vanish at r=0 and r $\rightarrow\infty$, since they are square integrable. In our grid calculation using a finite radial interval, this is approximated by assuming the functions to vanish at the last point of the mesh. This reads

$$f(0) = 0 = f(r_m). \tag{2.49}$$

On this mesh, the radial integrals are therefore approximated by

$$\int_0^\infty f(r)dr = \frac{r_m}{g(1)} \int_0^\infty g'(x) f\left(r(x)\right)dx \approx \approx \frac{hr_{N_r}}{g(1)} \sum_{j_r=1}^{N_r-1} g'(x_j) f(r_j). \quad (2.50)$$

This relation is used to calculate the scalar product of two radial functions [12].

2.4.1 Radial discretization of the wave function

As usual in grid calculations, the potential terms of $\widehat{H_0}$ and $\hat{V}$ are represented by diagonal matrices composed of their values at mesh points. Therefore we see that the matrix $\hat{V}$ of the time-dependent potential is fully diagonal in both its angular and radial representations.

Using quasiuniform grid as described above, the second-order differential operator appearing in $\widehat{H_0}$ reads as

$$\frac{d^2}{dr^2} = \left[\frac{g(1)}{r_m\, g\prime(x)}\right]^2 \left[\frac{d^2}{dx^2} - \frac{g\prime\prime(x)}{g\prime(x)} \frac{d}{dx}\right], \quad (2.51)$$

where g' and g'' are respectively the first and second derivatives of g. The differentiation operators over x can be discretized with the $(2\,N_d + 1)$- point finite-difference formulae. The first-order derivative reads

$$\left(\frac{df}{dx}\right)_{x_{j_r}} \approx h^{-1} \sum_{k=-N_d}^{N_d} c_k{}^{(1)}\, f(x_{j_r+k}), \quad (2.52)$$

with $c_0{}^{(1)} = 0$ and, for $k \neq 0$,

$$c_k{}^{(1)} = (-1)^{k-1} \frac{(N_d!)^2}{k\,(N_d-k)!(N_d+k)!}. \quad (2.53)$$

We have then $c_{-k}{}^{(1)} = -c_k{}^{(1)}$. The second derivative is given by

$$\left(\frac{d^2f}{dx^2}\right)_{x_{j_r}} \approx h^{-2} \sum_{k=-N_d}^{N_d} c_k{}^{(2)}\, f\left(x_{j_r+k}\right), \quad (2.54)$$

with, for $k \neq 0, c_k{}^{(2)} = 2\, c_k{}^{(1)}/k$. Here we have $c_{-k}{}^{(2)} = c_k{}^{(2)}$. When *k=0,*

$$c_0^{(2)} = -2 \sum_{j_r=1}^{N_d} j_r^{-2} \,. \tag{2.55}$$

The second-order derivative over radial components of the wave function expressed in the spherical-harmonic basis can then be approximated by

$$\left(\frac{d^2 \bar{\Psi}_\vartheta^{m_I}}{dr^2}\right)_{r_{j_r}} \approx \sum_{j'_r=0}^{N_r} d^{(2)}_{j_r j'_r} \, \bar{\Psi}_\vartheta^{m_I}(r_{j'_r}) \,, \tag{2.56}$$

where $d^{(2)}$ is the matrix whose elements are

$$d^{(2)}_{jj'} = \\ = \begin{cases} \left[\frac{g(1)}{h\, r_m\, g''(x_j)}\right]^2 \left[c^{(2)}_{(j'-j)} - h\, \frac{g''(x_j)}{g'(x_j)}\, c^{(1)}_{(j'-j)}\right] & if\ |j'-j| \le N_d\,; \\ 0 & otherwise. \end{cases} \tag{2.57}$$

Because of the time evolution process, the wave function, which is initially a bound state of the halo nucleus, develops a long-range breakup component. This tail evolves rather quickly towards large *r*. Therefore, the last point of the mesh r_{N_r} has to be chosen so as to ensure that the wave function does not reach the boundary of the mesh. In most of the cases, r_{N_r}, could be chosen equal to 800 fm.

As for the number of angular functions, the number of radial-mesh points N_r is chosen in order to keep enough accuracy on the values of the cross section. We have found empirically that choosing $\frac{r_{N_r}}{N_r} \sim 1$ fm ensures that the evolution calculation has converged with regard to the radial discretisation. This ratio corresponds approximately to the mean radial step. The fact that this value is related to the convergence of the scheme is not surpiring. It indeed characterizes the point density and so the accuracy of the discretisation. Therefore, with a mesh extending up to $r_{N_r} = 800$ fm, we consider $N_r = 800$ points for practical calculations.

2.4.2 The results of solving stationary SE: the energy spectrum of bound states

Using these numerical methods described above, the energy levels of the ^{11}Be nucleus were calculated. The results of calculation of the discrete spectrum of the ^{11}Be are shown in Table 1 and are compared with the experimental [17] and theoretical data of [12].

The parameterization of the potential between the neutron and ^{10}Be core is discussed in detail at next section. Here the eigenvalue problem (2.18) (the system of used units and some details of the solution of SE see in appendix A) was solved with two different set of parameters in order to compare results.

Table 1 − The energies of computed bound states of ^{11}Be [50] in comparison with the experimental [17] and theoretical data of [12].

J^{π}	l	E_{exp} (MeV) [17]	E_{th} (MeV) [12]	E_{th} (MeV)
$\frac{1^+}{2}$	0	-0.503	-0.502	-0.5013
$\frac{1^-}{2}$	1	-0.183	-0.184	-0.1844

The first set is from earlier work [12, 45], where the standard value is V_{ls}=32.8 MeV fm^2 for the depth of the *ls* potential for a p-shell nucleus, the depth of the Woods-Saxon potential is V_0= - 59.5 MeV (l=0) and V_1= - 40.5 MeV (l=1), radius R_0=2.669 fm, diffuseness a=0.6 fm (set 1 in table 2). The theoretical values of the energy from [12] were taken with these parameters. The second set of parameters is V_{ls}= 32.8 MeV fm^2, V_0= - 62.52 MeV (l=0) and V_1= - 39.74 MeV (l=1), R_0=2.585 fm, a=0.6 fm [are taken from 11] (set 2 in table 2). The last column (E_{th}) of table 1 was reproduced with this set.

For approximating of Eq.(2.40) with respect to the radial variable r, a second order finite-difference approximation on a quasiuniform grid has been used on the interval $r \in [0, r_m]$ with $r_m = 800$ fm in this section as in [12]. The grid has been realized by the mapping r→x of the initial interval onto $x \in [0,1]$ by the formula $r = r_m(e^{8x} - 1)/(e^8 - 1)$ [12].

Table 2 illustrates the convergence of the computational scheme as Δr→0 (Δx→0) using as a test the calculation of the binding energy of the ^{11}Be ground state (l=0). For comparison, the computations are performed for two different set of potentails in a similar quasiuniform radial mesh [49].

Table 2 − Convergence of the computational scheme on a uniform and quasiuniform radial grid

uniform radial grid			quasi uniform radial grid			
N_r	Δr	E_0 [12]	N_x	Δx	E_0 (1-set)	E_0 (2-set)
2000	0.4	-0.722	125	0.008	-0.50177	-0.50497
4000	0.2	-0.552	250	0.004	-0.50140	-0.50459
8000	0.1	-0.514	500	0.002	-0.5013	-0.50450
16000	0.05	-0.504	1000	0.001	-0.50129	-0.50448

Results also were compared with the calculations of [12] on the uniform grid. The analysis shows that the second order finite-difference approximation on a quasiuniform grid with N_x= 500 points ($\Delta x = 0.002$), leads to a considerably more accurate value of energy E_0 than the scheme on the uniform grid with N_r=2000 points ($\Delta r = 0.4$ fm). As seen in table 2, for computing the eigenvalue E on the uniform grid with a 1% accuracy, the number of grid points must be increased 8 times (N_r= 16000, $\Delta r = 0.05$ fm), which proves the efficiency of using a quasiuniform grid as proposed in [12].

2.5 The parameterization of the interaction between the neutron and core

The time evolution of $\Psi(\mathrm{r},\mathrm{t})$ following from Eq. (2.1) is calculated according to the above scheme starting from the initial state $\Psi(\mathrm{r},\mathrm{T_{in}}) = \phi_{2s}(\mathrm{r})$, where $\phi_{2s}(\mathrm{r})$ is the ground state of the ^{11}Be. The eigenfunctions of Hamiltonian H_0 with energy E are denoted as $\phi_{ljm}(E,r)$,

$$H_0\phi_{ljm}(E,r) = E\phi_{ljm}(E,r), \tag{2.58}$$

here j is a projectile total momentum $j=l+s$, resulting from the coupling of the orbital momentum l and spin s of the neutron, m is a magnetic quantum number.

Following the parameterization suggested in [17], the interaction $V(r)$ between the neutron and the ^{10}Be core is chosen for bound and resonance states as the sum of a spherical Woods-Saxon potential $V_l(r) = -V_l f(r)$, where $f(r) = 1/(1 + exp(\frac{r-R_0}{a}))$ and of a standard spin-orbit interaction

$$V_l^s(r)ls = V_{ls}\frac{1}{r}\frac{d}{dr}f(r)(ls). \tag{2.59}$$

The standard value V_{ls}=21 MeV fm^2 is used for the depth of the ls potential for a p-shell nucleus [53]. The parameters of the Woods-Saxon potentials, as radius R_0, diffuseness a and depth V_l are given in Table 3 and the selection of these parameters will be discussed further in detail for bound and resonant states separately [54].

Table 3 – Parameters of potentials

$V_{l\ \mathrm{even}}$ (MeV)	$V_{l\ \mathrm{odd}}$ (MeV)	V_{LS} (MeV fm^2)	a (fm)	R_0 (fm)	States
62.52	39.74	21.0	0.6	2.585	$1/2^+$, $1/2^-$, $5/2^+$, $3/2^+$
–	6.8*	21.0	0.35	2.5	$3/2^-$

* we found this parameters at [3].

The depths of the Woods-Saxon potentials have been determined as V_l= 62.52 MeV (l-even) and V_l= 39.74 MeV (l-odd) [11] in order to reproduce the $1/2^+$ ground state of ^{11}Be at -0.503 MeV, the $1/2^-$ excited state at -0.183 MeV and two resonance states $5/2^+$ and $3/2^+$ with the position of peaks at $E_{5/2^+} = 1.232$ MeV and $E_{3/2^+} = 3.367$ MeV [27, 28] (see table 4). As it is shown in Table 3 for all these states, except the resonance $3/2^-$, the radius is R_0=2.585 fm and the diffuseness is a=0.6 fm.

Thus, in solving of the radial Schrodinger equation (2.58) for a neutron-core system four set of potentials were used. In the discrete spectrum the parameter V_l=62.52 MeV of the Woods-Saxon potential reproduces ground state at E= -0.503 MeV (l=0, $1/2^+$) and the depth V_l=39.74 MeV describes the first excited state (l=1, $1/2^-$). In the continuous spectrum (E>0) for l=2 with the set of parameter V_l=62.52 MeV from [11], we got the positions of two resonances $3/2^+$ (l-*1/2*) and $5/2^+$ (l+*1/2*) as $E_{5/2^+} = 1.232\,MeV$ and $E_{3/2^+} = 3.367\,MeV$ (see table 4) [27, 28] . To fix the position of the $3/2^-$ resonance (l=1) close to the experimental [28] and theoretical [27] value $E_{3/2^-} = 2.789\,MeV$ (table 4), we tuned the set of parameters V_l, a and R_0 ourselves (see Table 3) [3], since the parameters of [11] do not reproduce the known position of resonance $3/2^-$. For $l \geq 3$, the spherical potential V(r) was set to zero [54].

Thereby our calculations reproduce the theoretical value of positions of resonances $5/2^+$, $3/2^-$ and $3/2^+$ from [27]. In this simplified single-channel approach, resonances are confined only by the centrifugal barrier and the coupling with the excited states of the core ^{10}Be is not taken into account. Nevertheless, the calculated resonance width Γ= 150 keV for resonance $5/2^+$ is in qualitative agreement with the experimental and theoretical ones (see Table 4). The widths of the resonances $3/2^-$ and $3/2^+$ in this simplified model of 700 keV and 600 keV significantly exceed the experimental and theoretical ones (see Table 4). However, it is not surprising, since a quantitative description of the widths of these resonances requires the inclusion in the model of coupling with the core excitation channels.

Table 4 – Theoretical and experimental energy of resonance states of ^{11}Be

	$5/2^+$		$3/2^-$		$3/2^+$	
	E, MeV	Γ, keV	E, MeV	Γ, keV	E, MeV	Γ, keV
Theory [24]	1.230	100	2.789	240	3.367	3
Exp [25]	1.281	120	2.898	122	2.387	<8

In figure 5 we present the radial part $\phi_{lj}(E,r)$ of the ground state ($1/2^+$) of ^{11}Be wave function $\phi_{ljm}(E,\boldsymbol{r}) = \phi_{lj}(E,r)Y_{lm}(\hat{r})$, which is the solution of the eigenvalue problem Eq.(2.58) with l=0 at discrete spectrum normalized to unity ($\int(\phi_{lj}(E,r))^2 dr = 1$). Here the internal Hamiltonian $H_0(\boldsymbol{r})$ (2.58) includes potentials, the summation of which translates the so-called effective potential of the relative neutron-core motion, with the parameterization for l=0 discussed above [54]. The effective potential (see Fig.6)

$$V_{eff} = V_l(r) + V_l^s(r)ls + \frac{\hbar^2 l(l+1)}{2\mu r^2}, \tag{2.60}$$

consists of a Woods-Saxon potential $V_l(r)$, a spin orbital term of interaction $V_l^s(r)ls$ and centrifugal barrier .

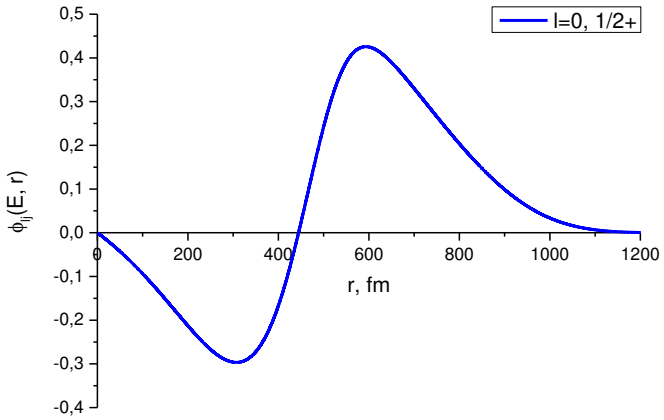

Figure 5 − The radial part $\phi_{lj}(E,r)$ of the wave function of the ground state ($1/2^+$) of ^{11}Be (l=0, m=0).

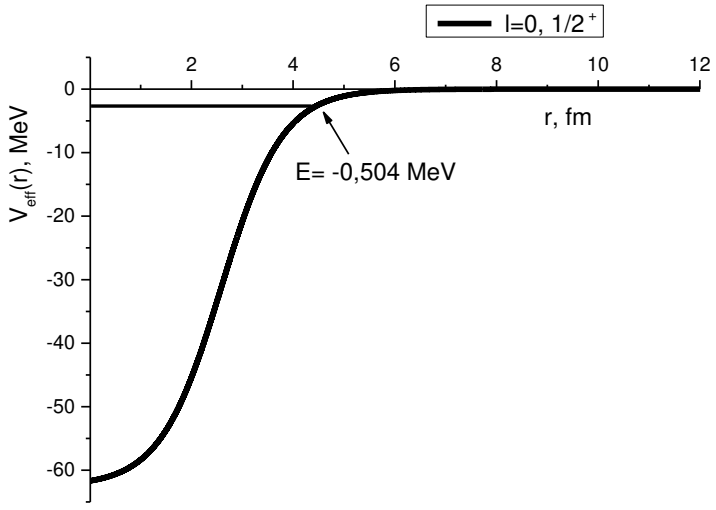

Figure 6 − The effective potential of the ground state ($1/2^+$) of ^{11}Be (for l=0, m=0).

As it is shown in figure 7, the position of the $3/2^-$ resonance (red line) overtop the shape of the potential, calculated with the set of parameters from [11], which shows the feasibility of selecting the potential by ourselves at [3] for this level.

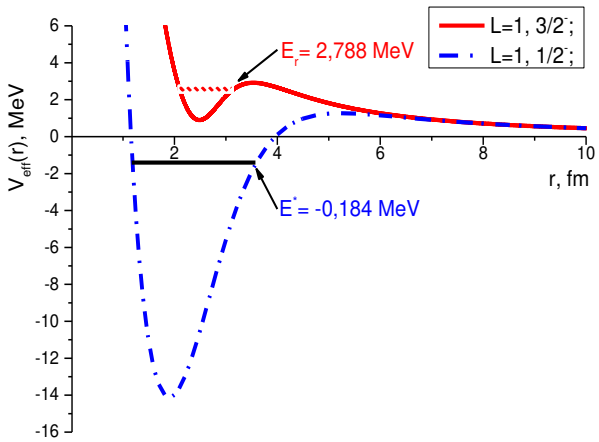

Figure 7 – The effective potential, describing first excited $1/2^-$ state (l-1/2) at E=– 0.184 MeV and resonance $3/2^-$ (l+1/2) with the position E=2.788 MeV (l=1).

Performing integration of the eigenvalue scattering problem (Equation (2.58)) when E>0) for l=2 with the parameters V_l= 62.52 MeV, R_0= 2.585 fm and a= 0.6 fm, we reproduce the position of peaks at $E_{5/2^+} = 1.232\ MeV$ and $E_{3/2^+} = 3.367\ MeV$ (table 4) [27, 28], which is shown in figure 8.

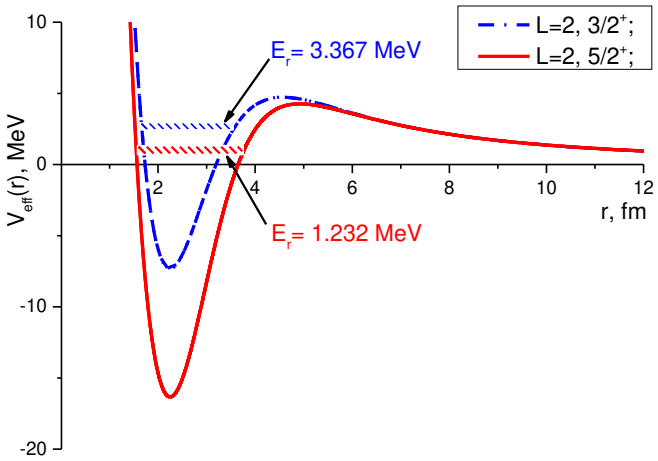

Figure 8 – The effective potential, calculated for l=2 to reproduce the resonance $3/2^+$ (l-1/2) with the position of the energy E=3.367 MeV (blue dashed dots) and $5/2^+$ (l+1/2) state with the peak at E=1.232 MeV (red line).

The radial p-wave function $\phi_{lj}\ (E,r)$ of excited (1/2$^-$) bound state (see fig. 9) and scattering p3/2 wave function (see fig. 10) $\phi_{lj}\ (kr)$ in the continuum are the solutions of the boundary value (2.58) on the same radial grid. The radial wave functions of a d3/2 and d5/2 scattering states are plotted at figures 11 and 12, respectively.

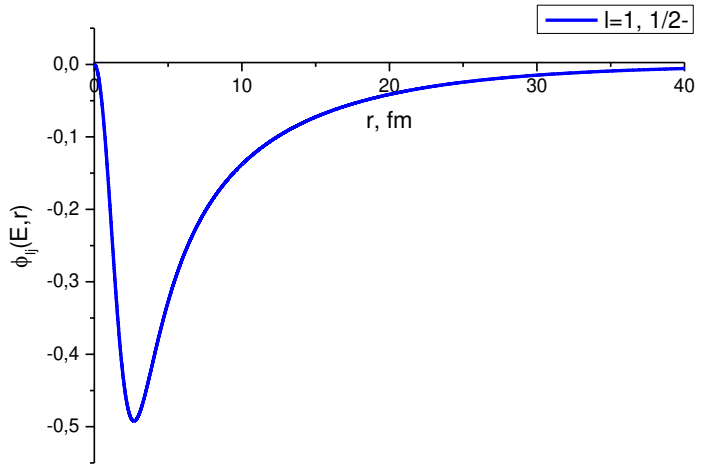

Figure 9 – The radial part of $p_{1/2}$ wave function $\phi_{lj}\ (E,r)$ of excited (1/2$^-$) bound state of discrete spectrum (l=1, m=0).

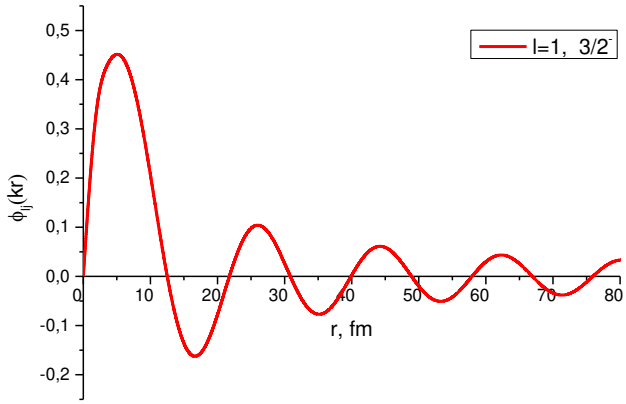

Figure 10 – The radial part of scattering $p_{3/2}$ wave function $\phi_{lj}\ (kr)$ in the continuum (l=1, m=0).

The scattering states are computed at energies corresponding to the positions of the three resonances $3/2^-$, $3/2^+$ and $5/2^+$. The radial part of the eigenfunction of the Hamiltonian $H_0(\boldsymbol{r})$ (2.58) $\phi_{lj}\,(kr)$ in the continuum spectrum (E> 0) is normalized $\phi_{lj}\,(kr) \to 0, \text{if } kr \to 0$ in accordance with the boundary condition $\phi_{lj}\,(kr) \to \frac{\sin(kr-\frac{\pi l}{2})}{k}, \text{if } kr \to \infty.$

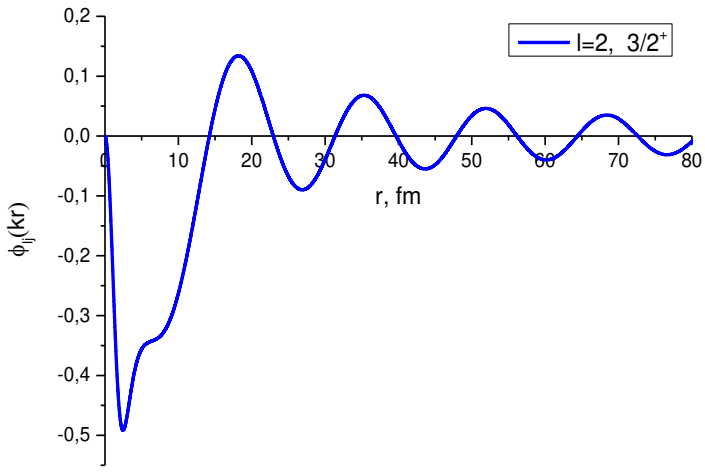

Figure 11 – The scattering $d_{3/2}$ wave functions $\phi_{lj}\,(kr)$ of $3/2^+$ resonance (l=2, m=0) of ^{11}Be nucleus.

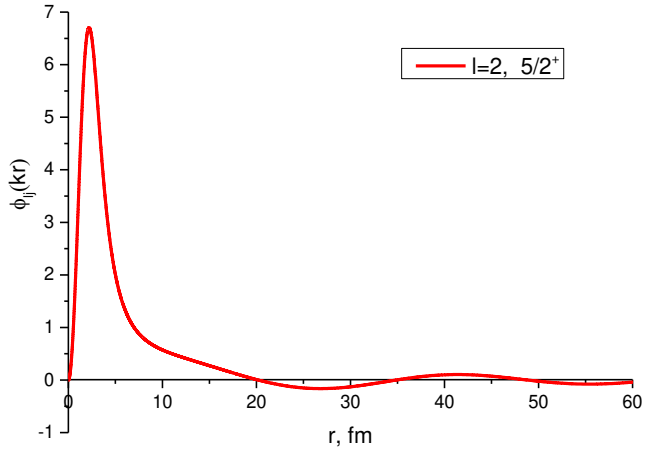

Figure 12 – The scattering $d_{5/2}$ wave functions $\phi_{lj}\,(kr)$ of $5/2^+$ resonance (l=2, m=0) of ^{11}Be nucleus.

Thus in subsection 2.3 the results of calculating the spectrum and resonant states of the ^{11}Be are described in depth, which is an important element of the computational scheme. Here we paid attention to discuss the parameterization of potential between the neutron and ^{10}Be core and how the resonant states were included in the analysis of the breakup reaction. Also, the internal effective potential for different partial and spin states of the ^{11}Be nucleus are illustrated.

Overall, in chapter 2 the modeling of the physical problem and computational methods used for solving the stationary and non-stationary Schrodinger equations are described. Also the numerical results of calculation of the bound states (which is a necessary initial value for integration of time-dependent Schrodinger equation (2.1)) and continuum resonant states of $H_0(\boldsymbol{r})$, that are important for breakup analysis of halo nuclei are presented.

3 THE CALCULATION OF BREAKUP CROSS-SECTION

The breakup component of wave function $|\Psi_{\rm bu}(\boldsymbol{r},t)>$ is obtained by eliminating the bound states from the calculated wave packet [12,13,53]

$$|\Psi_{\rm bu}(\boldsymbol{r},t)\rangle = \left(1 - \sum_{\nu\in \rm bound} |\phi_\nu(\boldsymbol{r})\rangle\langle\phi_\nu(\boldsymbol{r})|\right)|\Psi(\boldsymbol{r},t)\rangle, \qquad (3.1)$$

where the sum runs over two bound states $1/2^+$ and $1/2^-$ of ^{11}Be calculated by integration of Eq. (2.58). The wave functions of the ^{11}Be bound states are normalized to the unity.

Then the total breakup cross section can be calculated as a function of the relative energy E between the emitted neutron and the core nucleus by the formula as in [12]

$$\frac{d\sigma_{bu}}{dE}(E) = \frac{4\mu k}{\hbar^2}\int_{b_{min}}^{b_{max}} \sum_{j=l+s}\sum_{lm} |\int j_l(kr)Y_{lm}(\hat{r})\Psi_{\rm bu}(\mathbf{r},T_{\rm out})d\boldsymbol{r}|^2\, bdb. \qquad (3.2)$$

Here $j_l(kr)-$ is a spherical Bessel function representing the l-wave component of the neutron wave function in the continuum spectrum E>0 ($k=\sqrt{2\mu E}/\hbar$) if the interaction between the core and the neutron is neglected.

Time evolution starts at initial time $T_{\rm in}$ and stops at final time $T_{\rm out}$ by iteration over N_T time steps Δt as explained in [13] The initial (final) time $T_{\rm in}$ ($T_{\rm out}$) has to be sufficiently big $|T_{in}|, T_{out}\to+\infty$, fixed from the demand for the time-dependent potential $V_C(\boldsymbol{r},t)$ to be negligible at the beginning (end) of the time evolution at t=$T_{\rm in}$ ($T_{\rm out}$). Following the investigation performed in Ref. [12, 13], the time interval is fixed as $T_{\rm in}$= -20$\hbar$/MeV and $T_{\rm out}$= 20$\hbar$/MeV, the time step Δt equals to 0.01 $\hbar$/MeV.

For discretizing with respect to the radial variable r, a sixth-order (seven point) finite-difference approximation on a quasiuniform grid has been used on the interval $r\in[0,r_m]$ with r_m= 1200 fm. The grid has been realized by the mapping $r\to x$ of the initial interval onto $x\in[0,1]$ by the formula $r=r_m(e^{8x}-1)/(e^8-1)$ [24].

The boundary of integration over the impact parameter b in formula (3.2) was chosen from the demand of accuracy (to be of the order of 1%) as b_{min}= 12fm and b_{max}= 400fm. It should be noted that the inclusion of the region [0, b_{min}] makes sense if the nuclear interaction between the target and the projectile is taken into account [3]. The demanded accuracy and the convergence of the integral (3.2) is discussed below.

The breakup component of wave function $|\Psi_{\rm bu}(\boldsymbol{r},t)>$ (3.1) was also used for exploring mean value of the transverse and longitudinal momenta between the emitted neutron (n) and the ^{10}Be core-nucleus in the breakup reaction ^{11}Be+^{208}Pb -> ^{10}Be+n+^{208}Pb at [13]. The details of this analysis is given in Appendix C.

3.1 Convergence of the computational scheme and accuracy of the approach

It is important to emphasize that all errors of the method are controlled and, in this section, the accuracy of the numerical technique is discussed.

In works [12, 13] and in subsection 2.2.2, it was shown the unitarity of the evolution operator of the computational approach for integration of the time-dependent Schrodinger equation (2.1). It ensures that the normalization of the neutron wave-packet to unity is preserved with the required accuracy at chosen T_{out}= 20$\hbar$/MeV. In these works a discussion is also given about the choice of T_{out} from the condition of convergence of breakup cross sections along this parameter. In [13] it is demonstrated that if r_m is chosen ≥ 800 fm, then at T_{out}= 20$\hbar$/MeV the component of the wave-packet describing the outgoing neutron does not reach the boundary of integration over r. The wave functions of the ^{11}Be bound states are normalized to unity [3].

The quasiuniform radial grid with 2000 mesh points (generated by the step $\triangle x = 5 \cdot 10^{-3}$) and the edge at r_m = 1200 fm gives the accuracy of integration of the order of about 1%. The step of integration over the time variable $\triangle t$ = 0.01 $\hbar$/MeV chosen in [12] keeps the same order of accuracy.

In the calculation of the breakup cross section the choice of edges of integration b_{min} and b_{max} must be carefully tested. It was investigated in previous calculations at [12, 13] that the integration over the interval [30 fm, 400 fm] gives about 60% of the calculated cross section near the maximum. A similar calculation in work [6] was made up to b_{max} = 30 fm. The piece from b>30fm to ∞ was taken into account according to the perturbation theory, which seems not very reasonable, as can be seen in this figure 13. Here the breakup cross-section from previous calculations [12] were made without taking into account resonance states. The dotted line represents the results obtained on a quasi-uniform grid Δx= 0.002 fm, r_m= 800 fm. The solid line shows the results calculated on the grid Δx= 0.0005 fm, r_m= 1200 fm. The triangle in graph indicates the results calculated with the Coulomb potential (2.3), and the full circle is the calculated one in the free neutron model, which takes into account the deviation of the projectile from a linear trajectory and the effect of post-acceleration. As shown in this work [12], the influence of these effects is negligible. The results obtained partially perturbatively [14] are presented as a dotted line, which was calculated numerically over the interval [b_{min}= 12 fm, b_{max}= 30 fm], and the remaining part was estimated using perturbation theory. Experimental data are taken from [16]. This shows the advantage of our approach, which allows integration up to such large values of b_{max} outside of perturbation theory.

Tables 5 and 6 illustrate the convergence of the integral (3.2) as a function of the upper bound b_{max} for a few relative energies E. The total breakup cross section calculated for an intermediate beam energy of 72 MeV/nucleon (table 5) and for a lower beam energy 10 MeV/nucleon (table 6) taking into account the low-lying resonance states ($3/2^+$,$3/2^-$ and $5/2^+$) of ^{11}Be nucleus (more detail at subsection 3.2.2). As it can be seen, the demanded accuracy (to be in order of one percent) in computing the integral (3.2) is achieved as b_{min}= 12 fm and b_{max}= 400 fm [3]. Here

the nuclear interaction effects were simulated by a cutoff b_{min}= 12 fm of the impact parameters at the formula (3.2).

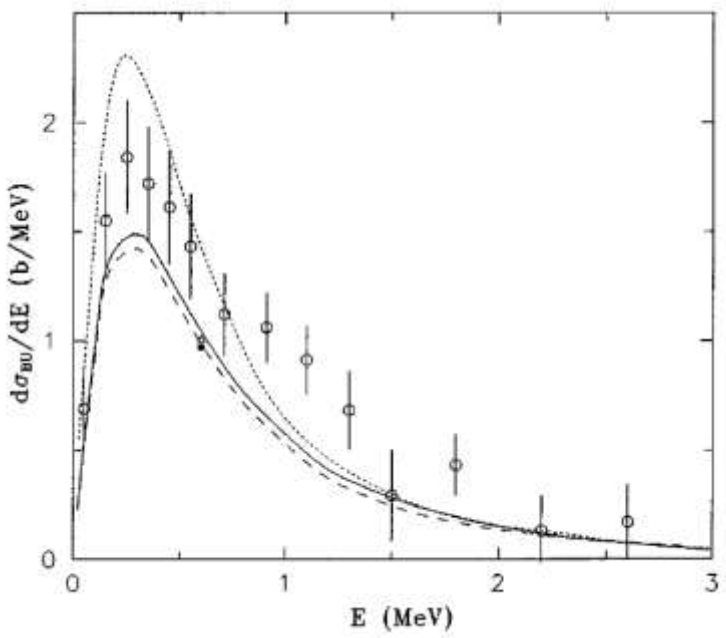

Figure 13 − The cross sections dσ(E,b_{max})/dE of previous calculations without including resonance states from [12] in comparison with the partly perturbative results of [45]. The experimental data are from [16]. The figure is taken from [12].

Table 5 − Convergence of the breakup cross section $d\sigma(E, b_{max})/dE$ in (b/MeV) at 72 MeV/nucleon over the edge of integration b_{max} (in fm) for different relative energies E (MeV). The calculations are performed for N=25 with including all three resonant states [3].

b_{max}	*E=0.1 MeV*	*E=0.4 MeV*	*E=0.8 MeV*	*E=1.2 MeV*	*E=1.6 MeV*	*E=2.0 MeV*	*E=2.8 MeV*	*E=3.0 MeV*	*E=3.3 MeV*
12	0.021	0.052	0.046	0.032	0.019	0.013	0.006	0.005	0.004
20	0.183	0.397	0.309	0.200	0.122	0.080	0.037	0.030	0.023
50	0.561	1.024	0.689	0.407	0.234	0.143	0.060	0.048	0.035
100	0.816	1.335	0.819	0.456	0.254	0.151	0.061	0.049	0.036
200	0.950	1.436	0.841	0.461	0.255	0.151	0.061	0.049	0.036
300	0.972	1.443	0.841	0.461	0.255	0.151	0.061	0.049	0.036
400	0.976	1.444	0.841	0.461	0.255	0.151	0.061	0.049	0.036

Table 6 − Convergence of the breakup cross section $d\sigma(E, b_{max})/dE$ in (b/MeV) at 10 MeV/nucleon over the edge of integration b_{max} (in fm) for different relative energies E (MeV). The calculations are performed for N=81 with including all three resonant states [3].

.

b_{max}	E=0.1 *MeV*	E=0.4 *MeV*	E=0.8 *MeV*	E=1.2 *MeV*	E=1.6 *MeV*	E=2.0 *MeV*	E=2.7 *MeV*	E=3 *MeV*	E=3.3 *MeV*
13	0.031	0.055	0.078	0.102	0.058	0.045	0.025	0.019	0.014
20	0.350	0.696	0.842	0.767	0.413	0.273	0.121	0.085	0.060
50	1.363	2.439	1.889	1.254	0.615	0.363	0.145	0.099	0.068
100	1.839	2.809	1.966	1.269	0.618	0.364	0.145	0.099	0.068
200	1.904	2.822	1.967	1.269	0.618	0.364	0.145	0.099	0.068
400	1.907	2.826	1.968	1.269	0.618	0.364	0.145	0.099	0.068

Overall, the splitting-up method gives a fast convergence with respect to the numbers of grid points N (angular) and N_x (quasiuniform radial). The computational time is directly proportional to the numbers N and N_x [12]. The convergence of the method with respect to angular points $N \to \infty$ is discussed below, it is investigated for the case of intermediate and lower beam energies individually [3].

In order to investigate the convergence of the numerical scheme by the angular grid, we calculated the cross section $d\sigma(E, b_{max})/dE$ for a beam energy 69 MeV/nucleon at different angular grid points N = 9, 25, 49 (the number of basis functions (2.5) in expansion (2.4)) with including all three resonance states $5/2^+$, $3/2^-$, $3/2^+$. As it is illustrated in fig.14, the approach achieves the convergence at N = 25.

One of the main task of our investigation is to extend the time-dependent approach for calculation of the breakup cross sections at low energy beams. Firstly, we investigate the convergence of computational scheme at low energies over the angular grid number N. For this the calculation of breakup cross section $d\sigma(E, b_{max})/dE$ for a beam energies of 20 MeV/nucleon (figure 15) and 5 MeV/nucleon (figure 16) is performed on different angular meshes N=9, 25, 49, 81 and 121.

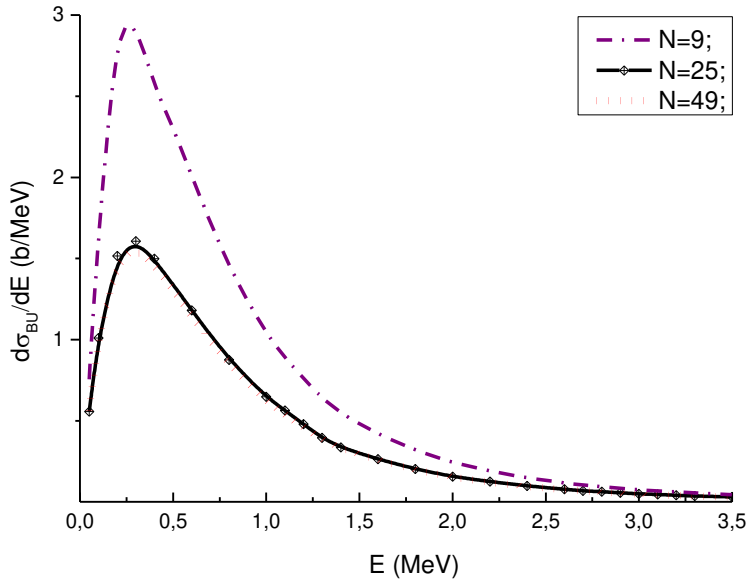

Figure 14 – The convergence of the breakup cross section $\frac{d\sigma_{bu}(E)}{dE}$ over the number N of angular grid points calculated by Eq. (3.2) including three resonances ($5/2^+$, $3/2^-$, $3/2^+$) at 69 MeV/nucleon.

As it is shown in figure 16, for computing the breakup cross section at beam energies ≥ 20 MeV/nucleon with demanded accuracy of the order of one percent, it is sufficient to use N=49. For lower energies (up to 5 MeV/nucleon) the basis should be extended to N=81 (see fig.16) due to the slowing down of convergence [3].

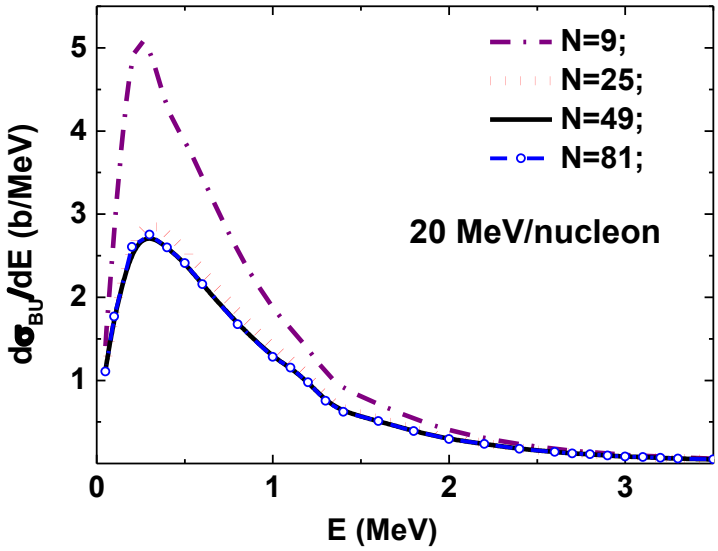

Figure 15 – The convergence over the angular grid number N of the calculated breakup cross sections with including resonant states $5/2^+$, $3/2^-$ and $3/2^+$ into the computational scheme at 20 MeV/nucleon.

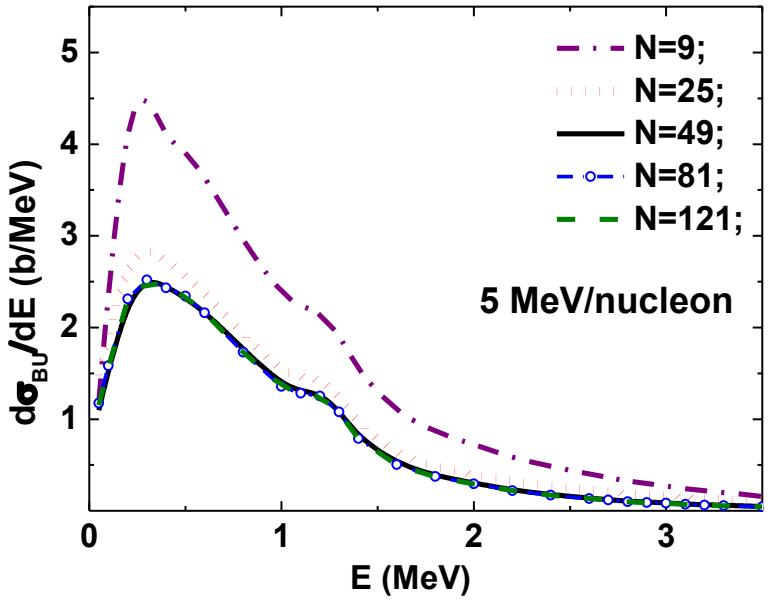

Figure 16 – The convergence over the angular grid number N of the calculated breakup cross sections at 5 MeV/nucleon. The cross sections were calculated by formula (3.2). The resonant states $5/2^+$, $3/2^-$ and $3/2^+$ were included into the computation.

The results of the computed breakup cross section $d\sigma(E, b_{max})/dE$ for 20 MeV/nucleon on different angular meshes N=9, 25, 49, 81 and 121 are presented at tables 6 and 7 below. The calculations were performed for different relative energies E (MeV) taking into account only two bound states ½+ and ½- (table 7) and adding three low-lying resonances $3/2^-$, $3/2^+$ and $5/2^+$ of ^{11}Be (table 8).

Thus, the convergence of the computational scheme and accuracy of the method are demonstrated in a wide energy range from intermediate (69 MeV/nucleon) to low beam energies (5 MeV/nucleon) including low-lying resonances in various partial and spin states of ^{11}Be.

Table 7 − Convergence of breakup cross section considering only bound states $d\sigma(E, b_{max})/dE$ on an angular grid points N=9, 25,49 and 81 at b_{max}=400 fm for a beam energy E=20 MeV/nucleon

E, MeV	$d\sigma(E, b_{max})/dE$, b/MeV													
	0.05	0.1	0.3	0.5	0.8	1.0	1.2	1.6	2.0	2.4	2.7	3.0	3.3	3.5
N=9	1.356	2.688	4.549	3.323	2.067	1.533	1.113	0.619	0.342	0.188	0.130	0.094	0.071	0.063
N=25	1.061	1.673	2.589	2.205	1.485	1.151	0.838	0.491	0.269	0.151	0.103	0.073	0.054	0.056
N=49	1.069	1.652	2.443	2.039	1.362	1.058	0.773	0.458	0.254	0.143	0.099	0.071	0.053	0.054
N=81	1.058	1.643	2.440	2.038	1.361	1.057	0.772	0.457	0.253	0.143	0.099	0.071	0.053	0.054

Table 8 − Convergence of breakup cross section taking into account two bound and 3 resonance states $d\sigma(E, b_{max})/dE$ on an angular grid points N=9, 25,49,81,121 at b_{max}=400 fm at E=20 MeV/nucleon

E, MeV	$d\sigma(E, b_{max})/dE$, b/MeV													
	0.05	0.1	0.3	0.5	0.8	1.0	1.2	1.6	2.0	2.4	2.7	3.0	3.3	3.5
N=9	1.413	2.869	5.062	3.896	2.520	1.859	1.384	0.714	0.397	0.229	0.153	0.104	0.072	0.059
N=25	1.113	1.799	2.910	2.585	1.814	1.396	1.062	0.537	0.310	0.184	0.125	0.086	0.060	0.050
N=49	1.118	1.777	2.756	2.411	1.676	1.283	0.978	0.510	0.296	0.178	0.121	0.084	0.059	0.049
N=81	1.107	1.768	2.754	2.410	1.676	1.282	0.976	0.510	0.296	0.178	0.121	0.084	0.059	0.049
N=121	1.110	1.770	2.751	2.410	1.676	1.282	0.976	0.510	0.296	0.178	0.121	0.084	0.059	0.049

3.2 Results and discussion

In this work, the influence of low-lying resonance states of ^{11}Be into breakup reaction at 69 and 72 MeV/nucleon are studied in the framework of time dependent approach as in [12,13]. We suppose that in the experimental data from [16,17], there are visible peaks near the energies 1.23, 2.78 and 3.3 MeV , which correspond to position of low-lying resonance states $5/2^+$, $3/2^-$ and $3/2^+$ [27] of ^{11}Be. The contribution of resonances into breakup reaction of ^{11}Be at a heavy target ^{208}Pb at intermediate beams is studied at subsection 3.2.1 below.

One of the main tasks of the dissertation is to extend and demonstrate the applicability of the computational model for solving the time-dependent Schrodinger equation in a nonperturbative algorithm [12,13] for calculations of breakup cross section at low collision energies. The subsection 3.2.2 provides the investigation of the resonance states' contribution to breakup at low beam energies of 5-30 MeV/nucleon.

3.2.1 Influence of resonant states on the breakup cross section of ^{11}Be at 69 and 72 MeV/nucleon

In the works [12] and [13] the breakup reaction $^{11}Be + {}^{208}Pb \rightarrow {}^{10}Be+n+{}^{208}Pb$ was successfully investigated at 69 and 72 MeV/nucleon with the non-perturbative time-dependent approach. As it is illustrated at [12, 13, 23], this method is the efficient tool for a quantitative analysis of the Coulomb breakup of halo nuclei. However, the resonant states of ^{11}Be were not included in these calculations. In particular, we assume that in the experimental data at these beam energies [16, 17], there are visible peaks near the energies 1.23, 2.78 and 3.3 MeV, which correspond to position of resonances: $5/2^+$, $3/2^-$ and $3/2^+$ [27]. Here, we overcome this drawback of the model: the resonant states $5/2^+$, $3/2^-$ and $3/2^+$ (see Table 4) are taken into consideration. Note that these resonances were also observed experimentally by Fukuda et.al. in the breakup of ^{11}Be on the light target (^{12}C) at 70 MeV/nucleon [17]. In Fig. 17, we demonstrate that the inclusion of the resonant states in the interaction between the neutron and the ^{10}Be-core gives a considerable contribution to the breakup cross sections. Thus, for a relative energy E= 1.2 MeV the 25% increase of the cross section is observed, for E= 3.3 MeV the increment is about 3% [3]. Overall, it is shown that the inclusion of the resonant states improves the agreement of the calculated breakup cross section with experimental data at 72 MeV/nucleon [16]. The calculations are performed on the angular grid with N = 25 grid points. Convolution of the calculation with the experimental resolution was not performed.

To clarify the contribution of the dominant resonance to the breakup cross section, we performed the computation at 69 MeV/nucleon, where most detailed and accurate experimental data are available [17]. The partial contribution of each resonance is illustrated in Table 9 [3]. It is shown that the resonances $3/2^-$ and $3/2^+$ make a slightly larger contribution to the cross section $d\sigma(E,b_{max})/dE$ than $5/2^+$ at such intermediate beam energies (~70 MeV/nucleon).

Table 9 – The contribution for different relative energies E (in MeV) of the resonant states $5/2^+$, $3/2^-$ and $3/2^+$ to the breakup cross section $d\sigma(E,b_{max})/dE$ (in b/MeV) at 69 MeV/nucleon. Here, 'b.s.' indicates the cross sections calculated with the interaction potential between the neutron and the ^{10}Be-core including only two bound states of ^{11}Be.

Energy, MeV	b.s.	b.s.+$5/2^+$	b.s. + $5/2^+$+$3/2^+$	b.s. + $5/2^+$+$3/2^-$	b.s. + 3 res
E=0.1	0.936	0.936	1.007	1.011	1.011
E=0.3	1.420	1.421	1.595	1.606	1.606
E=0.8	0.704	0.708	0.865	0.875	0.875
E=1.0	0.555	0.562	0.639	0.647	0.648
E=1.2	0.383	0.378	0.473	0.479	0.479
E=2.0	0.138	0.137	0.155	0.156	0.156
E=2.7	0.056	0.056	0.070	0.069	0.069
E=3.0	0.043	0.044	0.051	0.050	0.050
E=3.3	0.036	0.036	0.037	0.037	0.037

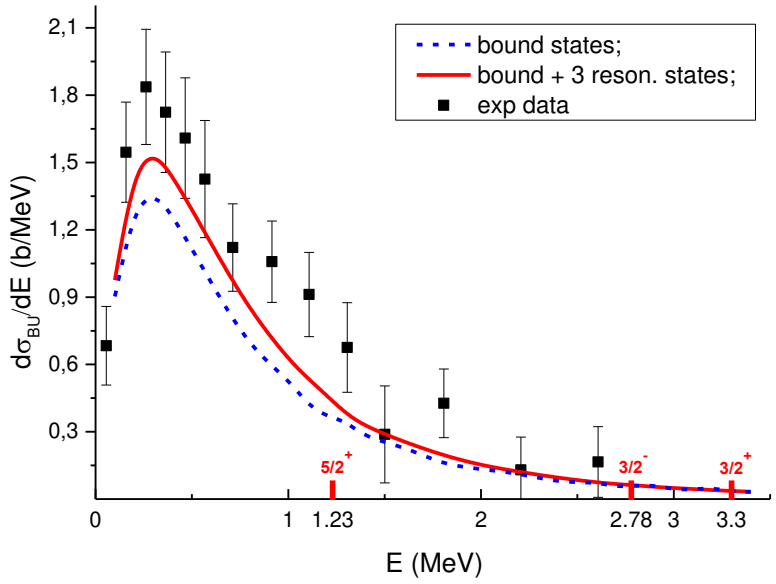

Figure 17 – The breakup cross sections $d\sigma(E,b_{max})/dE$ including into interaction between the neutron and the ^{10}Be-core only $1/2^+$ and $1/2^-$ bound states, and bound and resonant states ($5/2^+$, $3/2^-$, $3/2^+$) in comparison with experimental data at 72 MeV/nucleon [16].

3.2.2 Breakup cross section of ^{11}Be at low beam energies

Despite the fact that research on the halo of the ^{11}Be nucleus dates back to the 80s of the last century, this topic is still one of the most relevant. Including the tool for studying the halo nuclei through the Coulomb breakup of the system is important. As already indicated above, experiments were performed at intermediate beam energies (69 and 72 A MeV) of ^{11}Be [16, 17] for the reaction ^{11}Be + ^{208}Pb -> ^{10}Be+n+^{208}Pb and many theoretical calculations and processing [11, 12, 13, 14, 45, 46] have been carried out. There is also an experiment at high energy beams - at 520 MeV/nucleon [44].

However there were several theoretical studies at low beam energies for Coulomb breakup reaction of ^{11}Be. In particular, in [11, 18] it was calculated the differential cross section of the breakup of ^{11}Be in the eikonal approximation at a beam energy of 20 MeV/nucleon. Also, authors of [19] studied postacceleration effects in the Coulomb breakup of neutron halo nuclei at low energies: 5-30 A MeV. In this section we extend the the non-perturbative time dependent approach for calculations of breakup cross section at low beam energies down to 5 MeV/nucleon and investigate the contribution of the ^{11}Be resonance states in this region [3].

In Fig. 13, we compare our results with the Coulomb wave Born approximation (CWBA) available for a beam energy of 30 MeV/nucleon [19]. Our calculations were performed with including only bound states (blue dash curve) and also with bound and three resonant states (red curve). They are compared with the CWBA calculations for the first order CWBA (green short dots) and the finite range CWBA (black dashed dots). Figure 18 shows a significant deviation of the CWBA calculation from our result at 30 Mev/nucleon, which increases with decreasing energy. This is consistent with the conclusion of the authors of [19] about the difficulty of using the CWBA for lower energies. The resonant states of ^{11}Be were not included in the CWBA calculations.

In Fig.19 we compare our results with the breakup cross section calculated in [11, 18] within the dynamical eikonal approximations at fixed relative energies E= 0.3 and 0.5 MeV at 20 MeV/nucleon. In the dynamical eikonal calculations the resonant states of ^{11}Be were not taken into account. Note that at an energy E= 0.3 MeV near the peak of the cross section, our calculation without including the resonant states of ^{11}Be gives a cross section rather close to the dynamical eikonal approach [18].

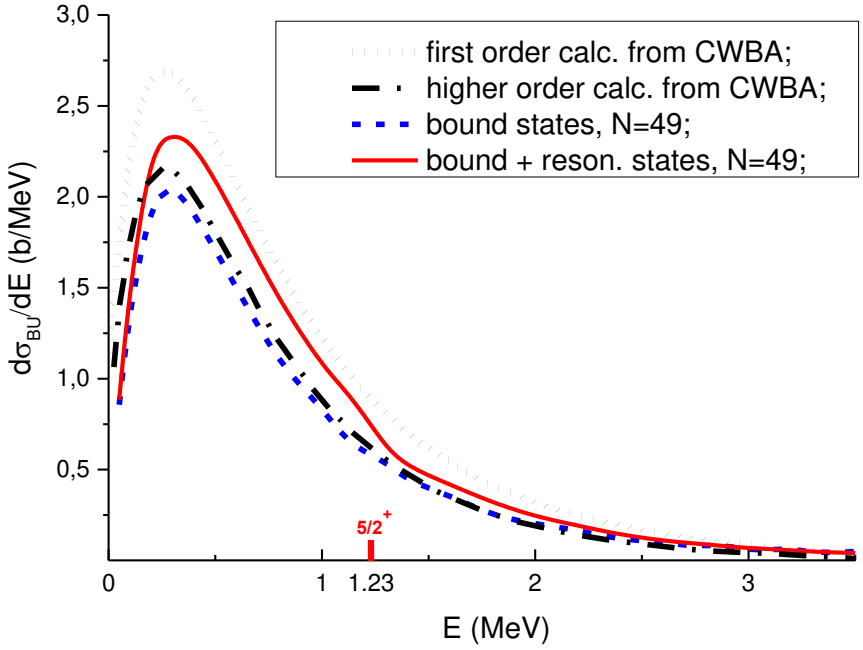

Figure 18 – The breakup cross section calculated by formula (3.2) at 30 MeV/nucleon in comparison with CWBA calculations of [19].

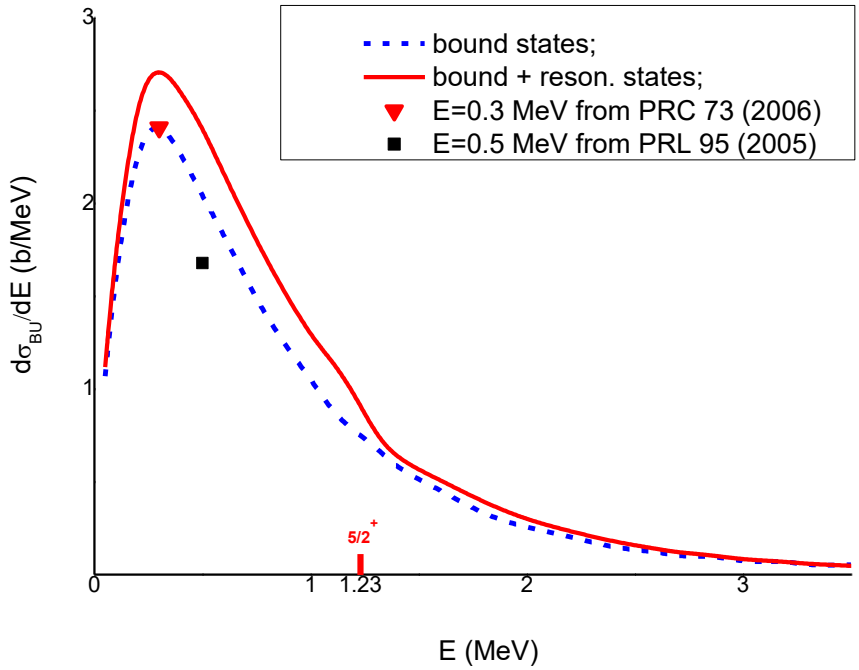

Figure 19 – The breakup cross sections calculated with only bound states of ^{11}Be in the computational scheme (blue dash curve) and including three resonances of ^{11}Be (red curve) at 20 MeV/nucleon in comparison with calculations of the dynamical eikonal approaches at E = 0.3 MeV [18] and E = 0.5 MeV [11].

The table 10 shows the total differential cross section data from [11] and [18] for relative energies E=0.5 MeV and E=0.3 MeV at a beam energy of 20 MeV/nucleon in comparison with our calculations for the angular grids N=9, N=25 and N=49 for bound states and with taking into account three resonant states. As can be seen, our calculations for bound states are close to the cross sections obtained in the dynamical eikonal approximation. In this graphs at Fig.13, Fig. 14 and table 10, the data from these papers [11] and [18] may have an error of ≈5%, because we could make some deviations while digitizing the data from the graphs of these works [11, Fig. 4] and [18, Fig. 11] and there are still errors in the numerical integration according to Simpson (the accuracy is $\varepsilon \approx 10^{-3}$, the integration step is h=0.25 fm).

Table 10 − The comparison of our data at E=0.5 MeV and E=0.3 MeV with the results of [11,18], calculated with eikonal approximation at 20 MeV/nucleon

$d\sigma(E = 0.5\ \text{MeV}, b_{max} = 400\ \text{fm})/dE$, b/MeV			by dynamical eikonal approximation from [11, Fig. 4]
angular grid	with only bound states (b.s.)	b.s. + 3 resonances	
N=25	2.205	2.585	1.678
N=49	2.0389	2.411	
N=81	2.0384	2.410	
$d\sigma(E = 0.3\ \text{MeV}, b_{max} = 400\ \text{fm})/dE$, b/MeV			by dynamical eikonal approximation from [18, Fig. 11]
angular grid	with only bound states	b.s. + 3 resonances	
N=25	2.5893	2.910	2.409
N=49	2.4425	2.756	
N=81	2.4398	2.754	

In several works [47, 48], it was considered the influence of the resonance state ($1/2^{\pm}$, $3/2^{\pm}$ and $5/2^{+}$) to the breakup of ^{11}Be nucleus at intermediate energies using different targets. These calculations, based on the no-recoil DWBA and XCDCC (the extended version of the continuum-discretized coupled-channels) methods, showed indeed that the main contribution to the lower energy angular distribution arises from the single-particle excitation mechanism populating the $5/2^{+}$ resonance, whereas for the higher energy angular distribution the main contribution comes from the excitation of the $3/2^{+}$ resonance due to the collective excitation of the ^{10}Be core [55, 56].

3.3 The breakup cross section including neutron interaction with the core in the final state

Since one of the main objectives of the work is to study the influence of resonant states of ^{11}Be on the reaction of its breakup, it becomes necessary to take into account the resonant and nonresonant nuclear interaction of the neutron with the core in the continuum spectrum in the final state of the reaction. Therefore, we also use the alternative formula for the breakup cross section including neutron interaction with the core in the final state of the breakup process [3, 13, 23]:

$$\frac{d\sigma_{bu}}{dE}(E) = \frac{4\mu k}{\hbar^2}\int_{b_{min}}^{b_{max}} \sum_{j=l+s}\sum_{lm} \left| \int \phi_{lj}(kr)\, Y_{lm}(\hat{r})\Psi(\mathbf{r}, T_{\text{out}}) d\boldsymbol{r}\right|^2 bdb. \qquad (3.3)$$

Here $\phi_{lj}(kr)$ is the radial part of the eigenfunction of the Hamiltonian H_0(r) (2.3.2) in the continuum spectrum ($E = \frac{k^2\hbar^2}{2\mu} > 0$)), normalized to $j_l(kr)$ as $kr \to \infty$ if $V(r)=0$. To find the states of the continuous spectrum of problem Eq. (2.20), we used the method of reducing the scattering problem to a boundary value problem, described in the work [24]. Summation over (l, m) in (3.3) includes all 16 partial waves up to $l_{\max}$= 3 inclusive, as in (3.2) [3].

Since the wave functions $\phi_{lj}(kr)$ of the continuum spectrum of the Hamiltonian Eq.(2.3.2) are orthogonal to the states of the discrete spectrum of the same Hamiltonian, the elimination (3.1) of the bound states from the neutron wave packet after collision with the target is not required here.

In Fig. 20, we demonstrate that including the resonant states between the neutron and the ^{10}Be-core into the model improves the agreement of the calculated breakup cross sections with most accurate experimental data available at 69 MeV/nucleon [17]. Here it is showed that the effect of interaction of the neutron with the core at the final state of the breakup reaction (3.3) does not make a significant contribution to the cross section at intermediate energies around 70 MeV/nucleon.

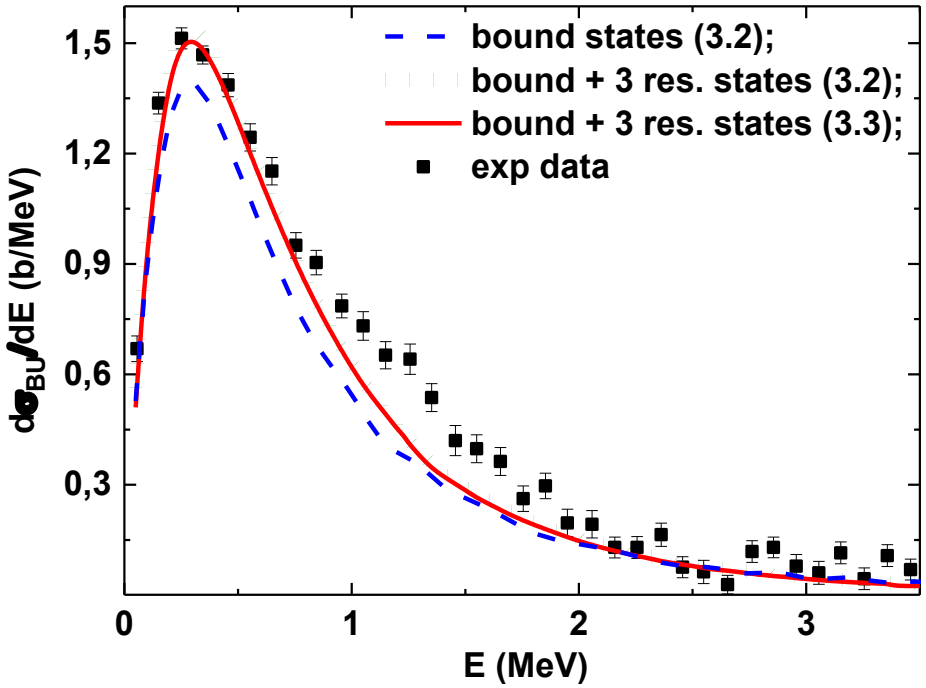

Figure 20 – Comparison of the calculated breakup cross sections with experimental data [17] at 69 MeV/nucleon. Calculations were performed by formula (3.2) with only bound states in the interaction between the neutron and the ^{10}Be-core (blue dashed curve) and with bound and three resonant states ($5/2^+$, $3/2^-$, $3/2^+$) in the interaction (green dots). The case of including both bound and resonant states, as well as the interaction of the neutron with the core in the final state of the breakup reaction by (3.3) is also presented (red solid curve). Convolution of the calculation with the experimental resolution was not performed.

Figure 21 and 22 demonstrate the contribution to the breakup cross sections of the resonant states $5/2^+$, $3/2^-$ and $3/2^+$ at a beam energy of 10 and 5 MeV/nucleon. The breakup cross sections were calculated by formula (3.2), which approximated the continuum of the neutron in the final state of the breakup by the Bessel functions (dashed and dotted curves). The differences on the peaks between the dashed and dotted curves is due to the influence of low-lying resonances ($5/2^+$, $3/2^-$ and $3/2^+$) [3]. Calculations with formula (3.3) taking into account the interaction of the neutron with the ^{10}Be-core at the final state of the breakup (red solid curve) are also presented here.

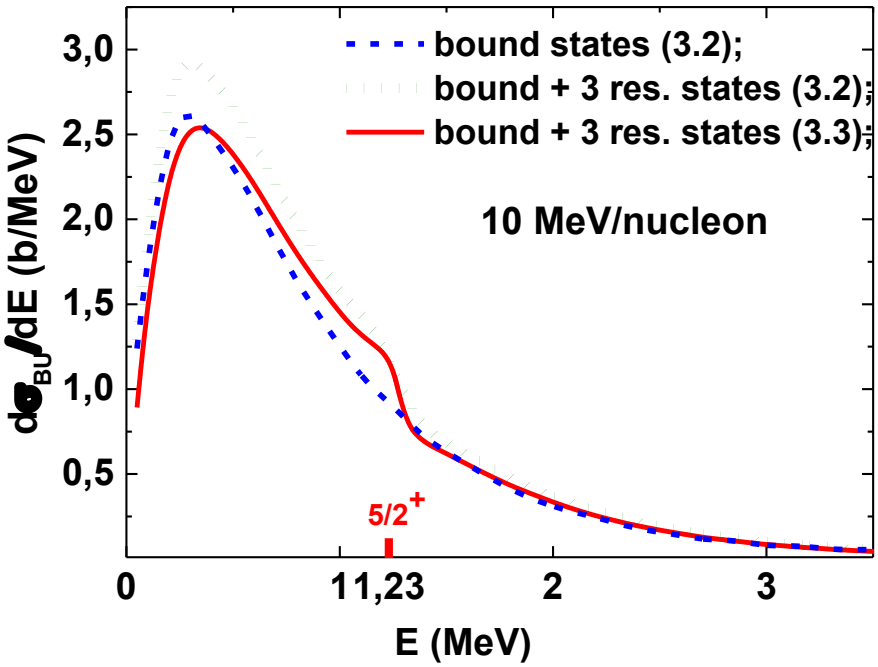

Figure 21 – The contribution to the breakup cross section of the resonant states and the neutron interaction with the core in the continuum at 10 MeV/nucleon. The calculations are performed at N = 81.

It is shown that the inclusion of the neutron-core interaction in the final state of the breakup reaction considerably corrects the breakup cross sections (see the difference between the dotted and solid curves in Fig.21 and Fig.22): taking into account the nuclear interaction (resonant and nonresonant) of the neutron released in the breakup reaction with the ^{10}Be core leads to a decrease in the breakup cross section and a shift of its peak to the region of higher energies. This effect decreases with increasing beam energy and practically disappears at 69 MeV/nucleon (see Fig.20).

Overall, the relative energy spectra of the fragments (neutron and core) were calculated for the Coulomb breakup of ^{11}Be on the ^{208}Pb target in the range 5 – 70 MeV/nucleon of beam energies. In Fig. 23 we present the results of the calculations, which take into account the influence of the resonant states ($5/2^+$, $3/2^-$, $3/2^+$) and the effect of the neutron-core interaction in the final state (3.3) to the breakup cross section of the ^{11}Be nucleus.

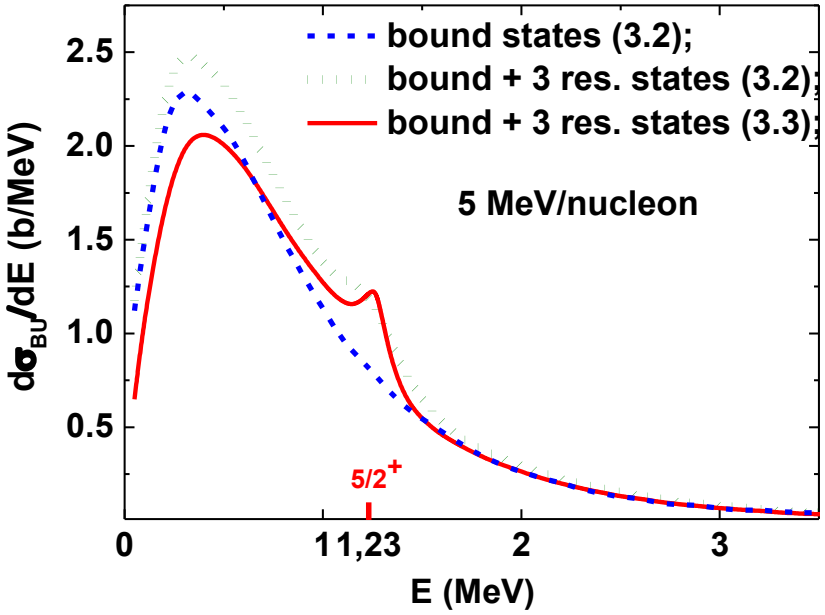

Figure 22 – The contribution of the resonant states and the neutron-core interaction in the final state to the breakup cross section at 5 MeV/nucleon. The calculations are performed at N = 81.

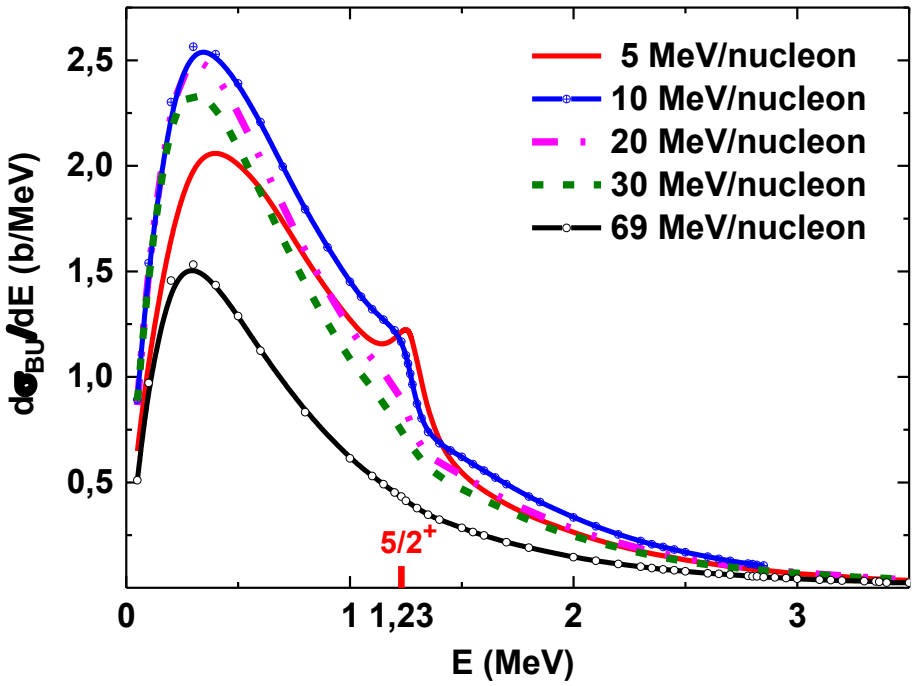

Figure 23 – The breakup cross section $d\sigma_{bu}(E)/dE$ calculated for different beam energies by formula (3.3). In the calculation the bound and three resonant states were included in the neutron-core interaction.

The analysis performed demonstrates a strong dependence of the calculated cross sections on the beam energy and an increase in their sensitivity to low-lying resonance $5/2^+$ with decreasing energy [57]. This also confirms the possibility of studying low-lying resonances in halo nuclei using their Coulomb breakup reactions [3].

3.4 Contribution to breakup of nuclear interaction between projectile and target

The interaction $V_C(\mathbf{r}, \mathrm{t})$ of the target with the projectile (Eq.(2.3) in subsection 2.1) was assumed to be purely Coulombic. As it has been shown in previous studies with time-dependent nonperturbative approach [13], for breakup reactions with a heavy target (^{208}Pb), the contribution of the nuclear part of the projectile-target interaction in the breakup cross sections is negligible around 70 MeV/nucleon. In this section we evaluate this effect at low beam energies following the approach of optical potential for the nuclear part $\Delta \mathrm{V}_N(\boldsymbol{r}, t) = \mathrm{V_{cT}}\,(\mathrm{r_{cT}}) + \mathrm{V_{nT}}\,(\mathrm{r_{nT}})$ between the target and projectile-nuclei interaction

$$V(\mathbf{r}, \mathrm{t}) = V_C(\mathbf{r}, \mathrm{t}) + \Delta \mathrm{V}_N(\mathbf{r}, \mathbf{t}). \tag{3.4}$$

Here $\mathrm{r_{cT}}$ and $\mathrm{r_{nT}}$ are the core-target $\mathbf{r}_{\mathrm{cT}} = \mathbf{R}(\mathrm{t}) + \mathrm{m}_n\mathbf{r}/\mathrm{M}$ and neutron-target $\mathbf{r}_{\mathrm{nT}} = \mathbf{R}(\mathrm{t}) - \mathrm{m_c}\mathbf{r}/\mathrm{M}$ relative variables and optical potentials $\mathrm{V_{cT}}$ and $\mathrm{V_{nT}}$ have the form:

$$\mathrm{V_{xT}}\,(\mathrm{r_{xT}}) = -\mathrm{V_x}\,\mathrm{f}(\mathrm{r_{xT}}, \mathrm{R_R}, \mathrm{a_R}) - \mathrm{i}\,\mathrm{W_x}\,\mathrm{f}(\mathrm{r_{xT}}, \mathrm{R_I}, \mathrm{a_I}) \tag{3.5}$$

with Woods-Saxon form factors $\mathrm{f}(\mathrm{r_{xT}}, \mathrm{R_R}, \mathrm{a_R}) = (1 + \exp(\frac{\mathrm{r_{xT}} - \mathrm{R}}{\mathrm{a}}))^{-1}$, where *x* stands for either core or neutron. More details of calculations with optical potential (3.5) are given in Appendix B.

In a simple analysis of this theory, the real term of (3.5) is reviewed as responsible for the elastic scattering while the imaginary part of (3.5) simulates the non-elastic processes. Because these processes somehow "absorb" the flux of probability from the elastic channel, the imaginary term is also known as the absorption term.

The analytical expression of such potentials is obtained by selecting the parameters of general form factors so as to fit the calculated scattering cross sections onto experimental data. A compilation of optical potentials for different projectiles and targets can be found in Ref. [58-61]. We use here the parameters of the optical potentials (3.5) from the paper [13], which are given in Table 11.

Table 11 − Parameters of the core-target and neutron-target optical potentials.

c or n	V_x (MeV)	W_x (MeV)	R_R(fm)	R_I(fm)	a_R(fm)	a_I(fm)
^{10}Be	70.0	58.9	7.43	7.19	1.04	1.0
n	28.18	14.28	6.93	7.47	0.75	0.58

In the previous sections, the Coulomb interaction is modeled by a point Coulomb potential while the nuclear interaction is simulated by a simple impact parameter cutoff. This is known as the black-disk approximation. It means that the interaction between the target and the projectile core and fragment is assumed to be purely Coulombic above a certain impact parameter b_{min}. Below that limit, the interaction is assumed to be dominated by nuclear forces that lead to strong inelastic reactions. From this viewpoint, only the trajectories with impact parameters above the cutoff are taken into account to compute the breakup cross section.

In the previous calculations for pure Coulomb approximation Eqs. (3.2 and 3.3), the nuclear interaction effects were simulated by a cutoff b_{min}=12 fm of the impact parameter. The inclusion of nuclear interaction $\Delta V_N(\boldsymbol{r}, t)$ between the projectile and the target requires the reduction of the impact parameters cutoff to b_{min}=5 fm [57].

Figure 24 illustrates the calculations of breakup cross section with pure Coulomb (3) and additional nuclear part of interaction (3.4) for lower beam energy of 10 MeV/nucleon taking into account bound and three resonant states [54]. Also the results obtained by Coulomb potential (3) with considering only two bound states are given for comparison. It is shown that the cutoff Coulomb approximation (3) underestimates the breakup cross section including the nuclear interaction between the projectile and the target (3.4) and the inclusion of three resonance states into the breakup reaction considerably corrects the breakup cross sections, especially near the resonant energy 1.23 MeV of the $5/2^+$ resonance [3, 54].

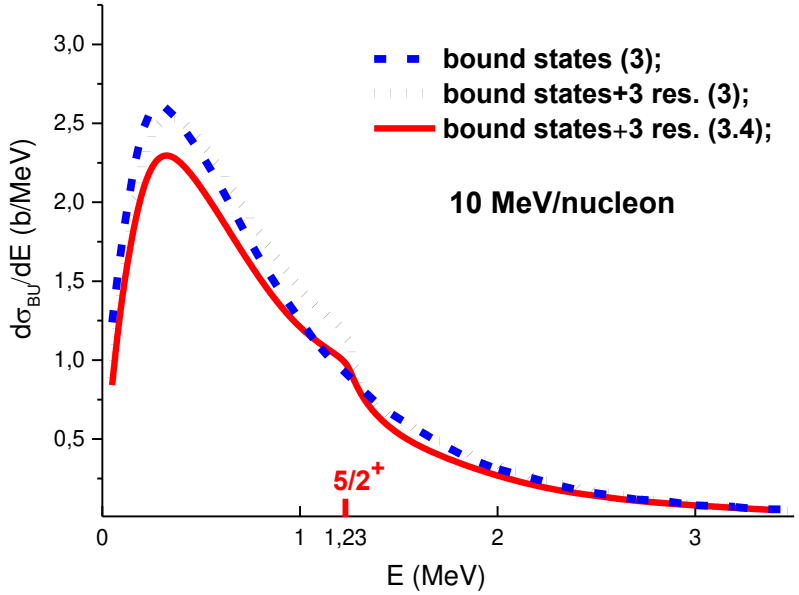

Figure 24 – Breakup cross sections calculated with only bound states (dotted curve) in the interaction between the neutron and the ^{10}Be-core and taking into account three resonant states (dashed curves) for pure Coulomb potential (3) and with (3.4) adding of nuclear interaction (full lines) between the projectile and target for the case of including both bound and resonant states ($5/2^+$, $3/2^-$ and $3/2^+$) at 10 MeV/nucleon.

The breakup cross sections calculated with Coulomb and additional nuclear part of interaction are compared in figures 25 and Fig.26 for beam energies of 30 (see Fig.25) and 20 (see Fig.26) MeV/nucleon. It is shown that the cutoff Coulomb approximation Eq.(2.3) underestimates the breakup cross section including the nuclear interaction between the projectile and the target Eq.(3.4) [3]. In the calculation, as well as in the previous sections, two bound states (ground ½+ and first excited ½- states) and three resonance states ($5/2^+$, $3/2^-$ and $3/2^+$) of ^{11}Be were taken into account. The calculation were performed on the angular grid giving convergent results with N=121 grid points. The difference between the linear and realistic trajectories is discussed in the next subsection 3.5.

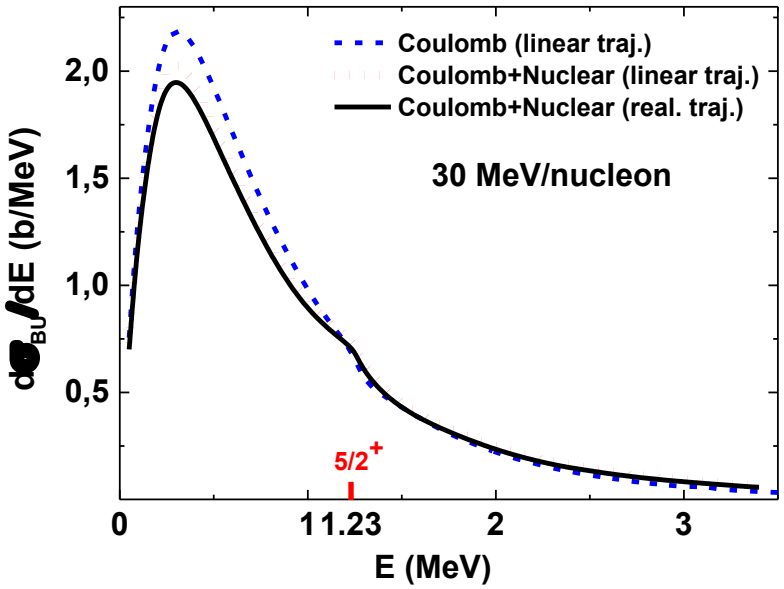

Figure 25 – Breakup cross sections calculated with semiclassical approach using linear trajectories of the projectile with pure Coulombic projectile-target interaction (Eq.2.3) and with inclusion of nuclear effects (Eq.3.4) at 30 MeV/nucleon. The solid curves indicate the $d\sigma_{bu}(E)/dE$ with quantum-quasiclassical approach including the Coulombic and nuclear projectile-target interaction (Eq.3.4).

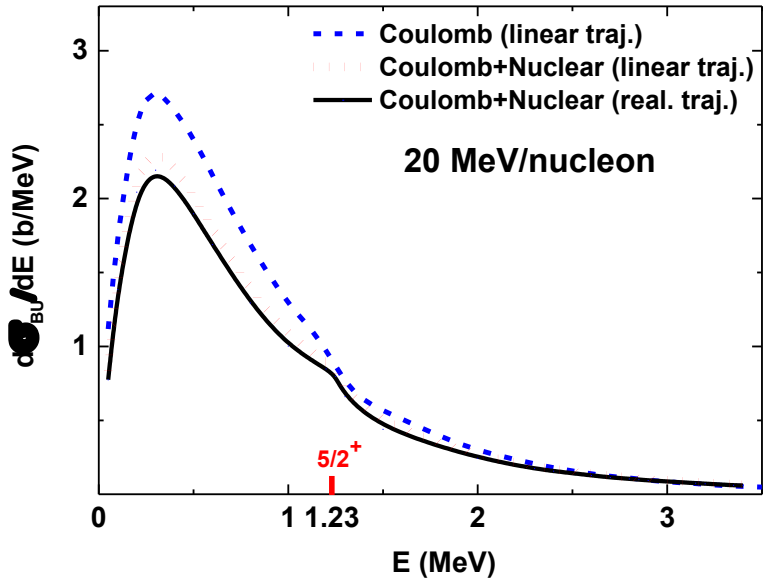

Figure 26 – Breakup cross sections calculated with linear trajectories of the projectile for pure Coulombic (Eq.2.3) and adding of nuclear interactions between projectile and target (Eq.3.4) at 20 MeV/nucleon. An account of the curvature of the projectile trajectory and nuclear effects in calculating the $d\sigma_{bu}(E)/dE$ are illustrated by solid lines.

In conclusion, it can be seen that with a decreasing of beam energy, the influence of the nuclear effect in the projectile-target interaction becomes more significant for the breakup cross section. The contribution from the resonance states remains noticeable when the nuclear interaction between the target and the projectile is included, and the peak due to the $5/2^+$ resonance is still clearly visible at low beam energies. Note that a noticeable manifestation of nuclear effects in the differential cross section for the breakup of the ^{11}Be on ^{208}Pb at 12.7 MeV/nucleon was also pointed out in the recent work [30], where the experimental data were analyzed with the CDCC method.

3.5 How good is the linear trajectory approach for projectile motion at low energies

To quantify how good the semiclassical approach with decreasing the projectile energy is, we also performed calculations with hybrid quantum-quasiclassical approach [25, 26], which includes the effect of deformation of the projectile trajectory and the transfer of energy from target to projectile and vice versa during a collision. In this approach [25] simultaneously with the time-dependent Schrödinger equation (2.1) for the halo-nucleon wave function $\Psi(\mathbf{r}, t)$ we integrate the set of Hamilton equations

$$\frac{d}{dt}\boldsymbol{P} = -\frac{\partial}{\partial \boldsymbol{R}} H_{BP}\left(\boldsymbol{P}, \boldsymbol{R}, t\right), \quad \frac{d}{dt}\boldsymbol{R} = -\frac{\partial}{\partial \boldsymbol{P}} H_{BP}\left(\boldsymbol{P}, \boldsymbol{R}, t\right), \tag{3.6}$$

describing relative projectile-target dynamics. Here, the classical Hamiltonian $H_{BP}(\mathbf{P}, \mathbf{R}, t)$ is given by

$$H_{BP}\left(\boldsymbol{P}, \boldsymbol{R}, t\right) = \frac{\boldsymbol{P}^2}{2M} + \left\langle \Psi(\boldsymbol{r}, t) \left| \frac{Z_C Z_T e^2}{\left|\frac{m_n \boldsymbol{r}}{M} + \boldsymbol{R}(t)\right|} + \Delta V_N(\boldsymbol{r}, t) \right| \Psi(\boldsymbol{r}, t) \right\rangle, \tag{3.7}$$

where the last term $\langle\Psi(\mathbf{r}, t)|...|\Psi(\mathbf{r}, t)\rangle$ represents the quantum-mechanical average of the projectile-target interaction over the halo-nucleon density instantaneous distribution $|\Psi(\mathbf{r}, t)|^2$ during the collision.

Thus, the Hamiltonian (3.7) defined in such a way has a parametric dependence on the halo-neutron position $\mathbf{r}(t)$ at every time moment. The inclusion of the strong coupling between the projectile and the target in the computational scheme insures that the effect of deformation and "vibration" of the projectile trajectory, as well as the transfer of energy from the target to the projectile and vice versa, are taken into account at the moment of collision. The required stability and accuracy of the integration of Eq. (3.6) with the same step of integration over time as the time-dependent Schrödinger equation (1) was ensured by using a computational difference scheme developed in [26, 62] based on the Störmer–Verlet method.

The breakup cross sections with the hybrid quantum-quasiclassical approach are presented in Figures 20-23 in comparison with the results of the semiclassical calculations using linear trajectories for a projectile for beam energies 30 (graph 25 at

subsection 3.4), 20 (graph 26 at subsection 3.4), 10 (graph 27) and 5 MeV/nucleon (graph 28). Dashed curves indicate results obtained with pure Coulombic projectile-target interaction (Eq.2.3) and dots—with the interaction (Eq.3.4) where nuclear effects are also included in the frame of semiclassical approach with linear projectile trajectories. The solid curves indicate the results of calculations with quantum-quasiclassical approach (realistic trajectory of the projectile) including the Coulombic projectile-target interaction as well as the nuclear interaction in the interaction potential (Eq.3.4)

The study shows that in the energy range 30–20 MeV/nucleon the difference between the two approaches does not exceed several percent (graphs 25 and 26 of previous subsection) and reaches a significant one starting from 10 MeV/nucleon (graph 27). For 10 MeV/nucleon, the discrepancy is about 10% (see Fig.27), and for 5 MeV/nucleon it reaches a value of more than 20% (as seen at graph 28). If for energies up to 10 MeV/nucleon this difference does not exceed the contribution of nuclear effects in the breakup cross sections, then for 5 MeV/nucleon this distinction already exceeds the effect of the nuclear interaction.

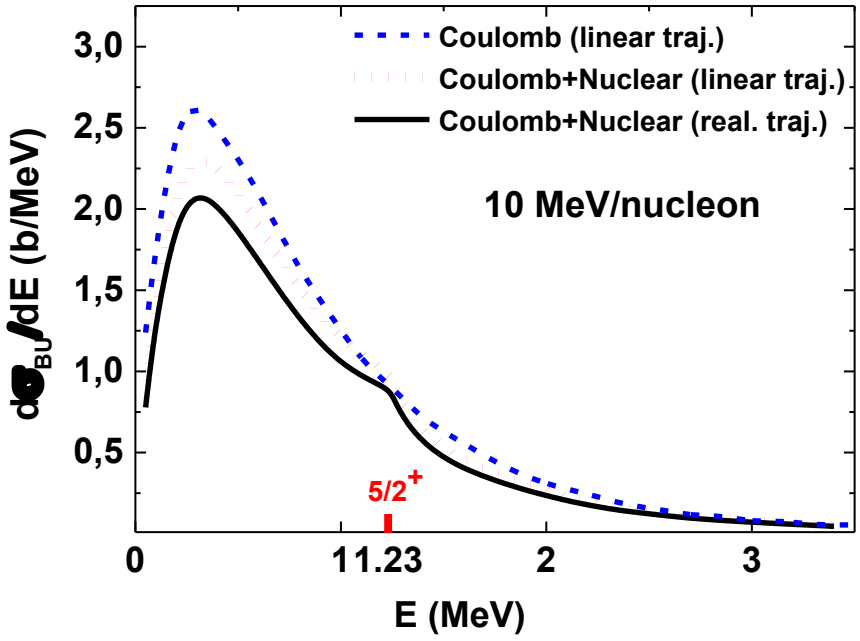

Figure 27 – Breakup cross sections with pure Coulombic projectile-target interaction and including nuclear effects calculated with linear and curvilinear (realistic) trajectories of the projectile for a beam energy of 10 MeV/nucleon.

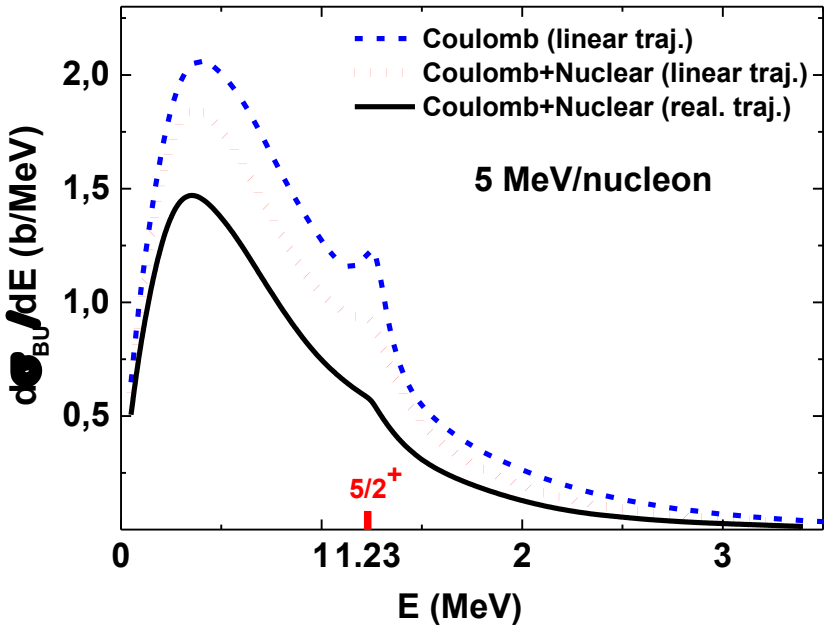

Figure 28 – Breakup cross sections calculated with semiclassical approach using linear trajectories of the projectile and with quantum-quasiclassical approach (realistic trajectory) at 5 MeV/nucleon for pure Coulombic and nuclear projectile-target interactions.

Figure 29 shows the dependence of the coordinates Z(X) (here the positions $Z=Z_0+\mathbf{v}t$, $X=\mathbf{b}$, which are formulate the relative coordinate between the projectile and target $\mathbf{R}(t) = \mathbf{b} + \mathbf{v}_0 t$ (Y=0)) in curvilinear coordinate at a fixed impact parameter (b= 311 fm) at different beam energies: 20, 30 and 69 MeV/nucleon. As can be seen from graphs, when the curvature of the projectile trajectory is taken into account, oscillations of the trajectory, i.e. deformation effect is visible.

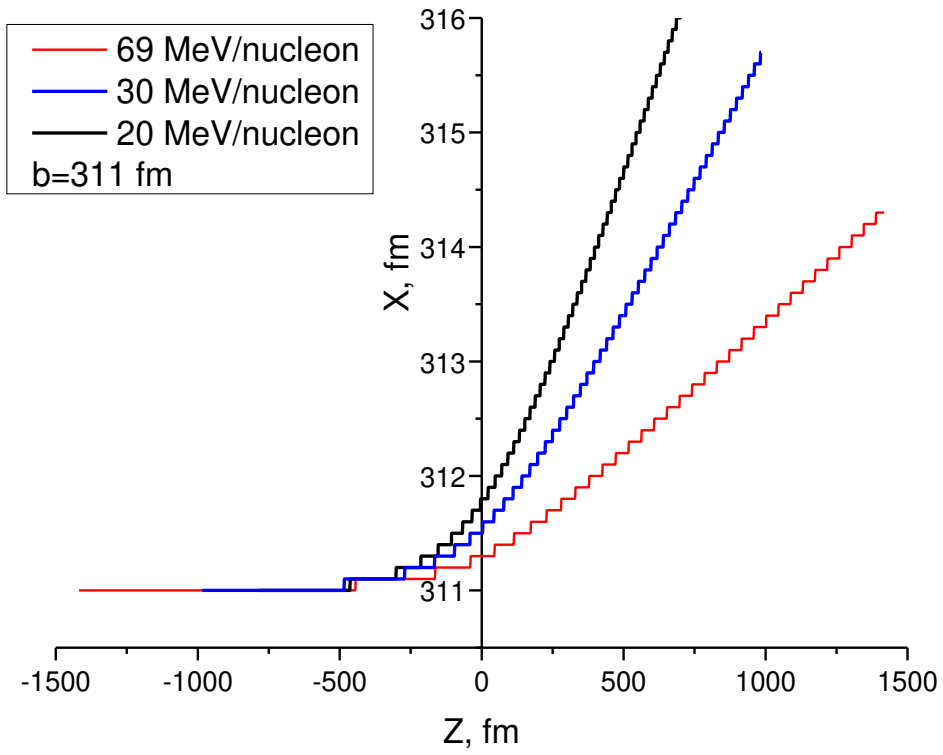

Figure 29 – Dependence of Z(X) in curvilinear coordinate at a fixed impact parameter b = 311 fm at different beam energies 20, 30 and 69 MeV/nucleon.

At figure 30 the dependence of the coordinates Z(X) of the projectile trajectory calculated by quantum-quasiclassical approach is illustrated for different impact parameters at the fixed collision energy of 20 MeV/nucleon.

Thus, the study performed demonstrates that the semiclassical approach with linear trajectories of the projectile provides a satisfactory accuracy in calculating the breakup cross sections of ^{11}Be up to 20 - 30 MeV/nucleon. It is shown that this approach is also useful at lower energies, where, however, a more adequate description is provided by the quantum-semiclassical approach [3].

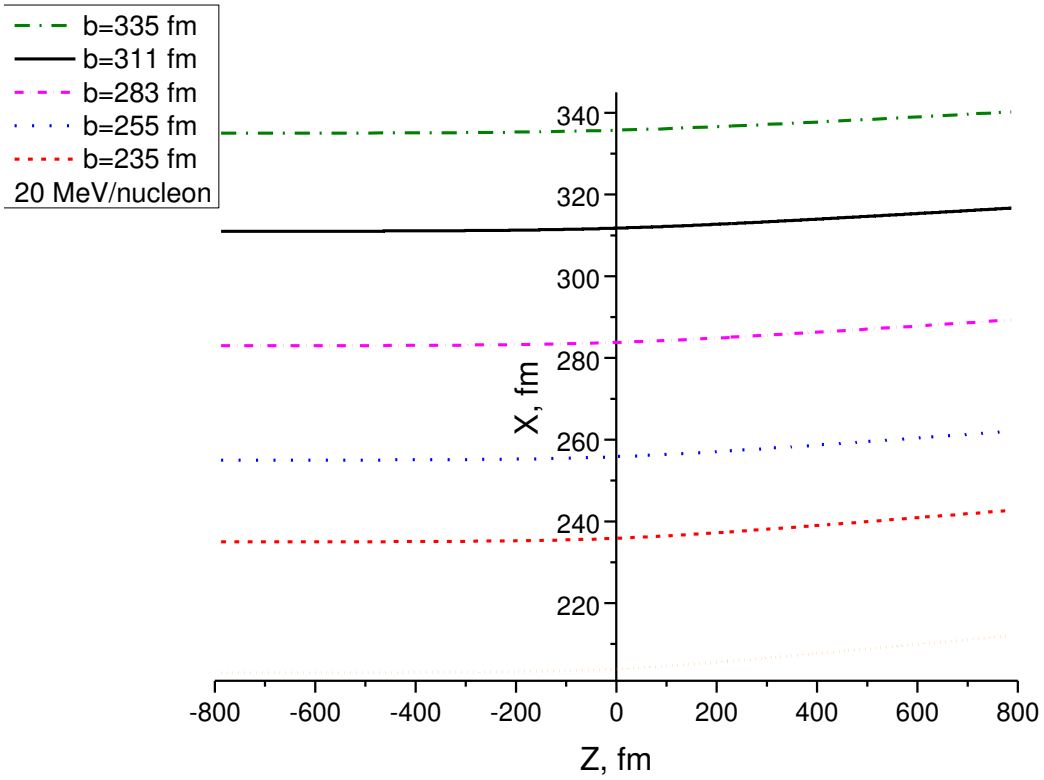

Figure 30 – Dependence of Z(X) in curvilinear coordinate at 20 MeV/nucleon for different impact parameters b.

3.6 Excitation of ^{11}Be in collision with ^{208}Pb

We have also calculated the transition probability P_{lj} during the collision of ^{11}Be with ^{208}Pb to the excited state ½- with the energy $E_{l=1,j=1/2}$= - 0.183 MeV

$$P_{lj}(b) = \frac{1}{2}\sum_m \left| < \varphi_{ljm}(E_{lj}, \boldsymbol{r}) \middle| \psi\,(\boldsymbol{r}, T_{out}) > \right|^2, \tag{3.8}$$

and the corresponding inelastic cross section

$$\sigma_{exc}(E) = 2\pi \int_0^\infty P_{lj}(b)\, b\, db \ . \tag{3.9}$$

First, in order to evaluate the contribution of the E1 transition in the excitation cross sections (3.9), we perform calculations using only the electric dipole term in the time-dependent potential (2.3). In other words, the time-dependent Coulomb potential is replaced by the first term of its multipole expansion:

$$V_C^{E_1}(\boldsymbol{r}, t) = -Z_C Z_T\, e^2\, \frac{m_n}{M} \frac{(\boldsymbol{r}\cdot\boldsymbol{R}(t))}{R(t)^3}\,. \tag{3.10}$$

The transition probabilities (3.8) and cross sections (3.9) were also calculated for pure Coulomb projectile-target interaction (3) and with including nuclear effects between the target and the projectile (3.4) [3, 57].

These results are presented in figure 31 for beam energy of 69 MeV/nucleon. They demonstrate a pure Coulomb mechanism of excitation of the $1/2^-$ state of ^{11}Be with the overhelming dominance of the E1 transition for impact parameters b > 15 fm. With a decrease of b, the excitation probability of the $1/2^-$ state sharply decreases due to the influence of the nuclear interaction between the target and the projectile [3].

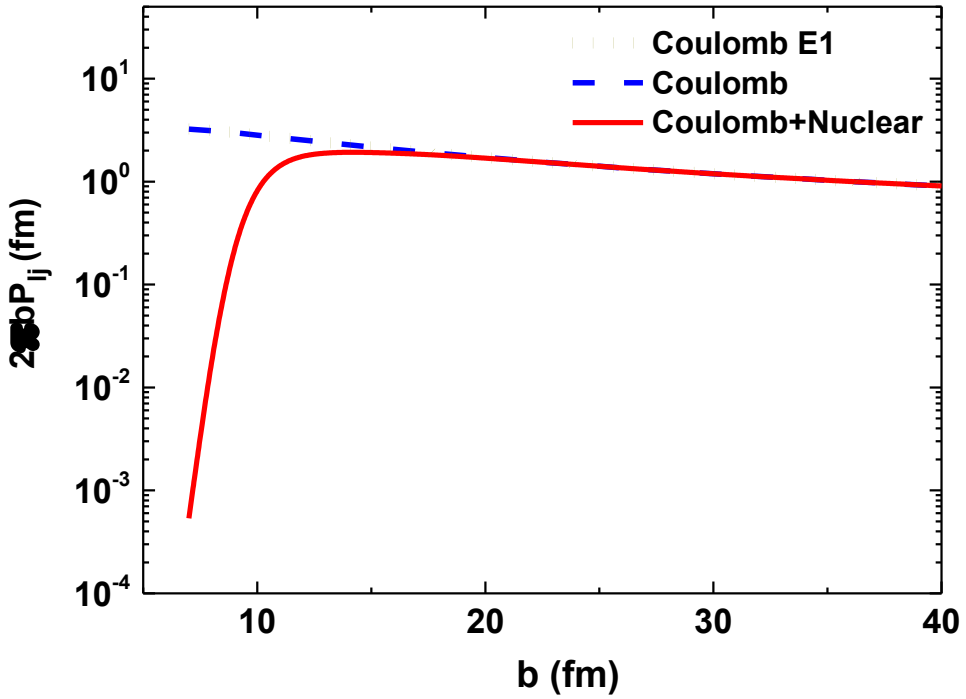

Figure 31 – The transition probabilities $P_{ij}(b)$ (multiplied by $2\pi b$) during the collision of ^{11}Be with ^{208}Pb to the $1/2^-$ state, calculated with optical potentials (full line) and with pure Coulomb excitation (dashed lines) in comparison with E1 dipole (dotted line) at 69 MeV/nucleon.

The excitation probabilities $P_{ij}(b)$ (multiplied by $2\pi b$) calculated at low colliding energies are presented in Fig.32. The probabilities calculated with including nuclear effects are smaller than those with a pure Coulomb interaction between the target and projectile. It is seen that the lower the projectile energy, the more influence has a nuclear effect. For all considered projectile energies starting from b = 15−20 fm the calculated excitation probabilities are determined by the Coulomb interaction between the projectile and the target. We may conclude that the choice of minimal impact parameter b_{min}= 12 fm as a cutoff approximation in the previous calculations for 72 MeV/nucleon at [13] was realistic, since the contribution of nuclear effects completely reduces the transition probability below b = 12 fm [57].

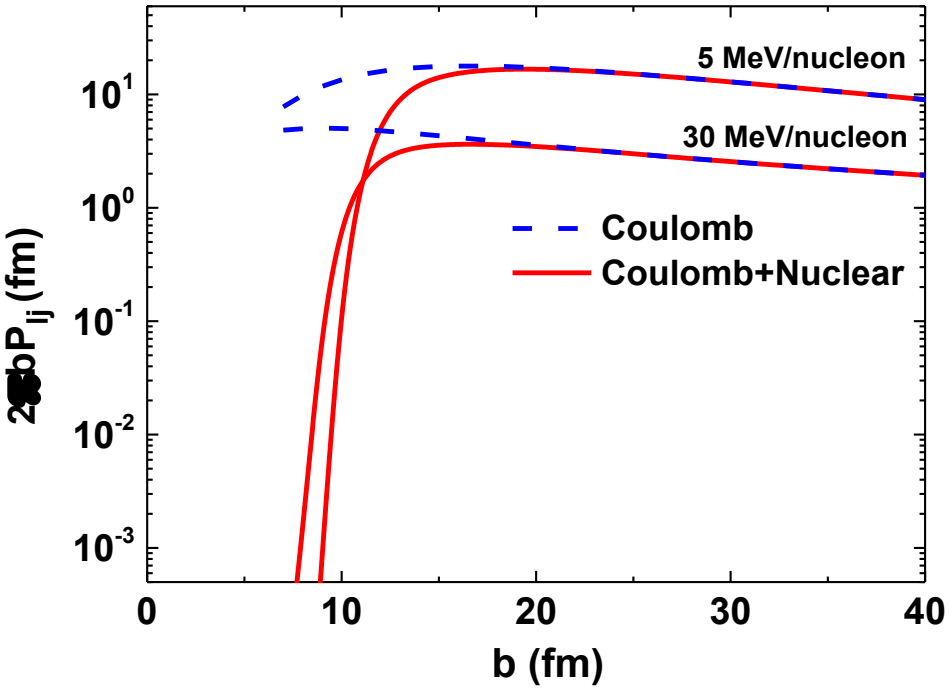

Figure 32 – Excitation probabilities $P_{ij}(b)$ (multiplied by $2\pi b$) of ^{11}Be in collision with ^{208}Pb to the 1/2$^-$ state, calculated with optical potentials (full line) and with only Coulomb excitation (dashed lines) at 30 and 5 MeV/nucleon.

The calculated excitation cross section of the 1/2− state of ^{11}Be (3.9) are given in Fig. 33 as a function of the projectile energy per nucleon for pure Coulomb and Coulomb plus nuclear induced excitations. A monotonic increase of the inelastic cross section (3.9) with decreasing projectile energy is observed. Also, it is noted that the difference between the calculation with only pure Coulomb projectile-target interaction and the one including also optical potentials increases for lower beam energies [3, 57].

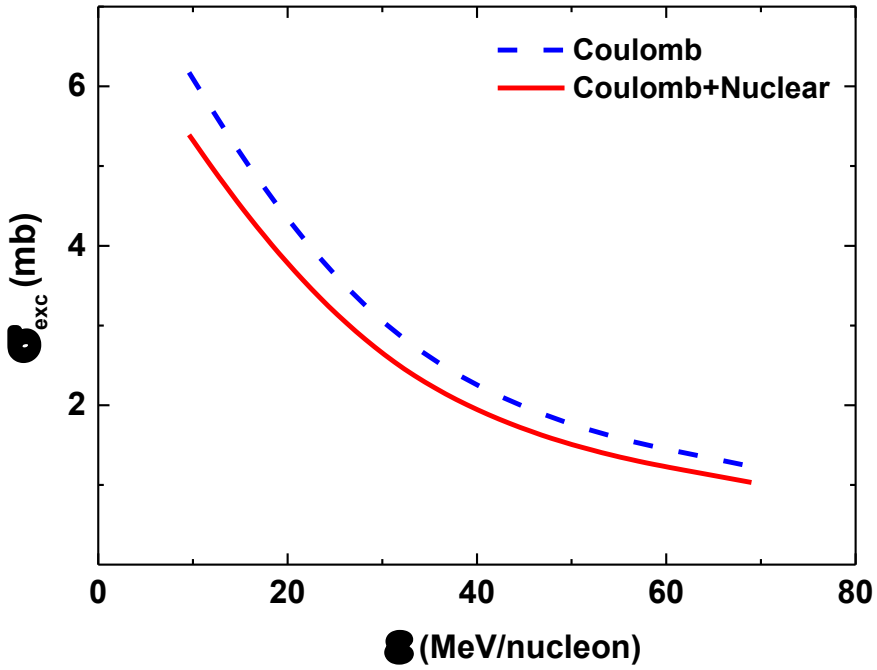

Figure 33 – Inelastic cross section to the ½⁻ excited state of ^{11}Be as a function of the projectile energy per nucleon ϵ (in MeV/nucleon) in comparison with pure Coulomb (dashed line) and with including nuclear interactions (full line).

The breakup probability per energy unit is given by

$$\frac{dP}{dE}(E,b) = \frac{2\mu}{\pi\hbar^2 k}\frac{1}{2j_0+1}\sum_{m_0}\sum_{ljm} | < \phi_{ljm}(E,r)|\psi^{(m_0)}(r,+\infty) > |^2, \quad (3.11)$$

where k is the wave number [13] . It includes a complete distortion of the scattering of the projectile's eigenstates. Then the alternative formula for the breakup cross section is:

$$\frac{d\sigma_{bu}}{dE}(E) = 2\pi\int_0^\infty \frac{dP}{dE}(E,b)bdb\ . \quad (3.12)$$

The breakup probabilities calculated with pure Coulomb (angular grid N=49) and adding nuclear (angular grid N=81) optical potential is illustrated in figure 34 as a function of the impact parameter b (fm) for a relative energies E=0.5 and 1,5 MeV at 72MeV/nucleon. The comparison of the breakup probabilities calculated with and without nuclear optical potential suggests that the cutoff impact parameter $b_{\min}$ should depend on energy in order to simulate nuclear effects. When we fit $b_{\min}$ to obtain the same breakup cross section in a pure Coulomb breakup approximation as in a calculation involving an optical potential the $b_{\min}$ values calculated at the energies of Fig. 34 are 12.5 fm at 0.5 MeV, 9.1 fm at 1.5 MeV. Therefore the choice of an adequate impact parameter lower bound $b_{\min}$ in a cutoff approximation is not straightforward. Because of the simplicity of the present treatment, the modeling of

the projectile-target nuclear interaction is better taken into account with an optical potential [13].

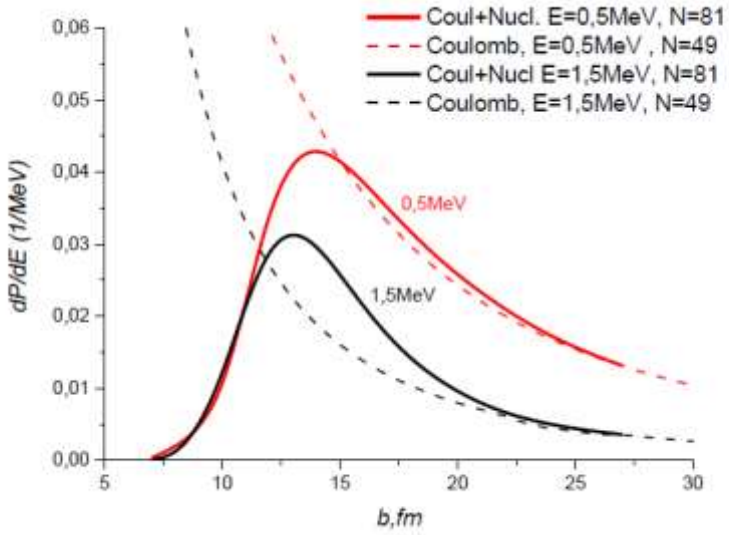

Figure 34 – Breakup probability per MeV of ^{11}Be on a ^{208}Pb as a function of the impact parameter b (fm) for E=0.5 and 1,5 MeV at 72MeV/nucleon with a pure Coulomb and adding nuclear interactions.

Overall, the influence of nuclear interaction to the Coulomb breakup of one-neutron halo nuclei on a heavy target has been studied within the non-perturbative time-dependent approach for low beam energies (5–30 MeV/nucleon) including the low-lying resonances in different partial and spin states of Be. The theoretical model, developed in [1, 8, 9], has been extended to low-energy region. In the frame of this model we evaluated the breakup cross sections of ^{11}Be on a heavy target of ^{208}Pb at energies 5– 30 MeV/nucleon with Coulomb and nuclear interactions between projectile and target. The performed research of the projectile trajectories demonstrates that the semiclassical approach with linear trajectories of the projectile provides a satisfactory accuracy in calculating the breakup cross sections of ^{11}Be up to 20 - 30 MeV/nucleon. However, a more adequate description is provided by the quantum-semiclassical approach for lower collision energies (5-10 MeV/nucleon).

CONCLUSION

The aim of the work is a theoretical study of the Coulomb breakup of the ^{11}Be halo nuclei on heavy target from intermediate (70 MeV/nucleon) to low energies (5 MeV/nucleon) within non-perturbative time-dependent approach. The Coulomb breakup of halo nuclei is one of the main tools in studying the properties of halo nuclei and provides useful information about the halo structure. A theoretical study of exotic nuclei by quantum-mechanical approach is relevant in connection with the planned experiments aimed to investigate the properties of light nuclei on radioactive beams.

The main results obtained in the dissertation:

In the first part of the research the theoretical determination of the exotic structure, the description of the halo nucleus is considered. The peculiar properties of exotic systems and some definitions of halo nuclei from theoretical view are described. It also provides an overview of some experiments with nuclear reactions that are important in the field of study of this topic. In this part of the thesis, the non-perturbative time-dependent approach in studying the Coulomb breakup of one-neutron halo nuclei is represented. The used three dimensional mesh approximations has the advantage that any local interaction is diagonal in such a representation. As a consequence, it allows avoiding the use of the multipole expansion of the time-dependent Coulomb interaction between the projectile and the target and the straight-line approximation for the projectile trajectory [25]. The splitting up procedure suggested in [12] and [62] permitted us to include correctly the resonances in different partial and spin states of ^{11}Be [3].

The following results were obtained:

– a quantitative model has been developed to describe the Coulomb breakup of one-neutron halo nuclei of ^{11}Be based on a nonperturbative solution of the time-dependent Schrodinger equation;

– the parameterization of potential between the neutron and ^{10}Be core and the results of calculating the spectrum and resonant states of the ^{11}Be, which is an important element of the computational scheme;

– the convergence of the computational scheme and accuracy of the approach is demonstrated in all considered range of the beam energy including the low-lying resonances in different partial and spin states of ^{11}Be.

The second part of the research is devoted to the calculations of the breakup cross-section, an account of low-lying resonances and the investigation of nuclear contribution into breakup reaction. Also in the framework of the dissertation thesis it was investigated the validity of using the linear trajectory approach to describe the breakup process at low collision energies.

As a result:

– The relative energy spectra of the fragments (neutron and core) were calculated for the Coulomb breakup of ^{11}Be on the ^{208}Pb target in the wide range of beam energies 5 –70 MeV/nucleon;

– The influence of the resonant states $5/2^+$, $3/2^-$ and $3/2^+$ of ^{11}Be on the breakup cross section was taken into account. These results have been compared with experimental data [16, 17] available at 69 and 72 MeV/nucleon and with existing alternative theoretical calculations of other authors [11, 18, 19] at 20 and 30 MeV/nucleon;

– In the numerical calculations performed for the incident beam energies at 5–30 MeV/nucleon, the contribution of the $5/2^+$ resonance state of ^{11}Be to the breakup cross sections is clearly visible, while at energies of 69 and 72 MeV/nucleon, resonant states $3/2^-$ and $3/2^+$ make the largest influence to breakup cross sections of ^{11}Be;

– The contribution of the neutron interaction with the core in the final state and an account of nuclear interaction between the target and projectile to the breakup cross sections was evaluated [57] at low beam energies (5 – 30 MeV/nucleon);

–The inelastic cross sections for the excitation of the ½- state of ^{11}Be in a collision with ^{208}Pb target at low beam energies are computed with inclusion of Coulomb and nuclear interactions between the target and projectile;

–The influence of the curvilinear trajectory for projectile motion is analyzed with decreasing the collision energies. It means that the effect of deformation of the projectile trajectory has been included within quantum quasiclassical approach. The differences between the linear and curvilinear (realistic) trajectories of the projectile in the analysis of the breakup reaction ^{11}Be+^{208}Pb->^{10}Be+n+^{208}Pb is about several percent in the energy range 30-20 MeV/nucleon, for 10 MeV/nucleon the discrepancy is 10% and reaches a value of more than 20% at 5 MeV/nucleon, which exceeds the effect of nuclear interaction.

The results are published in the articles and conference papers. **The tasks in the dissertation** are fully solved: the inclusion of the resonant states of ^{11}Be into the computational scheme leads to a significant improvement of the theoretical model, which gives a better agreement of the model description of the experimental data on the breakup cross sections [16, 17]. We summed up theoretical and practical experience of the carried out investigations and carefully research the processes of the Coulomb breakup of the halo nucleus of ^{11}Be, also proposed a solution to insufficiently explored problems in the region of low energies. . A lot of graphs and tables were given to illustrate the results of the work.

Recommendations. Summarizing, the results obtained in the dissertation our approach can potentially be used in further investigation of breakup reactions at low energies. In addition, the developed theoretical approach could easily deal with nuclear effects between the target and the projectile [57], which are supposed to be important in the breakup of halo nuclei on light targets. Another interesting, but more difficult application of the developed theoretical model may be breakup reactions of two-neutron halo nuclei.

In conclusion, I would like to express my hope that this dissertation work demonstrates new significant results and solutions, methods and concepts that contribute to the further development and deeper understanding of fundamental science.

In conclusion, I would like to express my deepest respect and gratitude to my first supervisor, mentor, Doctor of Physical and Mathematical Sciences, Professor Minal Dineikhan for his great contribution to my education, instilled love for science and decency, for the enormous scientific influence that he had. Under his leadership, young students of Kazakh National University got the opportunity to study and engage in science in Dubna and still closely cooperate with JINR scientists.

I would like to express my special thanks and sincere gratitude to the foreign consultant, Doctor of Physical and Mathematical Sciences, Professor Vladimir Stepanovich Melezhik for his great participation in my scientific activities, support and assistance at all stages of the work and for the discussions that took place in the N.N. Bogolyubov Laboratory of Theoretical physics of the Joint Institute for Nuclear Research, during my doctoral studies, and became the basis of my dissertation work.

I also want to thank my scientific consultant Zhaugasheva Saule Amanbaevna, Candidate of Physical and Mathematical Sciences, Associate Professor, for guidance, support and professional assistance during the dissertation research. And of course I am grateful to my family, parents and husband for their great support and understanding, patience and for giving me the opportunity to develop professionally.

REFERENCES

1 Tanihata I., Hamagaki H., Hashimoto O., Shida Y., Yoshikawa N., Sugimoto K., Yamakawa O., Kobayashi T. and Takahashi N. Measurements of interaction cross sections and nuclear radii in the light p-shell region // Physical Review Letters. – 1985. –Vol. 55. –P. 2676-2679.

2 Tanihata I. Neutron halo nuclei // Journal of Physics G: Nuclear and particle physics. –1996. –Vol. 22. –P. 157-198.

3 Valiolda D., Melezhik V.S., Janseitov D. Investigation of low-lying resonances in breakup of halo nuclei within the time-dependent approach // The European Physical Journal A. – 2022. – Vol. 58. –P 341-343.

4 Al-Khalili J. An introduction to halo nuclei, Chapter in Lecture Notes in physics. – Berlin: Springer Heidelberg, 2004. – 491 p.

5 Hebborn C., Capel P. Low-energy corrections to the eikonal description of elastic scattering and breakup of one-neutron halo nuclei in nuclear-dominated reactions // Physical Review C. –2018. –Vol. 98. –P. 0446101-0446107.

6 Typel S., Baur G. Coulomb dissociation of ^{8}B into ^{7}Be+p: Effects of multiphoton exchange // Physical Review C. –1994. –Vol. 50. –P. 2104-2115.

7 Esbensen H., Bertsch G. F. Effects of E2 transitions in the Coulomb dissociation of ^{8}B // Nuclear Physics A. –1996. –Vol. 600. –P. 37-62.

8 Tostevin J.A., Rugmai S., Johnson R.C. Coulomb dissociation of light nuclei // Physical Review C. –1998. –Vol. 57. –P. 3225-3236.

9 Suzuki Y., Lovas R.G., Yabana K., Varga K. Structure and reactions of light exotic nuclei. – London: Taylor and Francis, 2003. –608 p.

10 Kamimura M., Yahiro M., Iseri Y., Kameyama H., Sakuragi Y., Kawai M. Chapter I. Projectile breakup processes in nuclear reactions // Progress of Theoretical Physics Supplement. –1986. –Vol. 89. –P.1-10.

11 Baye D., Capel P., Goldstein G. Collisions of halo nuclei within a dynamical eikonal approximation // Physical Review Letters. –2005. –Vol. 95. –P. 0825021-0825024.

12 Melezhik V.S., Baye D. Nonperturbative time-dependent approach to breakup of halo nuclei // Physical Review C. –1999. –Vol. 59. –P.3232-3239.

13 Capel P., Baye D., Melezhik V.S. Time-dependent analysis of the breakup of halo nuclei // Physical Review C. –2003. –Vol. 68. –P. 0146121-01461213.

14 Kido T., Yabana K., Suzuki Y. Coulomb breakup mechanism of neutron drip-line nuclei// Physical Review C. –1994. – Vol. 50. –P. R1276-R1279.

15 Esbensen H., Bertsch G.F., Bertulani C.A. Higher-order dynamical effects in Coulomb dissociation // Nuclear Physics A. –1995. –Vol. 581. –P. 107-118.

16 Nakamura T., Shimoura S., Kobayashi T., Teranishi T., Abe K., Aoi N., Ishihara M. Coulomb dissociation of a halo nucleus ^{11}Be at 72A MeV // Physics Letters B. –1994. –Vol. 331. –P. 296-301.

17 Fukuda N., Nakamura T., Aoi N., Imai N., Ishihara M., Kobayashi T., Iwasaki H., Kubo T., Mengoni A., Notani M., Otsu H., Sakurai H., Shimoura S.,

Teranishi T., Watanabe Y.X., Yoneda K. Coulomb and nuclear breakup of a halo nucleus ^{11}Be // Physical Review C. –2004. –Vol. 70. –P. 0546061-05460612.

18 Goldstein G., Baye D., Capel P. Dynamical eikonal approximation in breakup reactions of ^{11}Be // Physical Review C. –2006. –Vol. 73. –P. 0246021-02460212.

19 Banerjee P., Baur G., Hencken K., Shyam R., Trautmann D. Postacceleration effects in the Coulomb dissociation of neutron halo nuclei // Physical Review C. –2002. –Vol. 65. –P. 0646021-0646027.

20 Al-Khalili J.S., Tostevin J.A., Brooke J.M. Beyond the eikonal model for few-body systems// Physical Review C. –1997. –Vol. 55. –P. R1018- R1022.

21 Aguiar C.E., Zardi F., Vitturi A. Low-energy extensions of the eikonal approximation to heavy-ion scattering // Physical Review C. –1997. –Vol. 56. –P. 1511-1515.

22 Fukui T., Ogata K., Capel P. Analysis of a low-energy correction to the eikonal approximation// Physical Review C. –2014. –Vol. 90. –P. 0346171-0346178.

23 Melezhik V.S., Baye D. Time-dependent analysis of the Coulomb breakup method for determining the astrophysical S factor // Physical Review C. –2001. –Vol. 64. –P. 0546121-05461211.

24 Melezhik V.S. Polarization of harmonics generated from a hydrogen atom in a strong laser field // Physics Letters A. –1997. –Vol. 230. –P. 203-208.

25 Melezhik V.S., Cohen J.S., Chi-Yu Hu. Stripping and excitation in collisions between p and He+(n⩽3) calculated by a quantum time-dependent approach with semiclassical trajectories // Physical Review A. -2004. –Vol. 69. –P. 0327091-032709113.

26 Melezhik V.S. Improving efficiency of sympathetic cooling in atom-ion and atom-atom confined collisions // Physical Review A. –2021. –Vol. 103. –P. 0531091-05310913.

27 Ershov S.N., Vaagen J.S., Zhukov M.V. Cluster model with core excitations. The ^{11}Be example // Physics of Atomic Nuclei. –2014. –Vol. 77, №8. –P. 989-998.

28 National Nuclear Data Center, https://www.nndc.bnl.gov/

29 Ershov S.N., Danilin B.V., Rogde T., Vaagen J.S. New Insight into Halo Fragmentation // Physical Review Letters. –1999. –V. 82. –P. 908-911.

30 Duan F.F. Yang Y.Y., Wang K., Moro A.M., Guimaraes V., Pang D.Y., Wang J.S., Sun Z.Y., Jin Lei, Pietro A.Di, Liu X., Yang G., Ma J.B., Ma P., Xu S.W., Bai Z., Sun X.X., Hu Q., Lou J.L., Xu X.X., Li H.X., Jin S.Y., Ong H.J., Liu Q., Yao J.S., Qi H.K., Lin C.J., Jia H.M., Ma N.R., Sun L.J., Wang D.X., Zhang Y.H., Zhou X.H., Hu Z.G., Xu H.S. Scattering of the halo nucleus ^{11}Be from a lead target at 3.5 times the Coulomb barrier energy // Physics Letters B. –2020. –Vol. 811. –P. 1359421-1359428.

31 Valiolda D., Melezhik V.S., Janseitov D. Contribution of Low-lying Resonances in the Coulomb Breakup of ^{11}Be Halo Nuclei// Acta Physica Polonica B Proceedings Supplement. –2021. –Vol. 14, № 4. –P. 687-692.

32 Tostevin J.A., Nunes F.M., Thompson I.J. Calculations of three-body observables in ^{8}B breakup // Physical Review C. –2001. –Vol. 63. –P. 0246171-02461710.

33 Al-Khalili J., Roeckl E. Lecture notes in Physics. –Berlin: Springer Heidelberg, 2003. –362 p.

34 Hansen P.G., Jonson B. The neutron halo of extremely neutron-rich nuclei // Europhysics Letters. –1987. –Vol. 4. –P. 409-414.

35 Riisager K., Fedorov D.V., Jensen A.S. Quantum halos // Europhysics Letters. –2000. –Vol. 49. –P. 547-553.

36 Kelley J.H., Kwan E., Purcell J.E., Sheu C.G., Weller H.R. Energy levels of light nuclei A=11 // Nuclear Physics A. –2012. –Vol. 880. –P. 88-195.

37 Hansen P.G. Studies of single-particle structure at and beyond the drip lines // Nuclear Physics A. –2001. –Vol. 682. –P. 310-319.

38 Millener D.J., Olness J.W., Warburton E.K., Hanna S.S. Strong E1 transitions in ^{9}Be, ^{11}Be, and ^{13}C // Physical Review C. –1983. –Vol. 28. –P. 497-505.

39 Nunes F., Thompson I.J., Johnson R.C. Core excitation in one neutron halo systems // Nuclear Physics A. –1996. –Vol. 596. –P. 171-186.

40 Gori G. Barranco F., Vigezzi E., Broglia R.A. Parity inversion and breakdown of shell closure in Be isotopes // Physical Review C. –2004. –Vol. 69. –P. R0413021- R0413025.

41 Vinh Mau N. Particle-vibration coupling in one neutron halo nuclei // Nuclear Physics A. –1995. –Vol. 592. –P. 33-44.

42 Shrivastava A., Blumenfeld Y., Keeley N., Zerguerras T., Aumann T., Bazin D., Chromik M., Crawley G.M., Glasmacher T., Kemper K.W., Maréchal F., Morrissey D.J., Nakamura T., Navin A., Pollacco E.C., Santonocito D., Sherrill B.M., Suomijärvi T., Thoennessen M., Tryggestad E., Varner R.L. ^{11}Be continuum studied through proton scattering // Physics Letters B. –2004. –Vol. 596. –P. 54–60.

43 Nakamura T., Motobayashi T., Ando Y., Mengoni A., Nishio T., Sakurai H., Shimoura S., Teranishi T., Yanagisawa Y., Ishihara M. Coulomb excitation of ^{11}Be// Physics Letters B. –1997. –Vol. 394. –P. 11-15.

44 Palit R., Adrich P., Aumann T., Boretzky K., Carlson B.V., Cortina D., Datta Pramanik U., Elze Th.W., Emling H., Geissel H., Hellström M., Jones K.L., Kratz J.V., Kulessa R., Leifels Y., Leistenschneider A., Münzenberg G., Nociforo C., Reiter P., Simon H., Sümmerer K., Walus W. Exclusive measurement of breakup reactions with the one-neutron halo nucleus ^{11}Be // Physical Review C. –2003. –Vol. 68. –P. 0343181-03431814.

45 Capel P., Goldstein G., Baye D. Time-dependent analysis of the breakup of ^{11}Be on ^{12}C at 67MeV/nucleon // Physical Review C. –2004. –Vol. 70. –P. 0646051-0646059.

46 de Diego R., Arias J.M., Lay J.A., Moro A.M. Continuum-discretized coupled-channels calculations with core excitation // Physical Review C. –2014. –Vol. 89. –P. 0646091-06460910.

47 William H. Numerical recipes in Fortran 77: the art of scientific computing. – Cambridge: Cambridge University Press, 1986. –933 p.

48 Cohen – Tannoudji C., Diu B., Laloe F. Mecanique quantique. –Paris: Hermann, 1973-898 p.

49 Valiolda D.S., Zhaugasheva S.A., Janseitov D.M., Zhussupova N.K. The study of the neutron halo of the ^{11}Be nucleus taking into account the influence of an external field// NEWS of the National Academy of Sciences of the Republic of Kazakhstan. –2018. –Vol. 318, №2. –P. 12-20.

50 Valiolda D.S., Janseitov D.M., Zhaugasheva S.A., Zhussupova N.K. Investigation of the neutron halo of the ^{11}Be nucleus// Recent Contributions to Physics. –2018. –Vol. 64, №1. –P. 81-88.

51 Kalitkin N.N. Numerical methods // Nauka Moscow. –1978. –512 p.

52 Melezhik V.S. New approach to the old problem of muon sticking in μCF // Hyperfine Interactions. –1996. –Vol. 101. –P. 365-374.

53 Kido T., Yabana K., Suzuki Y. Coulomb breakup mechanism of neutron-halo nuclei in a time-dependent method // Physical Review C. –1996. –Vol. 53. –P. 2296-2303.

54 Valiolda D., Melezhik V.S., Janseitov D. Study of bound and resonance states of ^{11}Be in breakup reaction // Eurasian Journal of physics and functional materials. –2022. –Vol. 6, № 3. –P. 165-173.

55 Crespo R., Deltuva A., Moro A.M. Core excitation contributions to the breakup of the one-neutron halo nucleus ^{11}Be on a proton // Physical Review C. –2011. –Vol. 83. –P. 0446221-0446224.

56 Moro A.M., Crespo R. Core excitation effects in the breakup of the one-neutron halo nucleus ^{11}Be on a proton target // Physical Review C. –2012. –Vol. 85. –P. 0546131-0546138.

57 Valiolda D., Melezhik V.S., Janseitov D. Study of nuclear contribution to breakup cross section of ^{11}Be halo nuclei within time-dependent approach // Physics of Particles and Nuclei Letters. –2022. –Vol. 19, №5. –P. 477-480.

58 Perey C.M., Perey F.G. Compilation of phenomenological optical-model parameters 1954–1975 // Atomic Data and Nuclear Data Tables. –1976. –Vol. 17. –P. 1-101.

59 Bechetti F.D., Greenless G.W. Nucleon-Nucleus Optical-Model Parameters, A>40, E<50 MeV // Physical Review. –1969. –Vol. 182. –P. 1190-1209.

60 Bonin, B., Alamanos, N., Berthier, B., Bruge, G., Faraggi, H., Lugol, J.C., Bauhoff, W. Alpha-nucleus elastic scattering at intermediate energies // Nuclear Physics A. –1985. –Vol. 445, №3. –P. 381-407.

61 Cook J. Global optical-model potentials for elastic scattering of ^{6,7}Li projectiles. Nuclear Physics A. –1985. –Vol. 388. –P. 153-172.

62 Melezhik V.S. Efficient computational scheme for ion dynamicsin RF-field of Paul trap // Discrete and Continuous Models and Applied Computational Science. –2019. –Vol. 27. –P. 378-385.

APPENDIX A
The system of units and some details of the solution of SE

In this work in solving problems, the outside system of units are used, which are often used in nuclear physics: where the energy, potential and mass are measured in energy units - MeV, and the radial coordinate and radius of the nucleus in fm (1 fm = 10^{-15} m), and the nuclear constant $\hbar c$=197.328 MeV·fm is used.

1) When we solve the stationary Schrödinger equation:

$$\left[-\frac{\hbar^2}{2\mu}\frac{d^2}{dr^2}+\frac{\hbar^2 l(l+1)}{2\mu\, r^2}+\boldsymbol{V}(r)\right]R_l(r)=E\,R_l(r). \qquad (A1)$$

In order to use the nuclear system of units, where r_0=1 fm, E_0=1 MeV, the Eq.(A1) is reduced to $r'=\frac{r}{r_0}$; $E'=\frac{E}{E_0}$:

$$\left[-\frac{\hbar^2}{2\mu\, {r_0}^2}\frac{d^2}{d\left(\frac{r}{r_0}\right)^2}+\frac{\hbar^2 l(l+1)}{2\mu\, {r_0}^2\,\left(\frac{r}{r_0}\right)^2}+V\left(\frac{r}{r_0}\right)\right]R_l\left(\frac{r}{r_0}\right)=E_0\left(\frac{E}{E_0}\right)R_l\left(\frac{r}{r_0}\right). \quad (A2)$$

The Woods-Saxon potential is rewrited as: $V(r)=\frac{V_0}{1+\exp(\frac{r'-R'}{a'})}=V\left(\frac{r}{r_0}\right)$; $\left(\frac{V_0}{E_0}\right)={V_0}'$. Then the radial SE:

$$\left[-\frac{\hbar^2}{2\mu\, {r_0}^2 E_0}\frac{d^2}{d{r'}^2}+\frac{\hbar^2 l(l+1)}{2\mu\, {r_0}^2\, E_0 {r'}^2}+\frac{{V_0}'}{1+exp(\frac{r'-R}{a})}\right]R_l(r')=E'R_l(r'). \qquad (A3)$$

Here the reduced mass $\mu=\frac{m_n M_{10}}{m_n+M_{10}}=\frac{m_n}{1+\frac{m_n}{M_{10}}}\approx m_n$ is then divided to the mass of neutron $m_n=939.565$ MeV. Taking into account corrections per unit, the constant in the equation (A3):

$$\frac{\hbar^2}{2\mu\, {r_0}^2 E_0}=\frac{\hbar^2 c^2}{2\,(\frac{\mu}{m_n})\,m_n\,c^2 {r_0}^2 E_0}=\frac{197{,}328^2\,\text{MeV}^2\,\text{fm}^2}{2\left(\frac{\mu}{m_n}\right)\cdot 939{,}565\ \text{MeV}\cdot 1\ \text{fm}^2\cdot 1\ \text{MeV}}=\frac{41{,}443}{2(\frac{\mu}{m_n})}.$$

Thus, the radial SE reduced to the nuclear system of units, is written as:

$$\left[-\frac{41{,}443}{2\left(\frac{\mu}{m_n}\right)}\frac{d^2}{dr^2}+\frac{41{,}443\ l(l+1)}{2\left(\frac{\mu}{m_n}\right)r^2}+\boldsymbol{V}(r)\right]R_l(r)=E\,R_l(r)\,\boldsymbol{.} \qquad (A4)$$

2) In solving the time-dependent Schrodinger equation:

$$i\hbar\,\frac{\partial\Psi}{\partial t} = [H_0(\boldsymbol{r}) + h(\boldsymbol{r},t)]\Psi(\boldsymbol{r},t). \tag{A5}$$

it is also necessary to introduce a correction for units, where time is measured in $\left[\frac{\hbar}{\text{MeV}}\right]$, since the energy is $E = \hbar\, w$, then $t_0 = \frac{2\pi\,\hbar}{E_0} = 2\pi\ \frac{\hbar}{\text{MeV}}$;

$$\frac{i\hbar}{E_0 t_0}\ \frac{\partial\Psi}{\partial(\frac{t}{t_0})} = E_0\left(\frac{H_0}{E_0}\right)\Psi(r,t) + E_0\left(\frac{h}{E_0}\right)\Psi(r,t). \tag{A6}$$

Thus the TDSE with the unit correction for time is written as:

$$\frac{i}{2\pi}\ \frac{\partial\Psi}{\partial\, t'} = (H_0{}' + h')\Psi(r,t'). \tag{A7}$$

3) Here at Eq.(A7) the time dependent Hamiltonian *h(r,t)* is the Coulomb potential:

$$V_C(r,t) = \frac{Z_c Z_T e^2}{|\frac{m_n r}{M} + R(t)|} - \frac{Z_c Z_T e^2}{R(t)} = Z_c Z_T e^2\ (\frac{1}{|\frac{m_n r}{M} + R(t)|} - \frac{1}{R(t)}). \tag{A8}$$

The product of the charges of the target (^{208}Pb) and the core (^{10}Be) is reduced to the units as:

$$Z_c Z_T e^2 = \frac{Z_c Z_T e^2\,\hbar c}{\hbar c} = \left|\alpha = \frac{e^2}{\hbar c} = \frac{1}{137.04}\right| = \frac{Z_c Z_T \cdot 197.3\ \text{MeV}\cdot\text{fm}}{137.04} = 1.44\ Z_c Z_T\ (\ E_0 r_0) \tag{A9}$$

The relative coordinate between the projectile and the target at Eq.(A8):

$$\boldsymbol{R}(t) = \boldsymbol{b} + \boldsymbol{v}\,t \tag{A10}$$

Here, the impact parameter is measured in units of length *[b]=1 fm,* an initial velocity is reduced to the speed of light: $\gamma = v/c$ *:*

$$\boldsymbol{v}\,t = 197.3\,\boldsymbol{\gamma}\,t \tag{A11}$$

Since $\boldsymbol{v_0}\,\boldsymbol{t_0} = \boldsymbol{r_0};\ \boldsymbol{v_0} = \frac{\boldsymbol{r_0}}{\boldsymbol{t_0}} = \frac{\mathbf{1\ fm\ MeV}\,\boldsymbol{c}}{\hbar\boldsymbol{c}} = \frac{\mathbf{1}}{\mathbf{197.3}}\boldsymbol{c}$.

The initial velocity at the Eq.(A10) is given by the initial energy of the projectile beam:

$$\frac{\boldsymbol{v}}{\boldsymbol{c}} = \sqrt{\mathbf{1} - \frac{\mathbf{1}}{\left(\mathbf{1} + \frac{\boldsymbol{T_i}}{\boldsymbol{A}\,\boldsymbol{m_N c^2}}\right)^{\mathbf{2}}}} \tag{A12}$$

Here T_i/A is the initial beam energy of the projectile, $m_N c^2 = A \cdot 931.5$ MeV . For example if the beam energy is T=72 MeV/nucleon, then from the formula (A12), the

initial velocity is v=0.37 c. Table A.1 below shows the values of all velocities calculated by this formula for the entire range of beam energies studied in our work.

Table A.1– Velocity values required in the computer program to set the initial beam energy.

T_i, the beam energy, MeV/nucleon	v/c, the initial velocity of the projectile
72	0.37
69	0.36
30	0.25
20	0.20
10	0.15
5	0.10

APPENDIX B
Details of the inclusion of nuclear interaction into the computational scheme

In the semiclassical approximation, the relative motion of the projectile and the target is treated classically. Therefore the target can be seen as following a classical trajectory in the projectile rest frame. The influence of the target onto the two-body projectile is then modeled by a time-dependent potential

$$V(\mathbf{r}, t) = V_{cT}(\mathbf{r}_{cT}) + V_{fT}(r_{fT}) - \frac{(Z_c+Z_f)Z_T e^2}{\mathbf{R}(t)}, \quad \text{(B1)}$$

simulating the projectile-target interaction consists of the residual interaction between the projectile fragments and the target. Here $\mathbf{R}(t)$, $\mathbf{r}_{cT}, \mathbf{r}_{fT}$ are the relative distances between the target and the projectile centre of mass, the core and the fragment respectively. As we consider a heavy target (^{208}Pb), the interaction (B1) approximated by a pure Coulomb interaction. For studying the nuclear effects, we should compute another classical trajectory with including a nuclear term of interaction.

The time-dependent potential with including the nuclear term of the projectile-target interaction in the breakup cross sections:

$$V(\mathbf{r}, t) = V_{cT}(r_{cT}) + V_{fT}(r_{fT}) + \frac{Z_c Z_T e^2}{r_{cT}} + \frac{Z_f Z_T e^2}{r_{fT}} - \frac{(Z_c+Z_f)Z_T e^2}{R(t)} =$$

$$= V_{cT}(r_{cT}) + V_{fT}(r_{fT}) + \frac{Z_c Z_T e^2}{|\mathbf{R}(t)+m_f\mathbf{r}/M|} - \frac{Z_c Z_T e^2}{R(t)} \quad \text{(B2)}$$

Here projectile-target potentials, describing the interaction of the core with the target $V_{cT}(r_{cT})$ and the fragment with the target $V_{fT}(r_{fT})$ are composed of the sum of real and imaginary potentials:

$$V_{cT}(r_{cT}) = -V_c\, f(r_{cT}, R_{Rc}, a_{Rc}) - i\, W_c\, f(r_{cT}, R_{Ic}, a_{Ic}), \quad \text{(B3)}$$

$$V_{fT}(r_{fT}) = -V_f\, f(r_{fT}, R_{Rf}, a_{Rf}) - i\, W_f\, f(r_{fT}, R_{If}, a_{If}). \quad \text{(B4)}$$

where $f(r_{xT}, R_R, a_R) = \frac{1}{1+\exp(\frac{r_{xT}-R}{a})}$ Woods-Saxon form factor, x stands for either core (c) or fragment (f).

The core target and fragment target coordinates are:

$$\mathbf{r}_{cT} = \mathbf{R}(t) + \frac{m_f \mathbf{r}}{M}, \quad \text{(B5)}$$

$$\mathbf{r}_{\mathrm{fT}} = \mathbf{R}(\mathrm{t}) - \frac{\mathrm{m_c}\mathbf{r}}{\mathrm{M}}\,. \tag{B6}$$

where $\mathrm{M}=\mathrm{m_c}+\mathrm{m_f}$ is a nucleus mass. Further substituting the values of $\mathbf{R}(\mathrm{t}) = \mathbf{b} + \mathbf{v_0}\mathrm{t}$, and after mathematical transformations, the core-target coordinates:

$$\mathrm{r_{cT}}=|\mathbf{R}(\mathrm{t}) + \mathrm{m_f}\mathbf{r}/\mathrm{M}| = \sqrt{(\mathbf{R}(\mathrm{t}))^2 + (\mathrm{m_f}\mathbf{r}/\mathrm{M})^2 + \frac{2\,\mathrm{m_f}}{\mathrm{M}}\,(\mathbf{r}\,\mathbf{R})},$$

$$r_{cT} = (b^2 + (vt)^2 + (m_f r/M)^2 + \frac{2\,m_f}{M} r\,(bsin\theta\,cos\varphi - vt\,cos\theta))^{\frac{1}{2}}\,. \tag{B7}$$

and the n-Pb (fragment-target) coordinates:

$$\mathrm{r_{fT}} = |\mathbf{R}(\mathrm{t}) - \mathrm{m_c}\mathbf{r}/\mathrm{M}| = \sqrt{(\mathbf{R}(\mathrm{t}))^2 + (\mathrm{m_c}\mathbf{r}/\mathrm{M})^2 - \frac{2\,\mathrm{m_c}}{\mathrm{M}}\,(\mathbf{r}\,\mathbf{R})}\,,$$

$$r_{fT} = (b^2 + (vt)^2 + (m_c r/M)^2 - \frac{2\,m_c}{M} r\,(bsin\theta\,cos\varphi - vt\,cos\theta))^{\frac{1}{2}}\,. \tag{B8}$$

Substituting Eq. (3.4) with nuclear part of interaction to Eq.(2.1), we get the scheme for TDSE:

$$\left[1 + i\frac{\Delta t}{2}(V_{coul} + V_{opt} + iW_{opt})\right]\boldsymbol{\psi}(r, t+\Delta t) = \left[1 - i\frac{\Delta t}{2}(V_{coul} + V_{opt} + \right.$$
$$\left. + iW_{opt})\right]\boldsymbol{\psi}(r, t)\,. \tag{B9}$$

Here the potentials $V_{coul} + V_{opt} = V$, the wave functions in time evolution $\psi(r, t+\Delta t) \rightarrow \psi^{n+1}$, $\psi(r,t) \rightarrow \psi^n$ are marked for conveniences. Then

$$\left[1 + i\frac{\Delta t}{2}(V + iW)\right]\psi^{n+1} = \left[1 - i\frac{\Delta t}{2}(V + iW)\right]\psi^n\,. \tag{B10}$$

Rewriting (B10) in matrix form:

$$\begin{pmatrix} 1 - \frac{\Delta t}{2}W & -\frac{\Delta t}{2}V \\ \frac{\Delta t}{2}V & 1 - \frac{\Delta t}{2}W \end{pmatrix}\begin{pmatrix} \psi^{n+1} \\ \overline{\psi^{n+1}} \end{pmatrix} = \begin{pmatrix} 1 + \frac{\Delta t}{2}W & \frac{\Delta t}{2}V \\ -\frac{\Delta t}{2}V & 1 + \frac{\Delta t}{2}W \end{pmatrix}\begin{pmatrix} \psi^n \\ \overline{\psi^n} \end{pmatrix}. \tag{B11}$$

$\overline{\psi^n}$ *and* $\overline{\psi^{n+1}}$ are the imaginary part of wave function. The solution of (B11):

$$\begin{pmatrix} \psi^{n+1} \\ \psi^{n+1} \end{pmatrix} = \hat{A}^{-1} \begin{pmatrix} 1+\frac{\Delta t}{2}W & \frac{\Delta t}{2}V \\ -\frac{\Delta t}{2}V & 1+\frac{\Delta t}{2}W \end{pmatrix} \begin{pmatrix} \psi^{n} \\ \psi^{n} \end{pmatrix}, \quad \text{(B12)}$$

where $\begin{pmatrix} 1-\frac{\Delta t}{2}W & -\frac{\Delta t}{2}V \\ \frac{\Delta t}{2}V & 1-\frac{\Delta t}{2}W \end{pmatrix} = \hat{A}$

the inverse matrix of $\hat{A}$:
:

$$\hat{A}^{-1} = \frac{1-\frac{\Delta t}{2}W}{(1-\frac{\Delta t}{2}W)^2+(\frac{\Delta t}{2}V)^2} \begin{pmatrix} 1 & \frac{\frac{\Delta t}{2}V}{(1-\frac{\Delta t}{2}W)} \\ \frac{-\frac{\Delta t}{2}V}{(1-\frac{\Delta t}{2}W)} & 1 \end{pmatrix}. \quad \text{(B12′)}$$

Then substituting the matrices $\hat{A}$ and $\hat{A}^{-1}$:

$$\begin{pmatrix} \psi^{n+1} \\ \psi^{n+1} \end{pmatrix} = \frac{1-\frac{\Delta t}{2}W}{\left(1-\frac{\Delta t}{2}W\right)^2+\left(\frac{\Delta t}{2}V\right)^2} \begin{pmatrix} 1 & \frac{\frac{\Delta t}{2}V}{\left(1-\frac{\Delta t}{2}W\right)} \\ \frac{-\frac{\Delta t}{2}V}{\left(1-\frac{\Delta t}{2}W\right)} & 1 \end{pmatrix} \times$$
$$\times \begin{pmatrix} 1+\frac{\Delta t}{2}W & \frac{\Delta t}{2}V \\ -\frac{\Delta t}{2}V & 1+\frac{\Delta t}{2}W \end{pmatrix} \begin{pmatrix} \psi^{n} \\ \psi^{n} \end{pmatrix}. \quad \text{(B13)}$$

$$\begin{pmatrix} \psi^{n+1} \\ \psi^{n+1} \end{pmatrix} = \frac{1}{\left(1-\frac{\Delta t}{2}W\right)^2+\left(\frac{\Delta t}{2}V\right)^2} \times$$
$$\times \begin{pmatrix} 1-\left(\frac{\Delta t}{2}W\right)^2-\left(\frac{\Delta t}{2}V\right)^2 & \Delta tV \\ -\Delta tV & 1-\left(\frac{\Delta t}{2}W\right)^2-\left(\frac{\Delta t}{2}V\right)^2 \end{pmatrix} \begin{pmatrix} \psi^{n} \\ \psi^{n} \end{pmatrix}, \quad \text{(B14)}$$

one can obtain the exact solution of the integral of TDSE - the outgoing wave function at each moment of time. The real part of wave function:

$$\psi(\boldsymbol{r}, t+\Delta t) = \frac{1}{(1-\frac{\Delta t}{2}W)^2+(\frac{\Delta t}{2}V)^2} \times \left[\left(1-\left(\frac{\Delta t}{2}W\right)^2-\left(\frac{\Delta t}{2}V\right)^2\right)\psi(\boldsymbol{r}, t) + \Delta t\, V\, \overline{\psi(\boldsymbol{r}, t)}\right], \quad \text{(B15)}$$

The imaginary part of wave function is

$$\overline{\psi(\boldsymbol{r}, t+\Delta t)} = \frac{1}{\left(1-\frac{\Delta t}{2}W\right)^2+\left(\frac{\Delta t}{2}V\right)^2} \times \times \left[-\Delta t V\, \psi(\boldsymbol{r}, t) + \left(1-\left(\frac{\Delta t}{2}W\right)^2-\left(\frac{\Delta t}{2}V\right)^2\right)\overline{\psi(\boldsymbol{r}, t)}\right]. \quad \text{(B12)}$$

APPENDIX C

The application of breakup wave function in analyzing the breakup dynamics

Let's write down the value of the coordinates x, y, z in spherical coordinates :

$$\begin{aligned} x &= r\,sin\theta cos\varphi \\ y &= r\,sin\theta sin\varphi \\ z &= r\,cos\theta \end{aligned} \quad , \tag{C1}$$

The average value of the coordinate Z in the breakup process is:

$$< Z >= \frac{<\Psi_{\mathrm{bu}}|Z|\Psi_{\mathrm{bu}}>}{<\Psi_{\mathrm{bu}}|\Psi_{\mathrm{bu}}>}, \tag{C2}$$

where Ψ_{bu}- is the wave function corresponding to the breakup [12,13] of the system ^{10}Be+n:

$$|\Psi_{\mathrm{bu}}(\boldsymbol{r},t)>=(1-\sum_{\vartheta\in bound}|\varphi_{\vartheta}(\boldsymbol{r})><\varphi_{\vartheta}(\boldsymbol{r})|)\,|\Psi(\boldsymbol{r},t)>, \tag{C3}$$

which consists of the sums of two bound states of ^{11}Be obtained from the solution of stationary Schrodinger equation:

$$\widehat{H_0}(r)\Psi(r)=\varepsilon\Psi(r). \tag{C4}$$

Substituting (2) into formula (1), we obtain the averaging of the coordinate over the breakup wave functions:

$$\begin{aligned} &< \Psi_{\mathrm{bu}}|Z|\Psi_{\mathrm{bu}} >< \Psi_{\mathrm{t}}|Z|\Psi_{\mathrm{t}} > -< \Psi_{\mathrm{t}}|Z|\Psi_0 >< \Psi_0|\Psi_{\mathrm{t}} > - < \Psi_{\mathrm{t}}|\Psi_0 > \\ &< \Psi_0|Z|\Psi_{\mathrm{t}} > +< \Psi_{\mathrm{t}}|\Psi_0 >< \Psi_0|Z|\Psi_0 >< \Psi_0|\Psi_{\mathrm{t}} > . \end{aligned} \tag{C5}$$

The normalization of the breakup wave function is found from the probability P_b of the system to be in a bound state:

$$< \Psi_{\mathrm{bu}}|\Psi_{\mathrm{bu}} >=< \Psi_{\mathrm{t}}|\Psi_{\mathrm{t}} > -< \Psi_{\mathrm{t}}|\Psi_0 >< \Psi_0|\Psi_{\mathrm{t}} >= 1-P_b, \tag{C6}$$

where the probability is $P_b =< \Psi_{\mathrm{t}}|\Psi_0 >< \Psi_0|\Psi_{\mathrm{t}} >$. The mean value of the coordinate x in breakup process is found in the same way.

In figures C1 and C2 the averaging of the coordinates Z(t) and X(t) over the breakup wave functions are illustrated, the dynamics of the breakup components along the mean value of coordinates was integrated over a wide time interval $t\epsilon[-10\,\hbar/MeV, +30\,\hbar/MeV]$ with the step of $dt = 0.02\hbar/MeV$. The z axis is chosen along $\boldsymbol{v_0}$ and the x axis is in the collision plane, according to the bound-neutron model with the straight-line trajectory $\mathbf{R}(t)=\mathbf{b}+\mathbf{v_0}t$ of the ^{11}Be projectile. The

impact parameter is chosen as b=12 fm and the selected relative velocity v=0.37c corresponds to 72 MeV per nucleon [12].

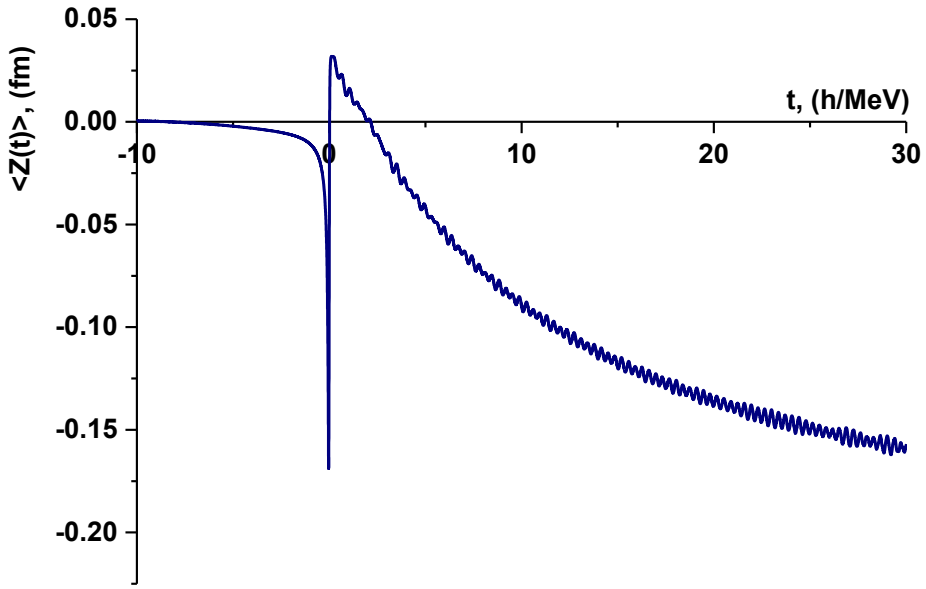

Figure C1– The averaging of Z(t) coordinate in a breakup process

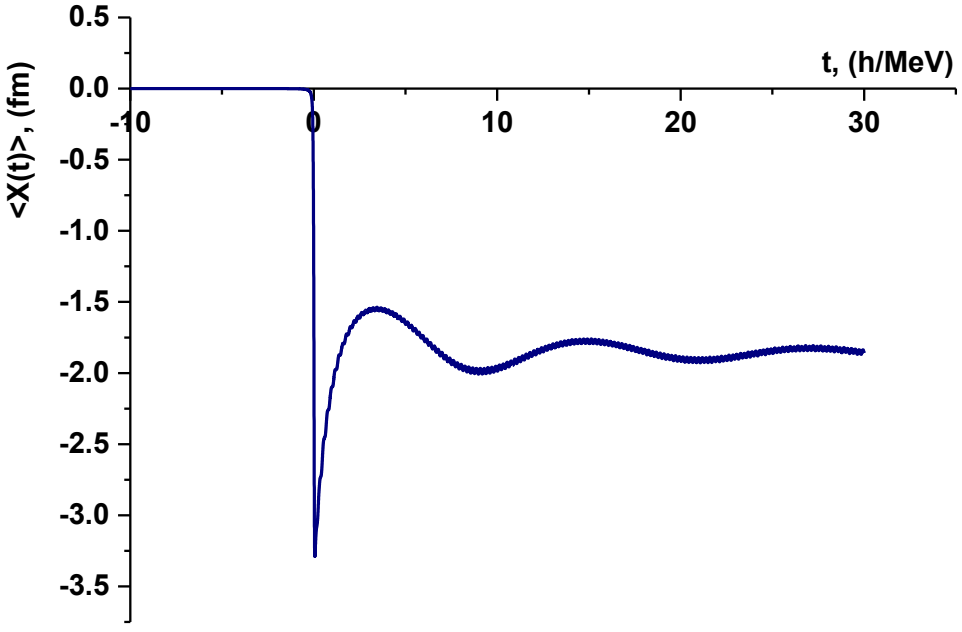

Figure C2– The averaging of X(t) coordinate in a breakup process

Now let's determine the mean value of the transverse and longitudinal momenta between the emitted neutron (n) and the ^{10}Be core-nucleus in the breakup reaction ^{11}Be+^{208}Pb -> ^{10}Be+n+^{208}Pb:

$$< k_Z >= \frac{\mu}{\hbar}\frac{<\Psi_{\mathrm{bu}}|\frac{dz}{dt}|\Psi_{\mathrm{bu}}>}{<\Psi_{\mathrm{bu}}|\Psi_{\mathrm{bu}}>}. \tag{C7}$$

where k_Z is the Z component of the wave vector. In the first approximation of $\frac{dz}{dt}$, a first-order differential (FOD) operation:

$$\frac{dz}{dt} = \frac{<z^{i+1}>-<z^{i}>}{\Delta t}, \tag{C8}$$

and for a higher accuracy, we write it in the second order differential (SOD) approximation:

$$\frac{dz}{dt} = \frac{<z^{i+1}>-<z^{i-1}>}{2\Delta t}. \tag{C9}$$

Then in a FOD approximation, substituting (C8), we obtain:

$$< k_Z >= \frac{\mu}{\hbar\Delta t}\left(\frac{<\Psi_{\mathrm{bu}}^{i+1}|Z|\Psi_{\mathrm{bu}}^{i+1}>}{<\Psi_{\mathrm{bu}}|\Psi_{\mathrm{bu}}>} - \frac{<\Psi_{\mathrm{bu}}^{i}|Z|\Psi_{\mathrm{bu}}^{i}>}{<\Psi_{\mathrm{bu}}|\Psi_{\mathrm{bu}}>}\right). \tag{C10}$$

Here the breakup components are: $<\Psi_{\mathrm{bu}}| =< \Psi(\mathrm{t})|(1-|\varphi_0><\varphi_0|)$ and $|\Psi_{\mathrm{bu}}>=|\Psi(\mathrm{t})> -|\varphi_0><\varphi_0|\Psi(\mathrm{t})>)$, φ_0 – is a wave function of bound states, i.e. the ground ($1/2^+$) and first excited ($1/2^-$) states of ^{11}Be.

The average value of the momentum component could be calculated in coordinate space in a direct way:

$$< p_Z >= \frac{<\psi_{bu}(\boldsymbol{r},t)|-i\frac{\partial}{\partial z}|\psi_{bu}(\boldsymbol{r},t)>}{<\psi_{bu}(\boldsymbol{r},t)|\psi_{bu}(\boldsymbol{r},t)>}, \tag{C11}$$

as it is known that $\widehat{p_Z} = -i\hbar\frac{\partial}{\partial z}$; $\widehat{p_Z} = \hbar\vec{k}_Z$.

In order not to lose accuracy during the numerical differentiation with respect to Cartesian coordinates, in equation (C11) we should calculate $< k_x >$ and $< k_Z >$ components through the matrix elements of the commutator $\left[\widehat{H}(\boldsymbol{r},t),Z\right]$:

$$< k_Z(t) >= i\frac{\mu}{\hbar^2}\frac{<\Psi_{\mathrm{bu}}(\boldsymbol{r},t)\left|\left[\widehat{H}(\boldsymbol{r},t),Z\right]\right|\Psi_{\mathrm{bu}}(\boldsymbol{r},t)>}{<\Psi_{\mathrm{bu}}(\boldsymbol{r},t)|\Psi_{\mathrm{bu}}(\boldsymbol{r},t)>} \tag{C12}$$

From the Hamilton equation:

$$\frac{dp_Z}{dt} = -\frac{\partial H}{\partial Z};\ \frac{dZ}{dt} = \frac{\partial H}{\partial p_Z}. \tag{C13}$$

Derivative of Z coordinate with respect to time:

$$\frac{dZ}{dt} = \frac{\partial Z}{\partial t} + \{H, Z\}\,, \tag{C14}$$

where $\{H, Z\} = \sum\{\frac{\partial Z}{\partial Z}\frac{\partial H}{\partial p_Z} - \frac{\partial H}{\partial Z}\frac{\partial Z}{\partial p_Z}\}$ written through Poisson brackets:

$$\frac{dZ}{dt} = \{H, Z\} = \frac{\partial H}{\partial p_Z} = \frac{\widehat{p_Z}}{\mu}\ , \tag{C14′}$$

as $\widehat{H} = \frac{p_x^2+p_y^2+p_z^2}{2\mu}$. Or it is written with a a commutator $[H, Z]$

$$\frac{dZ}{dt} = \frac{\partial Z}{\partial t} - \frac{i}{\hbar}[H, Z]. \tag{C15}$$

Then

$$\frac{dZ}{dt} = -\frac{i}{\hbar}[H, Z] = \frac{\widehat{p_Z}}{\mu} = \hbar\frac{\widehat{k_Z}}{\mu}\,. \tag{C16}$$

Thereby we calculate the average longitudinal and transverse momentum by $\widehat{k_Z} = -i\frac{\mu}{\hbar^2}[H, Z]$ or $\widehat{k_Z} = \frac{\mu}{\hbar}\frac{dZ}{dt}$ and compare these formulas. Accordingly, the average value $< k_Z(t) >$ as mentioned above, will be determined through the following formulas:

$$< k_Z(t) >= i\frac{\mu}{\hbar^2}\frac{< \Psi_{\mathrm{bu}}(\boldsymbol{r}, t)\big|\big[\widehat{H}(\boldsymbol{r}, t), Z\big]\big|\Psi_{\mathrm{bu}}(\boldsymbol{r}, t) >}{< \Psi_{\mathrm{bu}}(\boldsymbol{r}, t)|\Psi_{\mathrm{bu}}(\boldsymbol{r}, t) >}\,, \tag{C17}$$

$$< k_Z(t) >= \frac{\mu}{\hbar}\frac{< \Psi_{bu}(\boldsymbol{r}, t)|\,\frac{\partial}{\partial Z}\,|\Psi_{bu}(\boldsymbol{r}, t) >}{< \Psi_{bu}(\boldsymbol{r}, t)|\Psi_{bu}(\boldsymbol{r}, t) >}\,. \tag{C18}$$

Then using transformations with FOD and SOD, the averaging of $< k_Z(t) >$ component:

$$< k_Z(t) >= \frac{\mu}{\hbar\Delta t}(< Z_{i+1} > - < Z_i >) \qquad \text{(FOD)} \tag{C19}$$

$$< k_Z(t) >= \frac{\mu}{2\hbar\Delta t}(< Z_{i+1} > - < Z_{i-1} >) \quad \text{(SOD)} \tag{C20}$$

where $< Z_i >$, $< Z_{i+1} >$ and $< Z_{i-1} >$ is solved through formula (C2), respectively.

With the developed model, we now analyze the dependence of the mean transverse and longitudinal momenta by bound-neutron model with a straight-line trajectory. In Figures C3 and C4, the calculated values of $< k_Z(t) >$ and $< k_x(t) >$ with a first order (FOD) and second order (SOD) differential approximations (Eqs. (C19) and (C20)) are given as a function of time.

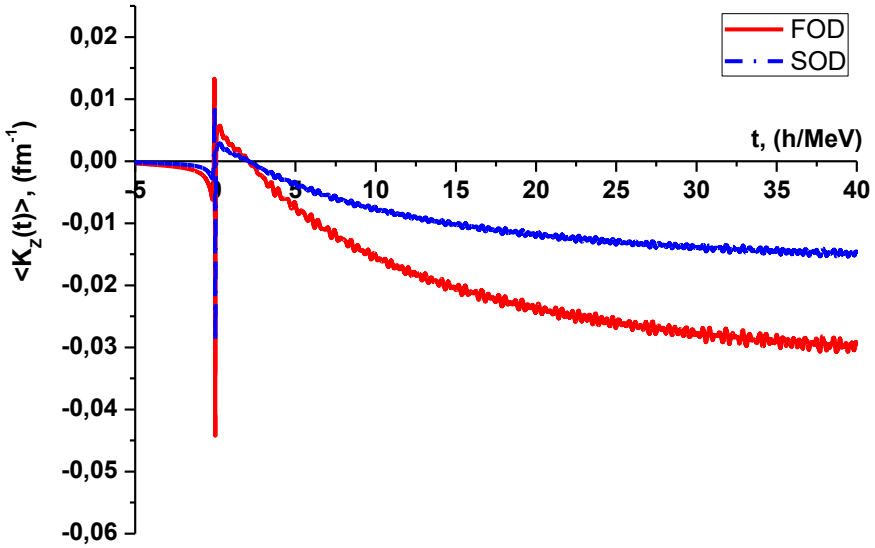

Figure C3 – Time dependence of the mean $< k_Z(t) >$ longitudinal momenta in comparison of the first order (FOD) and second order (SOD) differential approximations.

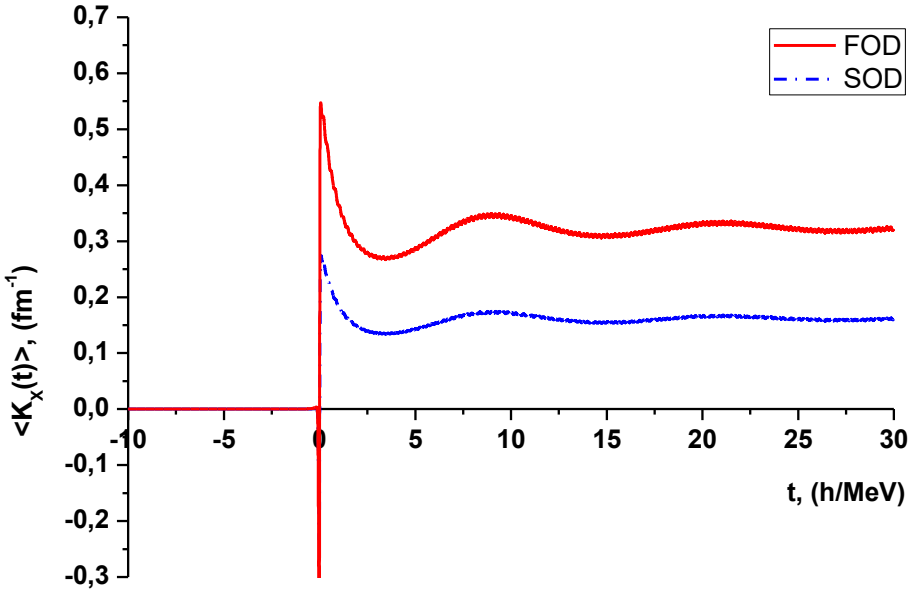

Figure C4 – Time dependence of the mean transverse $< k_x(t) >$ momenta in comparison of first order (FOD) and second order (SOD) differential approximations.

At table C1 below, the difference between our results and the previous ones [14] can be explained by the use of a more detailed radial grid and by the avoidance of a multipole expansion of the operator of the Coulomb interaction in the present calculations as in [14].

Table C1 – Analyses of the longitudinal momentum between the neutron and the core nucleus in comparison with the works [12, 14].

t ($\hbar$/MeV)	r_m=1200 fm Δx=0.0005 Δt=0.02$\hbar$/MeV the calculations with the FOD	r_m=1200 fm Δx=0.0005 Δt=0.02$\hbar$/MeV the calculations with the SOD	r_m=1200 fm Δx=0.0005 Δt=0.02$\hbar$/MeV calculations of V.S. Melezhik [12]	Calculations of T. Kido [14]
10	0.0154	0.0076	0.0156	0.019 (*); 0.026 (**)
15	0.0207	0.0104	0.0159	
20	0.0241	0.0121	0.0158	
25	0.0266	0.0133	0.0154	
30	0.0276	0.0138	0.0148	
40	0.0298	0.0148		

(*) the same parameters of the Woods-Saxon potential were used in the calculations, which were used in the works of V.S. Melezhik and in our calculations;
(**) calculations were made for other parameters of the depth of the Woods-Saxon potential.